(B) SPIN NETWORKS : QUANTUM GLASSES

Suppose we now consider a network of spins - a "spin net" in which we now have a set of M 2-level systems $\{\underline{\tau}_i\}$ with a set of interactions U_{ij} which may or may not be controllable.

For many years physicists have been studying regular lattices of spins in various dimensions, with fixed interactions. However these are a small fraction of the possible spin nets we might be interested in, and not really the most interesting. In both classical and quantum spin systems it has been found that very rich behaviour can emerge when we have what is called "frustration", and this has led to a very extensive study of what are called "glasses" (although there is no generally accepted definition of a glass). In recent years much more general types of spin network have been studied, with applications to fields ranging from neural networks, genetic networks, the dynamics of systems ranging from the internet to proteins, and even problems in computer science (notably optimisation problems).

Perhaps the most exciting development has involved spin nets in which one can vary the couplings in a controlled way to do quantum information processing. In some ways the theoretical structures & problems that arise in this new field are clearly related to existing ideas, notably in the theory of topological quantum fluids. Thus our study of glasses leads into some very interesting territory.

In what follows we begin with a brief review of experiments on glasses. We then take a closer look at the physics of dipolar glasses. These include both dipolar spin glasses & dipolar electric glasses. They are a useful example to begin with because they have a well-defined Hamiltonian, which is fairly simple, but they also exhibit all the important features of glasses, both quantum and classical. We then proceed to a more theoretical discussion of spin glasses, introducing some of the key concepts in this field. Finally, we look at the application to some related problems.

B.1 REVIEW OF EXPERIMENTS/PHENOMENOLOGY

There is a colossal experimental literature on glasses, both spin glasses & otherwise, and one recieves a salutary lesson on the way in which "experiments come laden with theory" when looking at it. The way that data are presented (and what is not presented), the kinds of experiments that are done, and the interpretational framework, all depend on some general theoretical ideas (or often just ideals) which sometimes have little justification apart from a historical pedigree. In this field one also finds a quite radical divorce between some of the theory and the experiments, and the development of differing schools of thought with quite different aims - the situation is reminiscent of string theory.

In this section we first look at the interesting experiments, some old, some new, in the quantum and classical regimes. We begin with spin glasses, and then discuss other related glasses (electric dipole glasses, electron glasses, amorphous glasses, random networks of superconductors, etc).

Finally, we look at some of the general ideas that can be used to interpret the data: the combination of disorder and frustration, hierarchies of timescales & "ultrametricity", quantum critical ideas, localisation, self-averaging, etc., and the "gauge theory" picture of glasses. This discussion will avoid formal details (which will come in section B.3).

(a) Experiments on Spin Glasses

The simplest phenomenological approaches to spin-glasses try to fit the experimental phenomena into modified ideas based around the theory of phase transitions. So we begin with some of the phenomena that naively resemble phase transitions, and then go on to discuss what is wrong with this, focussing on the dynamics. At the end we return to a discussion of the "static" phenomena for a 2nd look.

(i) Some Key Experimental Systems: The vast majority of condensed matter systems show glassy behaviour at low T, and often at quite high T. As far as magnetic systems are concerned, there are 3 broad criteria which are commonly used to decide whether a system is behaving as a spin glass, viz.,

- Below some temperature T_G it apparently shows frozen moments
- The moments are not ordered in the usual way - there is certainly no long-range order of the usual kind.
- Even below T_G (whose very definition depends on the timescale of interest) there are long-time relaxation phenomena in the spin distribution going on, along with remanence, aging, and hysteresis. All this occurs over timescales ranging from 10^{-11} secs up to astronomical times, with an apparently continuous range of relaxational timescales.

Note that there is no properly defined thermodynamic phase transition at T_G. This is best understood by looking at the data on magnetic susceptibility and specific heat (see below).

We begin by briefly describing some well-known categories of experimental system that have been examined, along with some representative examples.

Metallic Spin Glasses: These materials are amongst the earliest studied in detail in this field. They include a large variety of TM and RE ions, embedded in simple metals such as the Noble metals (Cu, Ag, Au), as in some cases in non-magnetic TM metals into which they easily go into solution (eg Pd, Pt, etc), or even light simple metals like Al. Many of these systems are classic Kondo systems. Systems that have been investigated particularly thoroughly include

Cu : Mn	Au : Mn	Pd : Fe	Zn : Mn	(1)
Cu : Fe	Au : Fe	Pd : Ni	Cd : Mn	
Cu : Ni	Au : Ni	Pt : Mn	Mg : Mn	

Typically the interactions between these impurities is supposed to be RKKY in nature, ie, we expect

$$\mathcal{H}_{int} = \sum_{ij} K_{ij}^{\alpha\beta}(\underline{r}_i - \underline{r}_j)\, S_i^{\alpha} S_j^{\beta} \qquad (2)$$

where when $k_F|\underline{r}_i - \underline{r}_j| \gg 1$,

$$K^{\alpha\beta}(\underline{r}_i - \underline{r}_j) \sim J_0^2 \frac{N(0)}{k_F^3 |\underline{r}_i - \underline{r}_j|^3} \cos\left(2k_F|\underline{r}_i - \underline{r}_j| + \delta\right) \qquad (3)$$

As with many simple theoretical prescriptions of this kind, the formula (3) gives a rough guide to the experiments, but is not quantitatively accurate. This can be seen in the figure at left, where a comparison is made between theory and experiment on some simple systems.

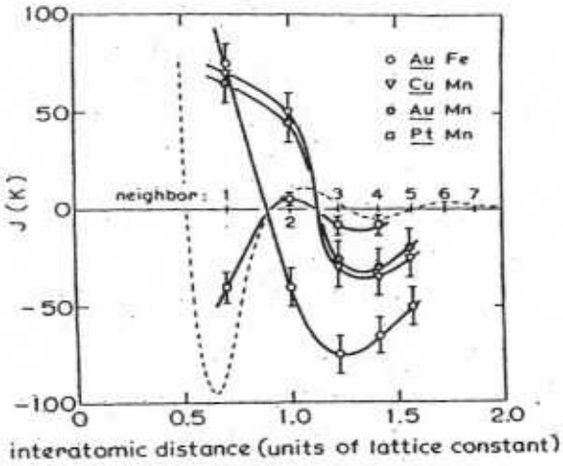

FIG. 6. Estimated exchange parameters J as a function of distance for four spin glass systems. The dashed line represents the RKKY conduction electron polarization around a Mn ion in Cu.

Note that whereas cases like Au:Mn or Cu:Fe are relatively simple (but see below), a system like Pd:Ni is more complicated because the Pd host is itself nearly ferromagnetic (the static susceptibility χ of Pd is roughly 10 times higher than the χ_0 expected from the band structure, indicating a very large Fermi liquid enhancement from low-energy spin fluctuations. In fact a single Fe ion, embedded in Pd, forms a huge moment $\sim 200\,\mu_B$ around it, by polarising the Pd spins. Nevertheless a concentration of $x \sim 10^{-6}$ of Fe in Pd allows the formation of a spin glass at mK temperatures. This shows that the long-range interaction between the "Fe/Pd spin clouds" is still RKKY-like at long ranges. The crucial point here is that if the spins are randomly distributed, then the distances $R_{ij} = |\underline{r}_i - \underline{r}_j|$ are also somewhat random, and thence the sign of the interaction also is largely random.

Note that magnetic anisotropy is crucial in these systems, since it allows each spin to freeze in some orientation at low T. It then finds itself subject to the field of its neighbours. So a good starting point for an effective Hamiltonian is

$$\mathcal{H}_{eff} = \sum_{k\sigma} \epsilon_k c^\dagger_{k\sigma} c_{k\sigma} + \sum_j \sum_k J\, \underline{S}_j \cdot (c^\dagger_{k\alpha} \hat{\sigma}_{\alpha\beta} c_{k\beta}) + \sum_{i \neq j} \sum_j K_{ij}^{\alpha\beta} S_i^\alpha S_j^\beta + \mathcal{H}_K(\underline{S}_j)$$
$$+ \mathcal{H}_{ph}(S_j, b_q) + \mathcal{H}_{Hyp}(\underline{S}_j, \{\underline{I}_k\}) - g\mu_B \sum_j \underline{S}_j \cdot \underline{H}_0 \qquad (4)$$

This Hamiltonian includes the conduction electrons, the local spins coupled to electrons via an exchange / Kondo term, plus the RKKY term, and also a coupling to phonons and nuclear spins. There is a UV cut-off implicit here - the interaction K_{ij} includes electron-hole pair terms above the UV cut-off, and the conduction electron k exchange terms only include electronic excitations below this cut-off. We note that first, (4) is a real simplification of the more realistic models we have seen in part A, and second, that (4) can be further mapped to a network of coupled two-level systems, with Hamiltonian:

$$\left.\begin{aligned} \mathcal{H}_{eff} &= \sum_j (\Delta_0 \hat{\tau}_j^x + \epsilon_j \hat{\tau}_j^z) + \sum_{ij} \bar{K}_{ij}^{\alpha\beta} \tau_i^\alpha \tau_j^\beta + \mathcal{H}_{osc} + \mathcal{H}_{sB} \\ \mathcal{H}_{osc} &= \sum_j \sum_q c_q^j x_q \tau_j^z + \tfrac{1}{2} \sum_q \left(\frac{p_q^2}{m_q} + m_q \omega_q^2 x_q^2 \right) \\ \mathcal{H}_{sB} &= \sum_j \sum_k (\underline{h}_k + \tau_j^z \underline{\omega}_k^j) \cdot \underline{\hat{\sigma}}_k + \sum_{kk'} V_{kk'}^{\alpha\beta} \sigma_k^\alpha \sigma_{k'}^\beta \end{aligned}\right\} \qquad (5)$$

in which the bosonic oscillators represent both the phonons and the electrons.

In these various experimental systems it has been possible to arrange a large variety of anisotropy fields. For example, one has

$$\left.\begin{array}{ll} Zn:Mn & \text{Ising (easy axis)} \\ Cd:Mn & XY \text{ (easy plane)} \\ Mg:Mn & \text{Heisenberg (no anisotropy).} \end{array}\right\} \quad (6)$$

In addition it can be shown that under many circumstances, the effect of the Dzyaloshinski-Moriya (DM) interactions is to mimic an anisotropy term

$$\mathcal{H}_K(S_j) \sim -\left(\underline{d}_j \cdot \underline{S}_j + (\underline{D}_j \cdot S_j)^2\right) \qquad (DM \text{ interaction}) \qquad (7)$$

with the first term breaking T-reversal symmetry.

This discussion of metallic glasses hardly touches the huge variety of possible systems that are available. Other materials upon which many experiments have been done include RE ions in metallic RE hosts, and both TM and RE ions in "semi-metals" (these have only very small "pocket" Fermi surfaces, and a very low concentration of conduction electrons - a well-known example is the semi-metallic

$$(Ti_{1-x}V_x)_2O_3 \qquad (\text{Ising semi-metal}) \qquad (8)$$

in which the spin-½ V ion is providing the spins.

Spins in Insulators: Here we have a huge choice of systems, since the spin ions can be embedded not just into simple insulating hosts, but also into more complicated compounds. There are literally thousands of such systems that have been studied in this context. We can divide these into several groups, as follows:

- Exchange-Dominated Systems: In relatively dense spin systems, the inter-spin interactions will be dominated by exchange or super-exchange couplings. This in itself will not lead to an spin glass phases unless there is some kind of competition between different interactions - we need some sort of frustration. This quite often happens - examples that have been studied in depth are, eg.,

  - The $Eu_xSr_{1-x}M$ systems, in which the species M can be varied a lot; examples are
    - $Eu_xSr_{1-x}S$: Here the nearest-neighbor $|J_{nn}| = 0.22K$, but the next-nearest neighbor $J_{nnn} = -0.1K$.
    - $Eu_xSr_{1-x}Te$: Here $|J_{nn}| < |J_{nnn}|$, so the system orders AFM when $x \sim O(1)$.
    - $Eu_xSr_{1-x}As_3$: Here crystal fields cause an orientational transition as well.

  Note that in $Eu_xSr_{1-x}S$, there are also dipolar interactions which are important when $x \ll 1$ (since these interactions are long-range).

  - The XY-anisotropy systems $\left.\begin{array}{ll} Y:Dy & Sc:Dy \\ Y:Tb & Sc:Tb \end{array}\right\}$ (9)

  in which large RE moments couple to each other by a mixture of superexchange & dipolar interactions.

  - Ising systems like Fe_2TiO_3. (with Fe & Ti randomly distributed).

- Dipolar-Dominated Systems : At lower concentrations dipole interactions will dominate in insulating spin systems. An spatially ordered set of dipoles will order magnetically at low T, but any spatial disorder is expected to give a glassy system. Thus all of the systems which are dominated by exchange interactions when $x \sim O(1)$ will be dominated by dipolar interactions when $x \ll 1$, making for a large number of candidates.

In recent years some interesting new systems have been studied very intensely. These include the class of systems like

$$Li R_x Y_{1-x} F_4 \quad ; \quad Ca R_x W_{1-x} O_4 \qquad (10)$$

in which R represents a large-spin Rare earth ions like Ho ($J=8$), Tb, etc. The most famous of these is the $LiHo_x Y_{1-x} F_4$ system, whose interesting phase diagram will be discussed below. In these systems the volume of the RE ion is very similar to that of the spinless ion it substitutes, and so there is little lattice distortion. Typically the anisotropy is strongly uniaxial in these systems. Experiments on the $LiHo_x Y_{1-x} F_4$ system are done routinely in the range $10^{-4} < x < 1$.; Even when $x = 1$, the interactions are dipolar-dominated.

Another very interesting class of spins which interact primarily via dipolar interactions is the large class of "single molecule magnets", which can be put into ordered lattice (so that they eventually should order magnetically) or in more disordered structures. Well-studied examples include the molecules

Mn-12	Fe-10	} (11)
Fe-8	Mn-84	
V-15	Ni-12	
Mn-4	Fe-18	

and there are many more. In some cases (e.g., Mn-4), once can also add non-negligible superexchange interactions as well.

The advantage of both the RE and SMM systems is that they typically have large spins, making the dipolar interactions stronger.

The effective Hamiltonian for these spins in insulators can also be reduced to the form in (5), where now the oscillators represent only phonons. There may also be non-trivial transverse coupling to phonons, described by a coupling

$$\mathcal{H}_\perp^{int} = \sum_q [C_q^+ \hat{c}_+ + H.c.] x_q \qquad (12)$$

and in many of these systems, the hyperfine couplings $\{w_k\}$ are very strong.

Amorphous Spin Glasses : In amorphous systems practically all reference to any regular crystalline or spatially-ordered structure has been lost, even at the microscopic scale. Many of these systems also have spins. Some well-studied examples include:

$Al_{1-x} Gd_x$	$Fe_x Ni_{1-x}$	} (13)
$La_{1-x} Gd_x$	$Tb_x Fe_{1-x}$	

which show spin glass physics. The first 2 above have RE ions in a non-magnetic insulating

amorphous medium. The latter 2 mix up 2 spin species in a random way. Another widely studied group is the "Aluminosilicates", like

$$\left.\begin{array}{l} MnO \cdot Al_2O_3 \cdot SiO_2 \\ CoO \cdot Al_2O_3 \cdot SiO_2 \end{array}\right\} \qquad (14)$$

with randomly positioned and oriented TM spins, and amorphous metallic glasses such as

$$(Fe_x Ni_{1-x})_{75} P_{16} B_6 Al_3 \qquad (15)$$

Clearly with systems like these, almost limitless possibilities open for study!

(ii) <u>The Spin Glass "Transition" at T_G</u> : In most spin glass systems something important clearly happens at a temperature T_G which depends on the concentration of spins in the systems; see the 2 examples in the figure below, which focusses on the magnetic susceptibility:

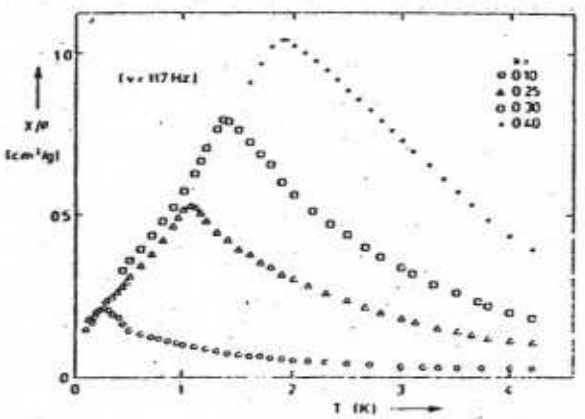

Real part χ' of the complex susceptibility $\chi(\omega)$ as a function of temperature for $Eu_xSr_{1-x}S$, at $\omega = 117$ Hz and various Eu concentrations as indicated in the figure.

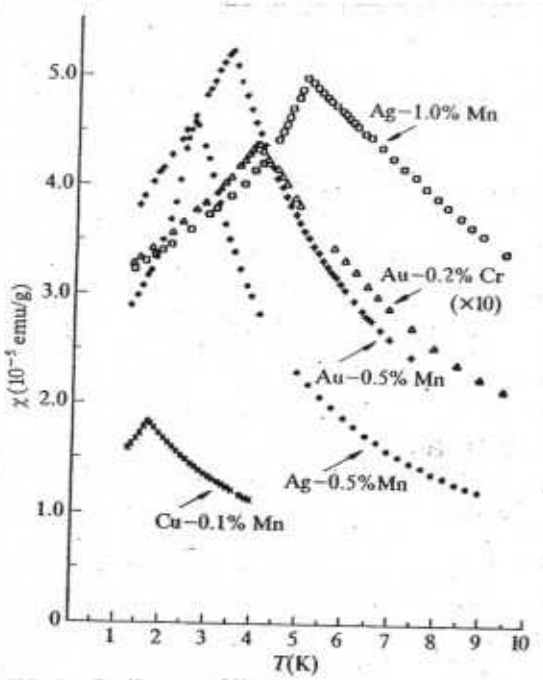

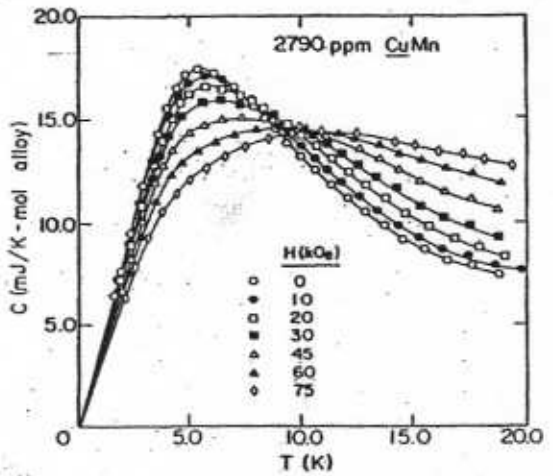

Magnetic contribution of the specific heat of CuMn spin glasses with 2.79 at. % Mn plotted vs temperature in various magnetic fields.

However we notice that this is not a sharp thermodynamic phase transition as usually understood. Consider, eg., the classic spin glass $Cu_{1-x}Mn_x$, which has a pronounced peak in the susceptibility around T_G. If we now look at the specific heat $C_p(T)$ for the same system (see left) we notice almost nothing unusual – there is virtually no trace of any transition, only a very broad "hump", which is not even centred exactly on T_G. As we will see below, part of this has to do with the timescales

involved, but it is worth noting that thermodynamic relations such as the Maxwell relation

$$\left.\frac{\partial^2 M}{\partial T^2}\right|_H = \frac{1}{T}\left.\frac{\partial C_M}{\partial H}\right|_T \qquad (16)$$

are still accurately obeyed around T_G in these systems.

A closer look at the transition in the susceptibility data reveals very interesting features; we look again at the Cu:Mn system.

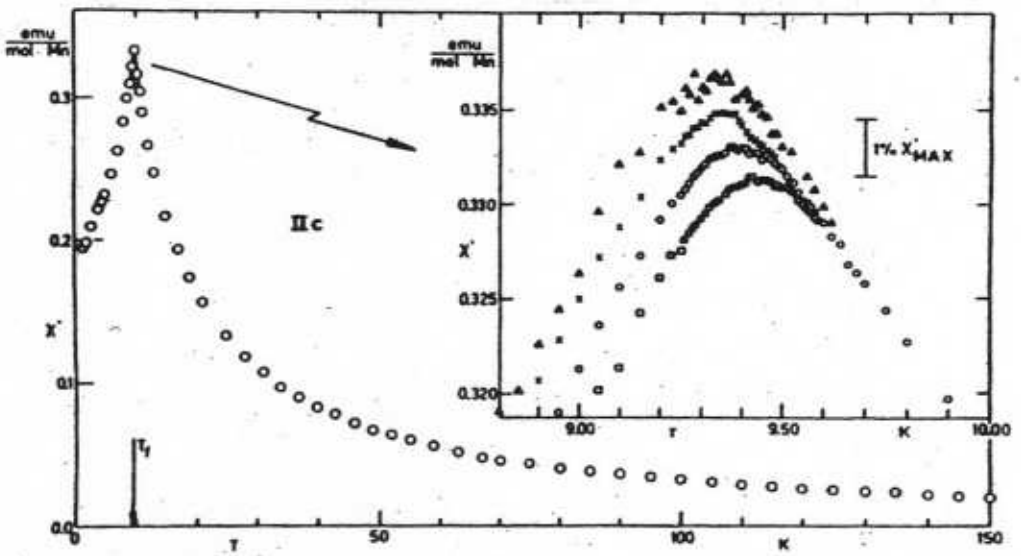

Real part χ' of the complex susceptibility $\chi(\omega)$ as a function of temperature for sample IIc (*Cu*Mn with 0.94 at. % Mn, powder). Inset reveals frequency dependence and rounding of the cusp by use of strongly expanded coordinate scales. Measuring frequencies: □, 1.33 kHz; ○, 234 Hz; ×, 104 Hz; △, 2.6 Hz.

The key point here is that the position of the "cusp" at T_G depends on the frequency at which the measurements are done - this is the first sign that we are dealing with a whole hierarchy of time scales. At first glance the data seem to indicate that this variation of T_G goes on over an unlimited range of frequencies; for example in Cu:Mn, one finds the relation

$$\frac{d \ln T_G(\omega)}{d \ln \omega} \approx 0.0022 \quad (Cu:Mn) \qquad (17)$$

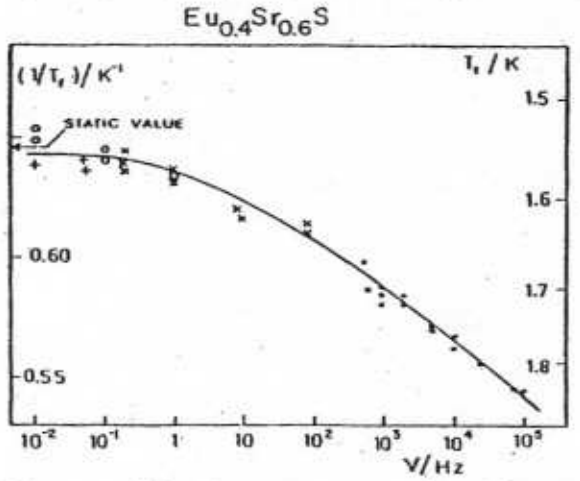

Inverse freezing temperature $T_f^{-1}(\omega)$ of $Eu_{0.4}Sr_{0.6}S$ plotted vs logarithm of measurement frequency. Different symbols indicate different measurement techniques.

is obeyed over a wide range of ω and of Mn concentrations (at least between $0.0094 < x < 0.064$ Mn concentration). This is quite remarkable - if extrapolated, it indicates that $T_G(\omega) \to 0$ as $\omega \to 0$, with no static transition at all. However at least in some systems one sees evidence for a "flattening off" of the ω-dependence at low ω. This is hard to look at experimentally since such low measuring frequencies are involved (see left).

A quantitative description of the results starts

from the Kramers-Kronig (ie., Hilbert transform) relations between $\chi'(\omega)$ and $\chi''(\omega)$. These are often written as follows for spin glasses:

$$\left.\begin{aligned} \chi'(\omega) &= \chi_S + \int_{\tau_{min}}^{\tau_{max}} d\ln\tau \; \frac{g(\tau)}{1+\omega^2\tau^2}\left[\chi_T(\tau) - \chi_S(\tau)\right] \\ \chi''(\omega) &= \int_{\tau_{min}}^{\tau_{max}} d\ln\tau \; \omega\tau \; \frac{g(\tau)}{1+\omega^2\tau^2}\left[\chi_T(\tau) - \chi_S(\tau)\right] \end{aligned}\right\} \quad (18)$$

where $\chi_S(T)$ and $\chi_T(T)$ are time-dependent generalizations of the iso-entropic (ie, adiabatic) & isothermal susceptibilities, and $g(T)$ is a weighting probability over a set of relaxation times τ. This distribution is extremely broad, and can be probed by a wide variety of experimental techniques for a given system, as we see in the figure at left. Over a wide frequency range one can approximately fit the data to forms like

$$\left.\begin{aligned} \chi'(\omega) &= \chi_0 + A\ln\left(\frac{1}{|\omega|}\right) \\ \chi''(\omega) &= \frac{\pi}{2} A \; \text{sign}\;\omega \end{aligned}\right\} \quad (19)$$

but these do not have a fundamental basis. The experimental techniques include global probes like neutron scattering or

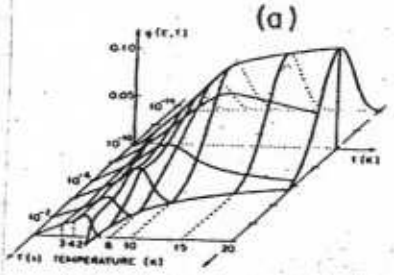

The distribution of relaxation times $g(\tau,T)$ as a function of time (10^0–10^{-14} s) and of temperature (0–20 K). The solid lines show several isotemporal and isothermal lines.

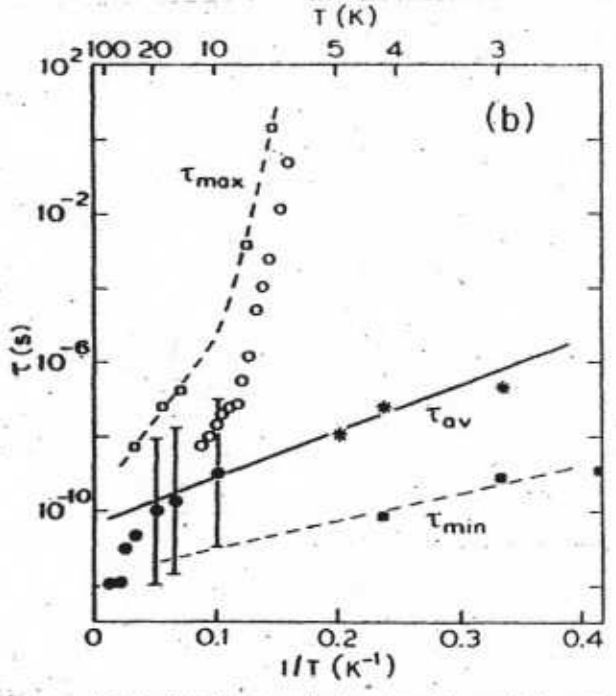

(a) The distribution of relaxation times $g(\tau)$ as a function of time (10^0—10^{-14} sec) and of temperature (0—20 K). The solid curves shows several isotemporal and isothermal lines. All data were obtained from an analysis of χ', χ'' for $(CoO)_{0.4}(Al_2O_3)_{0.1}(SiO_2)_{0.5}$ in the frequency range from 0.64 Hz to 30 MHz. (b) Relaxation times as obtained from χ'' measurements, plotted vs inverse temperature: □, maximum relaxation time; *, average relaxation time; ■, minimum relaxation time. Open circles are deduced from the frequency dependence of $T_f(\omega)$ [where $\chi'(\omega)$ has its peak] and solid circles are the μSR measurements

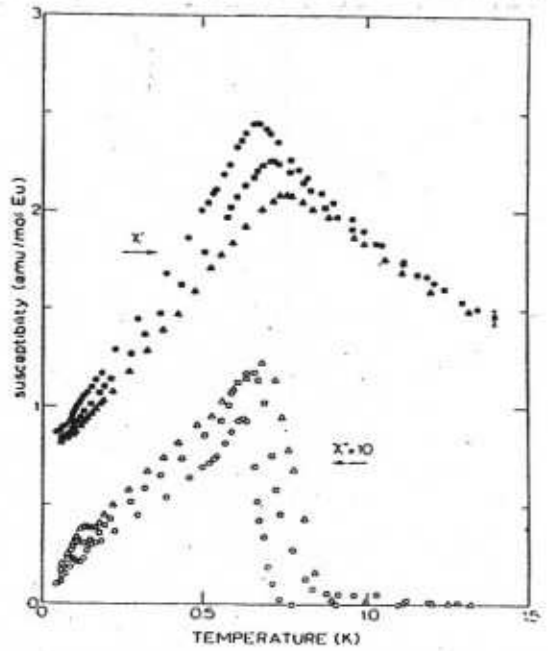

Temperature dependence of the dispersion χ' (solid symbols) and absorption χ'' (open symbols) for $Eu_{0.2}Sr_{0.8}S$ at an applied field $H \approx 0.1$ Oe. Frequencies: ●, ○, $\omega = 10.9$ Hz; ■, □, 261 Hz; ▲, △, 1969 Hz.

neutron spin echoes, or local probes like Mossbauer spectroscopy, ESR & μSR, out of course susceptibility and relaxation measurements. One result that does seem to have remarkably wide applicability is the "Vogel-Fulcher" fit, according to which timescales like τ_{max} in (18) obey:

$$\tau_{max} \sim \tau_0 e^{E_a/k(T-T_0)} \qquad \text{(VOGEL-FULCHER)} \qquad (20)$$

where E_a is an "activation" energy, and T_0 some characteristic temperature - this implies a fit for $T_G(\omega)$ of form

$$T_G(\omega) - T_0 \sim \frac{E_a}{\ln(\omega\tau_0)} \qquad (21)$$

which often fits reasonably well to experiments.

General theoretical considerations (to be discussed below) indicate that one should really be looking for signs of a transition in the "non-linear susceptibility", defined as follows:

$$M/H = \chi(T) - H^2\chi_3(T) + O(H^4) \qquad (22)$$

and there should be some sort of sharp cusp in the non-linear coefficient $\chi_3(T)$ around the glass transition.

BELOW: PLOT OF THE NON-LINEAR $\chi_3(T,H)$ IN $LiHo_xY_{1-x}F_4$ FOR $x = 0.167$, $T = 0.098$ K, AS A FUNCTION OF THE TRANSVERSE FIELD (WHICH CONTROLS THE TUNNELING SPLITTING).

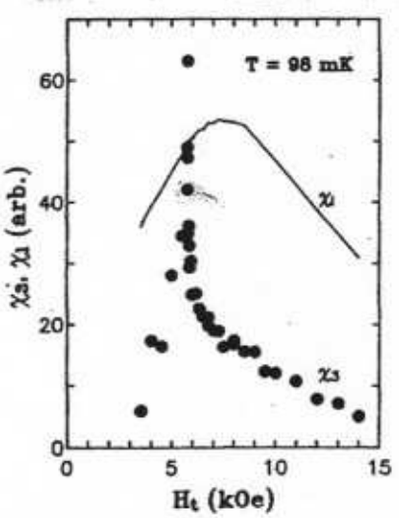

Divergence of the non-linear susceptibility χ_3 at the classical spin-glass transition. The linear susceptibility χ_1 is rounded at the 1.5 Hz measuring frequency.

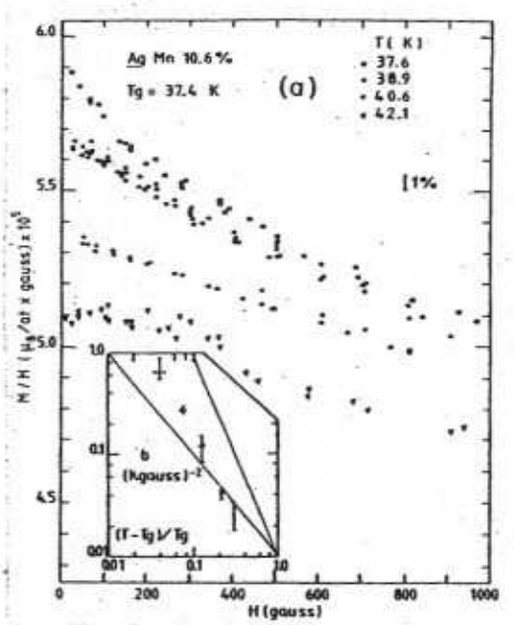

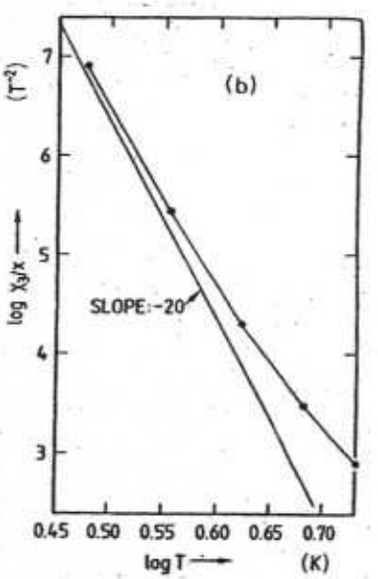

ABOVE (a) PLOTS OF THE NON-LINEAR χ_3 FOR $Ag_{1-x}Mn_x$, WITH $x = 0.106$. HERE WE HAVE M/H PLOTTED AGAINST H. THE INSET SHOWS $\chi_3(T)$ AGAINST $T_G/(T-T_G)$ [THE STRAIGHT LINES SHOW $T_G/(T-T_G) \propto [T_G/(T-T_G)]^2$].

(b) PLOT OF $\chi_3(T)$ AGAINST $\ln T$ FOR $Eu_xSr_{1-x}S$, WITH $x = 0.48$. THE STRAIGHT LINE PLOTS $\chi_3 \sim T^{-20}$.

(iii) Remanence, Aging, & Hysteresis

: Let us now focus on the dynamics, which in many ways are the most fundamental property of glassy systems. Let's concentrate here on the sort of observations that can be made, beginning with plots for the decay of magnetization in samples that had previously been polarized. The plots on the left are for a standard metallic glass, whereas the one below refers to the "quantum relaxation" of a set of Mn-12 molecules.

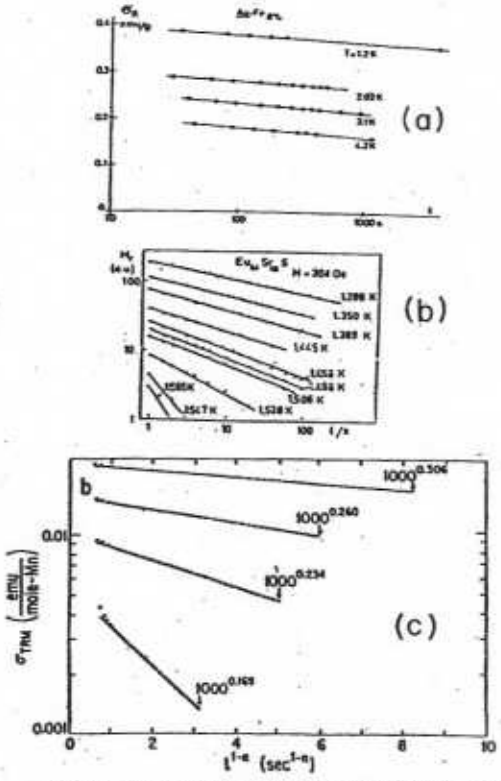

(a) Isothermal remanent magnetization of *Au*Fe with 8 at. % Fe, plotted vs the logarithm of time. From Holtzberg *et al.* (1977). (b) Log-log plot of the saturated thermo-remanent magnetization σ_{TRM} vs time for $Eu_{0.4}Sr_{0.6}S$ at various temperatures close to $T_f = 1.55$ K. From Ferré *et al.* (1981). (c) Logarithm of the saturation value of the thermo-remanent magnetization of *Ag*Mn with 2.6 at. % Mn plotted vs t^{1-n} at four temperatures, for a time range of about $1-10^3$ sec

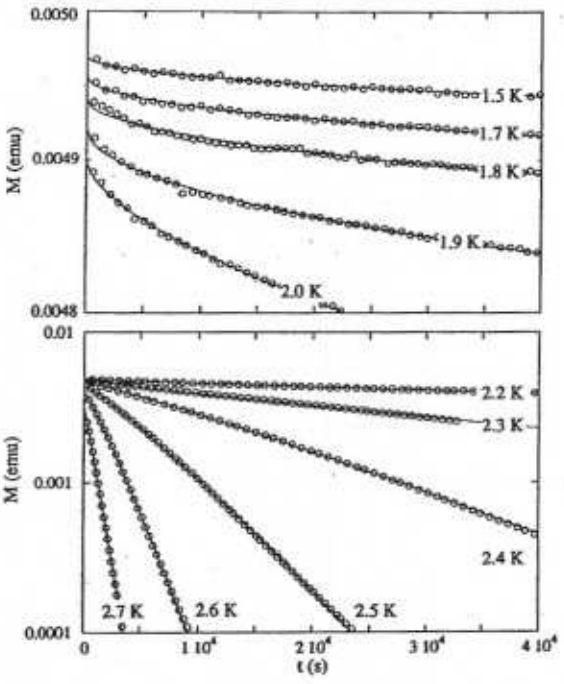

Time decay of the magnetization, measured in the remanent state at different temperatures. Note that the magnetization decay, plotted in logarithmic scale, is in general non-exponential. Lines show the fit of the data points to a stretched exponential function.

ABOVE: TIME RELAXATION OF CRYSTAL OF Mn-12 MOLECULES, AFTER FIELD-COOLING (FC).

BELOW LEFT: UNIVERSAL SCALING PLOT FOR Mn-12 RELAXATION

BELOW RIGHT: FIT OF THE LOWER T Mn-12 DATA TO A $\sqrt{t}$ FORM.

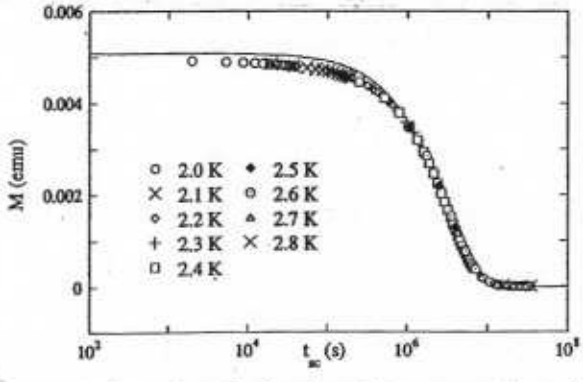

Scaling plot of relaxation data, measured at nine different temperatures, between 2.0 and 2.8 K. For clarity, only about 5% of the data points have been plotted. The continuous line shows the fit of the master curve to an exponential function.

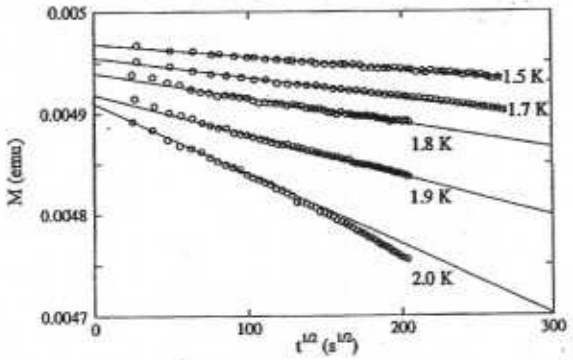

Time decay of the remanent magnetization measured at low temperature, plotted as a function of the square root of the time. Lines show linear fits.

One of the most interesting results is shown at the bottom left of the last page - it shows that one can put all of the decays on a single scaling curve. The short-time behaviour on this scaling curve falls on a simple form, in which one has

$$|M(t) - M(t=0)| \sim A\left(t/\tau_0\right)^{\frac{1}{2}} \qquad (\tau_0 < t < \tau_D) \tag{23}$$

We can see this in other similar systems - below we see plots for the Fe-8 molecular magnet. The real time plots gave no real clue that there is a universal time dependence, and in fact the universal plots were not made until after the theoretical predictions.

BELOW: RELAXATION OF A FIELD-COOLED (FC) CRYSTAL OF Fe-8 MOLECULES, AFTER RELEASING THE FIELD. INTERACTIONS BETWEEN Fe-8 ARE DIPOLE.

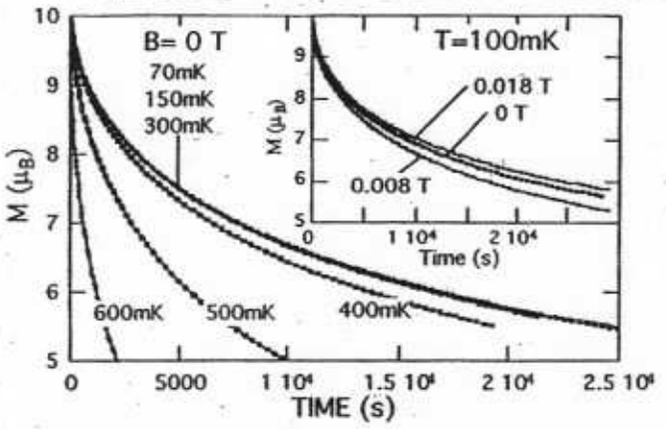

Relaxation of the magnetization measured at $B = 0$ after first saturating in a field of 3.5 T. For $T < 400$ mK curves superimpose showing that the relaxation is independent of T. Inset shows subtle field dependence near resonance.

BELOW: PLOT OF RELAXATION OF Fe-8 AGAINST $\sqrt{t}$. AT 40 mK ALL THE RELAXATION IS QUANTUM, MEDIATED BY NUCLEAR SPINS, & DIPOLAR COUPLINGS

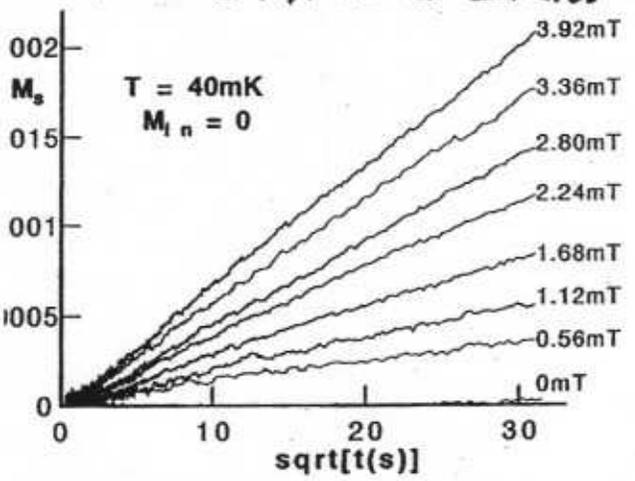

Typical square root of time relaxation curves for an crystal measured at 40 mK. For each curve, the sample first thermally annealed at $H = 0$ (ZFC), then a small field applied and the relaxation of magnetization was measured ig 1000 s. The slope of the lines gives Γ_{sqrt} when plotted ist the square root of t as shown.

What the Mn-12 & Fe-8 systems have in common is that (a) they were both done at low T, and (b) the molecules both interact via dipolar interactions. The results on the Au:Fe system were done at higher T, and while they are fit by a logarithmic relaxation form

$$|M(t) - M(0)| \sim A \ln t \tag{24}$$

it is important that they can be fit as well, or even better, by some power law relaxation, or even by a stretched exponential, ie.

$$|M(t) - M(0)| \sim A\left(1 - e^{-Ct^{\alpha}}\right) \tag{25}$$

Unlike the square root form in the quantum regime for dipole systems, the forms in (24) & (25) do not have a real theoretical justification.

It will be noticed that in these experiments the system is relaxing after some sudden change in the external conditions (in this case, the external field). It is perhaps not surprising that these systems also exhibit "aging" and "memory" effects in the relaxation. Such phenomena are very common, not just in spin

glasses but many other systems, as we'll see later. Rather than dwell on spins here, let's look at some hysteresis curves which give another perspective on the same physics. The key point in the first set of data on $Cu_{0.75}Mn_{0.25}$ is the difference between the ZFC (zero-field cooled) and FC (field-cooled) data. The ZFC protocol requires cooling a high-T annealed sample to low-T, and then cycling the field. The FC protocol slowly cools in a strong field, so the system is polarized at the beginning of the low-T cycle. This data is shown below left, both hysteresis & relaxation data.

Even more striking is the data at right below - as we will see, this maps the distribution of internal fields in a set of Fe-8 molecules with time. The top curve is FC data, the bottom curve is ZFC. We will see later how to interpret all this data.

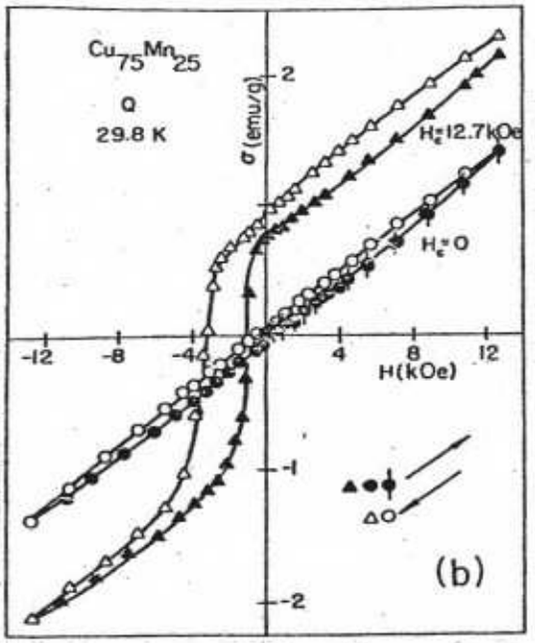

ABOVE: HYSTERESIS FOR $Cu_{0.75}Mn_{0.25}$ UNDER ZFC & FC CONDITIONS.

BELOW: SAME SYSTEM - NOTE HOW SMALL H IS IN THE FC EXPT HERE.

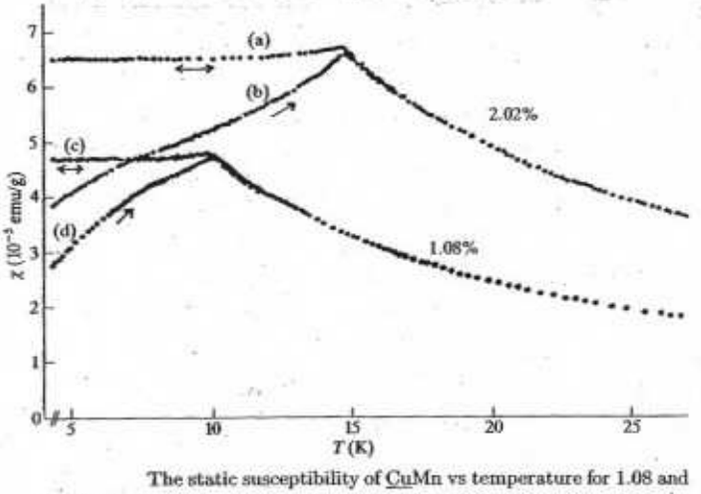

The static susceptibility of CuMn vs temperature for 1.08 and 2.02% Mn. After zero-field cooling ($H < 0.05$ Oe), initial susceptibilities (b) and (d) were taken for increasing temperature in a field of $H = 5.90$ Oe. The susceptibilities (a) and (c) were obtained in the field $H = 5.90$ Oe, which was applied above T_f before cooling the samples

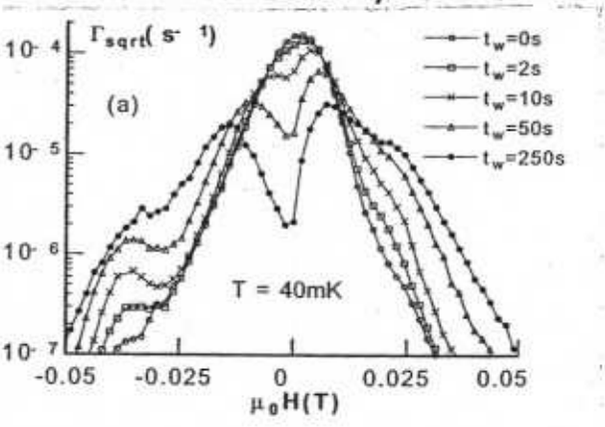

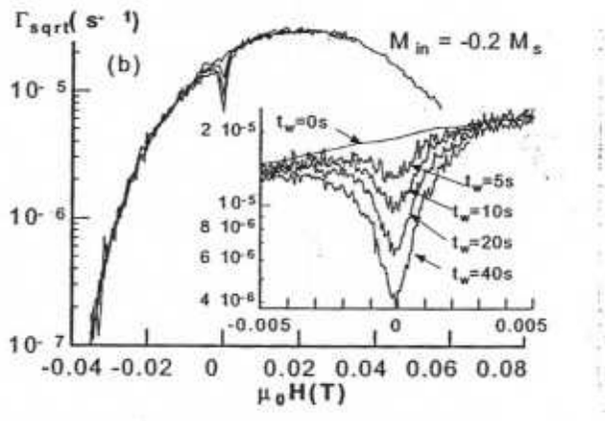

Tunneling distributions: the field dependence of the short-time square-root relaxation rates $\Gamma_{sqrt}(\xi_H)$ are presented on a logarithmic scale showing the depletion of the molecular spin states by quantum tunneling at $H = 0$ for various waiting times. (a) Tunneling distributions for the initial magnetization starting from saturation $M_{in} = -M_z$. For each point, the sample was first saturated in a field of -1.4 T and at a temperature of about 2 K and then rapidly cooled to 40 mK. After applying a "waiting field" of $H_w = 0$, we let the sample relax for a "waiting time" t_w (after $t_w = 2$, 10, 50, and 250 s, the reversed fraction of magnetization is 0.008, 0.030, 0.077, and 0.159 of M_z, respectively). Finally, we applied a small field to measure the short-time relaxation which could be fit accurately to a square-root law yielding Γ_{sqrt}. Because Γ_{sqrt} is proportional to the spins which are still free to tunnel, one obtains the distribution $P(\xi_H, H_w, t_w)$. (b) Tunneling distributions as in (a), but now for each point, the sample was first annealed (FC) to a value $M_{in} = -0.2M_z$. The inset enlarges the low field part around the waiting field H_w. After $t_w = 5$, 10, 20, and 40 s, the reversed fraction of the magnetization is 0.0012, 0.0020, 0.0032, and 0.0049 of M_z, respectively. At the resonance, the depletion develops very rapidly with elapsed time, even though the total magnetization and the internal demagnetization field hardly change during this time. Notice that the parabolic shape of $\Gamma_{sqrt}(\xi_H)$ shows it is accurately Gaussian, with a half-width of 0.030 T. This Gaussian profile is found for $|M_{in}| < |0.5M_z|$ (but with a half-width E_D depending on M_{in}).

(IV) Magnetic Phase Diagram

: We can now properly consider the different kinds of phase diagram that appear in experiments. There are many different possibilities, so here we just look at a couple of them. We begin with the $Eu_xSr_{1-x}S$ system, in which there is competition between FM and AFM interactions. The plot shows the phases as a function of concentration x and temperature - one can also show plots of phases as functions of H and T for a fixed x.

We notice that the spin glass phase only exists over a range of concentrations - when x is too large, the disorder or frustration is not strong enough to overcome the FM interactions and it orders. When x is too small, one might still imagine a spin glass phase at very low T, but we note that this is an insulating system, so the nn. and nnn interactions are short range exchange interactions. In fact the spin glass phase in this system disappears for $x \lesssim 0.11$, which is quite close to the "percolation threshold" of $x = 0.136$ for nnn interactions in an fcc lattice. In principle one might expect very weak spin glass order because of the dipolar interactions in the system, but these interactions are apparently too weak to cause any dipolar ordering (although it would be interesting to see what happens in the very long time limit in this system, when it has had time to relax).

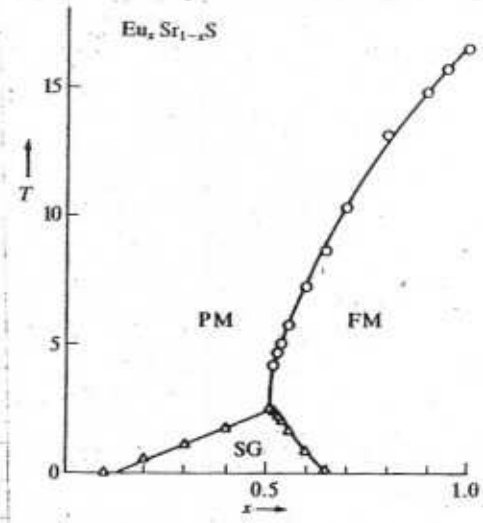

PHASE DIAGRAM OF $Eu_xSr_{1-x}S$

As an example where dipole interactions do cause interesting effects is the by now familiar $LiHo_xY_{1-x}F_4$ system. Here we can neglect any exchange interactions between the Ho ions, even when $x \approx 0(1)$. Because the Ho spins have $J = 8$, the dipolar interactions are strong. Below we see at left the phase diagram for $x = 1$, as a function of $H_\perp$ (applied perpendicular to the easy axis) and at right, we see the phase diagram as a function of x and T for a specific applied transverse field. The transverse field drives tunneling transitions, and at first glance the system looks a perfect example of the transverse field quantum Ising model (the archetypal quantum critical system). However we will see later that things are much more complex than this (and more interesting!).

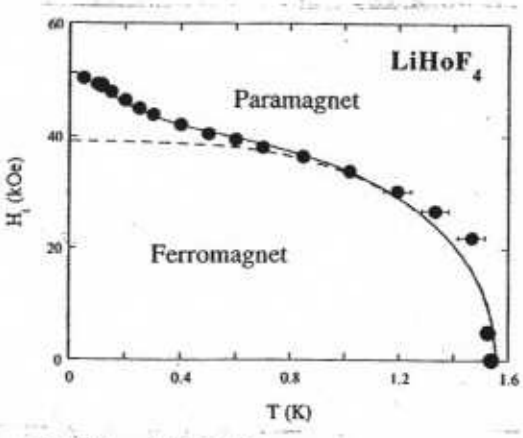

ABOVE: PHASE DIAGRAM FOR PURE $LiHoF_4$. THE UPTURN AT LOW T IS CAUSED BY THE Ho NUCLEI.

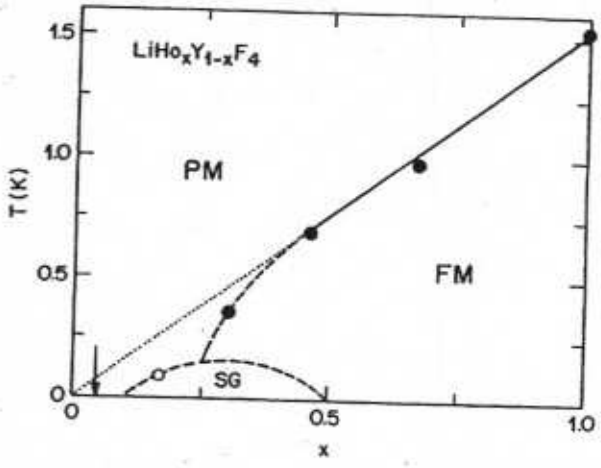

The phase diagram as a function of dipole concentration x for the Ising magnet/glass, $LiHo_xY_{1-x}F_4$. PM = paramagnet, FM = ferromagnet, SG = spin glass. In the dilute limit, the system only freezes for temperature $T = 0$ (arrow).

(b) Other Glasses: Low-Temperature Experiments

Given that the vast majority of condensed matter systems in Nature show some level of glassy behaviour, it is actually important to try & classify the different systems, & the different phenomena that are observed. The following general categories may be distinguished:

Defect Glasses: In these systems, there is short-range or even long-range crystalline order, but there are also defects. These defects may be interstitial foreign species, or simple vacancies in the system. In more complex versions they may be dislocations. Most such systems are electrically insulating, and the main effect of the defects is seen in their mechanical properties, and in thermodynamic properties such as specific heat. All mechanical properties are affected, as is heat transport, sound velocity & damping, etc. One may also look at metals, in which defects at low T significantly affect electronic transport. We assume the defects are dilute here.

Amorphous Glasses: This vast collection of systems includes supercooled liquids, indeed almost any liquid of any complexity which has been cooled at a finite (not infinitesimal) rate. It also includes disordered conductors (the "electron glass") including those undergoing Anderson localisation. The insulating systems range in complexity from simple systems like SiO_2 (this includes window glass), with only one or 2 atomic species, up to hugely complex polymers and organic materials, including materials in living things. Again, all mechanical properties are affected, and all transport properties.

We may also distinguish 2 temperature regimes of interest, viz:

(a) High-T regime ($T \sim T_g$): Much occurs around the glass temperature; again, this temperature is ill-defined, and depends on the previous history of the system, including cooling rates, etc. There is no real phase transition, only a rapid change in dynamics with T.

(b) Low-T regime ($T \lesssim 10\text{-}30\,K$): At low T there is an interesting crossover to a "quantum glass" regime. Quite remarkably, this regime has universal properties, which constitute a major mystery. The quantum collective behaviour is fascinating and suggests interesting connections to both quantum spin glasses and spin liquids. The role of topology & topological charge is of considerable interest.

In what follows we will focus mostly on the low-T regime, with connections made to the higher-T behaviour. The low-T regime is conventionally described by a model of interacting 2-level systems, and this immediately makes it relevant to the whole quantum computation enterprise. We shall see that the role of the quantum environment is crucial here.

Before beginning, the following cautionary remarks should be made:

- You will notice many similarities between glasses & spin glasses. It is important to note the differences as well. Later on I will try to summarize both, & to understand them.

- There is no generally accepted theory of glasses at either high or low T. The

low T systems are better understood, however, and we can make considerable quantitative progress with these; but there are still deep problems to be solved.

There is no question that these problems are both practically important and quite fundamental. The quote from Anderson, at right, comes from the time period of his near maximum activity in high-T_c! The low-T behaviour forces us to reflect on some very deep questions, as we will see see when we come to them – many of the experimental results are very surprising, and demand radical ideas as well as new theoretical methods.

"The deepest and most interesting unsolved problem in solid state theory is probably the theory of the nature of glass and the glass transition. This could be the next breakthrough in the coming decade. The solution of the problem of spin glass in the late 1970s had broad implications in unexpected fields like neural networks, computer algorithms, evolution, and computational complexity. The solution of the more important and puzzling glass problem may also have a substantial intellectual spin-off. Whether it will help make better glass is questionable."—P. W. Anderson [*Science* **1995**, *267*, 1615]

We will begin with a brief description of some of the key systems, and then go on to discuss their main experimental properties.

(1) **Some Key Experimental Systems** : We begin with the simplest systems here, looking at some representative examples, and then go on to some of the more complicated ones. It is convenient to divide the discussion between weak (defect) and strong (amorphous) disorder, or between insulating and conducting systems.

Tunneling Defects (DILUTE) : In even very good insulating crystals there will still be substitutional impurities, or interstitial species (which may or may not be impurities), and vacancies. Some of these systems have been studied in great detail.

Perhaps the best studied of these systems are the alkali halide systems with various substitutional impurities. Examples are

$NaF:OH^-$ $NaF:OD^-$ $NaCl:OH^-$ $NaCl:OD^-$ $KCl:OH$ $KCl:OD^{-1}$		<100>	6 minima
$NaBr:F$ $NaBr:Ag$ $RbCl:Ag$		<110>	12 minima
$KCl:Li$	$KCl:CN$	<111>	8 minima

(26)

Typically one adds rather small dopant concentrations, in the range $x = 10^{-6}$-10^{-4}. Typically the dopant finds it has a choice of several different energetically equivalent low energy sites, and it can tunnel between them – the example of KCl:Li, where the Li sites are oriented in a "<111> cage" is shown here.

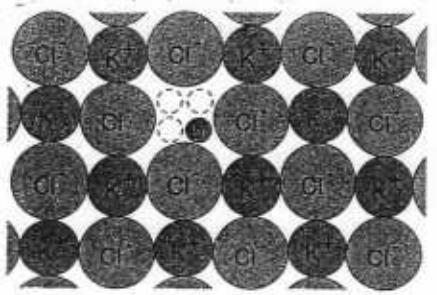

Schematic representation of a (001) plane of KCl after the replacement of a K^+ ion by a Li^+ ion. Eight sites are accessible to the lithium ion, namely four above and four below the plane of the drawing

It is useful to look at the example of KCl:Li in more detail. The tunneling between the 8 states is predominantly along the direct paths between them (there is a potential hill in the middle of the case, with much smaller barriers between sites along the edge paths). We define the set of 8 "quasi-localised" states shown, and we deal with an 8-well problem. Calling these states $|abc\rangle$, with $a,b,c = \pm 1$, we then form the eigenstates

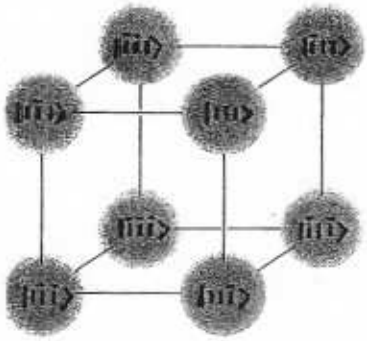

THE EIGHT LOW-ENERGY STATES OF Li IN THE KCl:Li SYSTEM ARE QUASI-LOCALISED AT THE SITES SHOWN - THEY TUNNEL ALONG THE CUBE "EDGES".

$$|\underline{K}\rangle = |K_1,K_2,K_3\rangle = \frac{1}{\sqrt{8}} \sum_{a,b,c} e^{i\pi \underline{K}\cdot\underline{r}} |abc\rangle \qquad (27)$$

where $\underline{r}$ is the displacement of the Li from the cube centre (measured in units of the cube size), and $K_j = \pm 1$. In this problem the states then divide up into irreducible representations of the cubic point group O_h, as follows:

$$\left.\begin{aligned} A_{2u} &: (1,1,1) \\ T_{2g} &: (1,1,-1)\ (1,-1,1)\ (-1,1,1) \\ T_{1u} &: (1,-1,-1)\ (-1,1,-1)\ (-1,-1,1) \\ A_{1g} &: (-1,-1,-1) \end{aligned}\right\} \qquad (28)$$

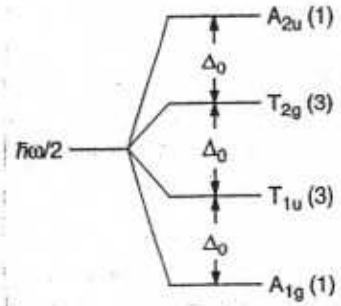

Level scheme of (111) tunneling systems taking only edge tunneling into account. The number of degenerate levels is given in brackets

These levels are organised as shown at left - the calculation of the scheme can of course be done directly, if we ignore the tunneling along "diagonals" of the cube, using the effective Hamiltonian

$$\mathcal{H}_{eff} = \frac{\Delta_0}{2} \sum_{\langle ab\rangle} (C_a^+ C_b + H.c) \qquad (29)$$

where a,b are nearest-neighbour sites. We assume here a tunneling amplitude $\Delta_0/2$ between these sites, which will be given by

$$\Delta_0 \sim \hbar\omega_0 \exp\left[-\tfrac{1}{\hbar}\int_{-d/2}^{d/2} dx \sqrt{2m^* V(x)}\right] \sim \hbar\omega_0 e^{-\frac{d}{2\hbar}(2m^*V_0)^{1/2}} \qquad (30)$$

where d is the cube size (distance between tunneling minima), m^* the effective of the tunneling impurity, and V_0 some average barrier height. The effective mass m will be quite strongly renormalised by coupling to phonons - in reality this is a dissipative tunneling process, described by the spin-boson model with a super-Ohmic coupling to phonons. Note that we can change m^* by using different Li isotopes (^{6}Li or ^{7}Li). This changes Δ_0 by a factor ~ 1.5, in experiments on this system.

One can do the same analysis for the other sets of tunneling paths in (26),

with the results shown in the figure below. It is an interesting exercise to work out the level schemes for these.

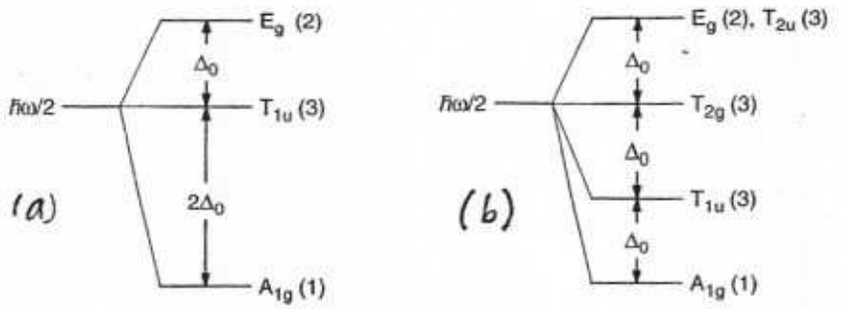

Level schemes of ⟨100⟩ tunneling systems (a) and ⟨110⟩ tunneling systems (b). The degree of degeneracy of the levels is given in brackets

These systems are all examples of "orientational glasses" in which each tunneling impurity behaves effectively as a quantum electric dipole, because in these ionic systems, the impurity is charged. This makes it relatively simple to probe the levels, since in an applied electric field, only certain transitions will be allowed, depending on the direction of the field. Thus, for the KCl:Li system, with 8 equivalent ⟨111⟩ sites, the allowed transitions must satisfy

$$|\underline{k} - \underline{k}'| = 1 \qquad (31)$$

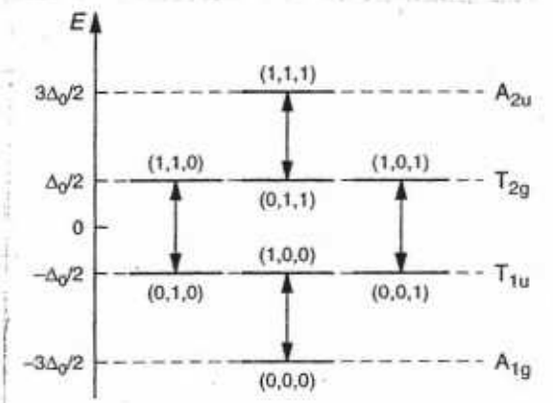

Electric dipole transitions in KCl:Li. *Arrows* mark the allowed transitions for an ac electric field applied in the ⟨100⟩ direction

for transitions between the eigenstates $|k\rangle$ given in (27) and (28). We see how this works out at left.

The great advantage in studying orientational glasses like these is that they do show all the relevant glassy features (as we will see), but they can be understood microscopically - we will be discussing how to do this in the next section.

There are many other orientational glasses produced by substitutional defects - some well-studied examples are

$$\left.\begin{array}{ll} KTaO_3 : Na, Nb, Li, \text{ etc.} & \\ K_{1-x}Li_xTaO_3 & (\text{"KTL"}) \\ KTa_{1-x}Nb_xO_3 & (\text{"KTN"}) \end{array}\right\} \qquad (32)$$

$$\left.\begin{array}{l} \text{neutron-irradiated quartz } (SiO_2) \text{ crystals} \\ \text{quartz } SiO_2 : K, OH, \text{ etc} \end{array}\right\} \qquad (33)$$

All of the above examples refer to insulating hosts. However there are plenty of systems where the host is metallic and/or superconducting. The principal interest of experiments in such systems is that one can vary the coupling to the bosonic bath - in metals one has an Ohmic coupling to the electrons, and in superconductors, the same Ohmic coupling decreases rapidly with temperature T when $T < T_c$.

Experiments have been done on a variety of metallic hosts, notably the well-understood alkali metals Na, K, and Rb, and the Noble metals Cu, Ag, and Au; the substitutional

defects include O, OH, H, and deuterium variants on these, as well as Li, F, etc., in the Noble metals. Typical superconducting hosts include Nb, Al, etc., with the same kinds of dopant. In the real world, any of these systems also has vacancies & dislocations.

An example is useful. The figure shows the Nb:O,H system (one can also use D instead of H). The interesting thing here is that the heavy O is almost immobile, and so adds an extra random potential acting on the H, which are themselves very mobile. This potential is just the strain field acting because the O distorts the Nb lattice - the strain is therefore long-range and creates a random bias on the H or D ions, in addition to the tunneling term. There is again a difference in effective mass for H and D, and one finds

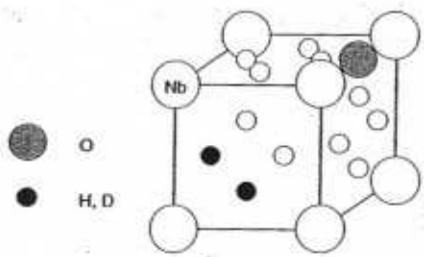

Niobium doped with oxygen and hydrogen.

$$\left.\begin{aligned} \Delta_0^H &= 1.4\,K \\ \Delta_0^D &= 0.18\,K \end{aligned}\right\} \qquad (34)$$

in this system. For H the tunneling distance $d = 1.17\,\text{Å}$ in this system, separating pairs of equivalent sites (2 of these are shown in dark in the Figure above).

Amorphous & "Dense Defect" Systems: The dilute defect systems considered above are very pure crystalline systems with a tiny concentration of vacancies or impurities. At high T the effect of these is rather feeble (except on the optical properties) but at low T, as we see below, they can have large effects.

Most systems in Nature are not nearly so simple. Even a relatively low concentration of defects causes overlap between the fields generated by the defects, just because the fields are long range. We can define a mean interaction strength $\bar{V}(x)$, where x is the concentration of defects; for $1/r^3$ interactions, we have

$$\bar{V}(x) \sim x V_0 \qquad (35)$$

where V_0 is the strength of nearest-neighbour interactions, the crossover between dilute and dense defect systems then occurs when

$$\bar{V}(x)/\Delta_0 \sim O(0.1) \qquad (36)$$

where we use 0.1 instead of 1 because percolation between the "polarisation clouds" of each defect starts at this point.

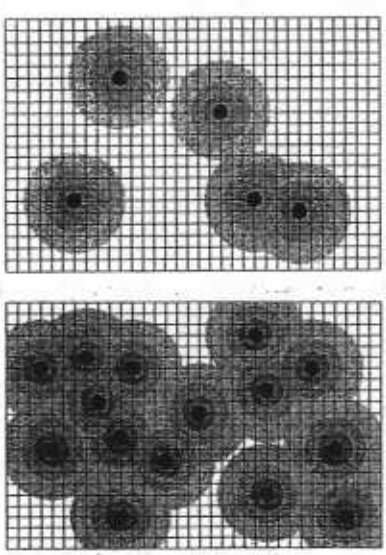

CONTRAST BETWEEN DILUTE DEFECT SYSTEM (TOP: $x \sim 10^{-3}$) AND A DENSER ONE (BELOW: $x \sim 10^{-4}$). THE "POLARISATION CLOUDS" ARE SHADED.

In the next section we discuss how strong these long-range interactions are - we shall see that once x exceeds 10^{-4} in most systems, we are getting into the "dense" regime.

As the defect concentration increases, one eventually loses all trace of a regular lattice structure - we then refer to the system as "amorphous". Experiments have been

done on a vast array of dense defect & amorphous systems, and here I will only list a few of the more common systems.

- Si- & Ge- based Glasses : Many of you may not realise quite how many "glasses" (in the sense of window glass, or optical glass) there really are out there! Amongst the Si-based glasses we have, eg.,

Irradiated / Disordered Quartz (SiO_2) crystals
SiO_2 : K, Na, etc ($x \gg 10^{-4}$)
Suprasil (SiO_2 : OH or OD)
Irradiated / disordered crystobalite (SiO_2) crystals
SiO_x ($x \neq 2$)
vitreous silica (SiO_2)
porous silica (Vycor, aerogel) : porosity 20-90%
spectrasil
Borosilicate glass (BK7)
} (37)

or more complex optical glasses like

Pyrex 7740 (SiO_2 : 80.5%, B_2O_3 : 12.9%, Na_2O : 3.8%, Al_2O_3 : 2.2%)
Corning Pyroceram 9606 (SiO_2 : 58%, MgO : 23%, Al_2O_3 : 12%, TiO_2 : 6%)
Corning 9623 (SiO_2 : 69%, Al_2O_3 : 15%, Li_2O : 9%)
} (38)

and amongst the Ge-based glasses one has

Amorphous GeS_2, GeS_4
" GeS_3
Corning 9754 (GeO_2 : 50%; Al_2O_3 : 25%, CaO : 15%, BaO : 5%, ZnO : 5%)
} (39)

Other glasses based on Si and O include the minerals.

$An_{50}Ab_{50}$ — An = Anorthosite ($CaAl_2Si_2O_8$); Ab = Albite ($NaAlSi_3O_8$)
plagioclase feldspar
} (40)

The variety here is of course huge & almost endless. Then we have

- Other (non-Si, non-Ge) optical glasses

B_2O_3 (amorphous)
B_2O_3 : Na, K, Li_2O, etc.
LASF (mixture of B_2O_3, La_2O_3, ThO_2, and some Ta_2O_3 & Nb_2O_5)
Amorphous B ; amorphous B_9C
Amorphous Se
Amorphous $CdGeAs_2$, or As_2S_3
KNO_3, $CaNO_3$ (amorphous) ; Nitride glasses [eg $[Ca(NO_3)_2]_{30}[KNO_3]_{50}:(H_2O)_x$
$LiCl:(H_2O)_x$
Amorphous MnF_2
$V52[(ZrF_4)_{(x+y)}(BaF_2)_x(ThF)_y]$.
LAPO [ie $(La_2O_3)_x(P_2O_5)_{1-x}$]
} (41)

One can also have experiments on simple organic compounds that form glassy states at low T. One that has been looked at extensively in experiments is

$$\text{glycerol} \quad (C_3H_5(OH)_3) \tag{42}$$

and there are many others.

– Low-T glasses from Polymers : Again, the number of systems here is huge, and it goes without saying that any polymer will become a glass at low T. Some of the systems upon which extensive experiments have been done include

epoxy resin , other natural resins (eg, amber)
Polystyrene
Polycarbonate , Polybutadiene
PMMA (Polymethylmethacrylate) , PEMA (Polyethylene Terephthalate)
PBM (Poly-n-Butyl-methacrylate
Mylar , Teflon
Stycast
PVC (polyvinyl chloride) , Polyvinyl phenolic
Scotch tape , apiezon grease , etc

(43)

and so on - the choice here has been dictated as much by the practical interest of the material as anything else. Many of these materials are commonly used by low-T physicists in their experimental cells.

– Metallic & Superconducting Glasses : Again, like the optical glasses above, these systems can be deliberately disordered, or they can be made amorphous , either by spin melting (pouring the molten metal onto a rapidly spinning cold spindle) or "splat cooling" (self evident !). These systems are usually alloys. Some examples are

$$Zr_{1-x}Pd_x \quad Zr_{1-x}Cu_x \quad Zr_{1-x}Be_x \quad Zr_{1-x}Ni_x \quad Zr_xNb_{1-x}$$
$$Pd_{1-x}Si_x \quad Pd_{1-x}Cu_x \quad Ti_xNb_{1-x} \quad Ti_xV_{1-x} \tag{44}$$
$$Ni_{1-x}P_x \quad Fe_{1-x}P_x \quad Co_{1-x}P_x$$

plus a host of more complicated multi-species ; some of these are

$$\begin{array}{ccc} Pd\,Si\,Cu & Pd\,U\,Si & Pd\,Si\,Ag \\ FeNiCrPB & FePCAlSi & NiPBAl \\ Ti\,Be\,Zr & Mo\,Ru\,P & Al\,Pd\,Mn \end{array} \tag{45}$$

and so on (here the elements are listed in decreasing order of concentration

– Other Popular low-T glassy systems : Apart from alloys, and glasses of the optical variety based on Si, Ge, or similar glasses, one also finds many experiments on insulating compounds which are actually mixtures of simpler compounds. Examples are :

$(NaCl)_x\,(NaCN)_{1-x}$ $\quad$ $(NaCl)_x\,(KCN)_{1-x}$
$(KBr)_x\,(KCN)_{1-x}$ $\quad$ etc.
$(BaF_2)_x\,(LaF_3)_{1-x}$ $\quad$ $(CaF_2)_x\,(LaF_3)_{1-x}$
Na, K - β - Alumina
$(ZrO_2)_{1-x}\,(CaO)_x$ $\quad$ $(ZrO_2)_{1-x}\,(Y_2O_3)_x$
$Rb_{1-x}(NH_4)_x\,H_2PO_4$ $\quad$ $Sr_{1-x}Ba_xNb_2O_6$
$YBaCuO$ $\quad$ L $\qquad$ (46)

The first few of the above materials are just mixtures of the "alkali halide" systems we have already seen. The β-alumina system has spinel (Al_2O_3) sheets separating 2-d layers, which are non-stoichiometric & disordered. The last 2 materials are well-known as high-T_c superconductors.

Finally many experiments have been done on amorphous films of C, Ge, Si, and C, prepared by sputtering or molecular beam techniques.

We see that these systems upon which experiments are done are often studied just because they are "there", lying around the lab for some other reason, or because they are by-products of some other activity (often technologically useful).

(ii) Experiments on Dilute Tunneling Defects : In the dilute limit, we can think of our system as a system of independent TLS, coupled to a phonon bath - the interactions between the TLS mediated either by phonons or photons (the electric dipole interaction) is going to be ignored to lowest approximation.

Experiments on the dilute systems bear these conclusions out in a rather spectacular way. Note first that we are dealing with a system which can be described approximately by the Hamiltonian

$$\mathcal{H}_{eff} \sim \sum_j \left(\Delta_0 \tau_j^x + \epsilon_j \tau_j^z\right) + \mathcal{H}_\phi + \mathcal{H}_E \qquad (47)$$

where the tunneling systems are assumed to all have the same Δ_0, but where the biases ϵ_j on each one may be different. The 2nd & 3rd terms are interactions with the phonons and electric fields, which we write as

$$\mathcal{H}_\phi = \sum_q \hbar\omega_q \left(b_q^\dagger b_q + \tfrac{1}{2}\right) + \sum_j \hat{\tau}_j^z \gamma_j^{\alpha\beta} \varepsilon_{\alpha\beta}(\underline{r}_j) \qquad (48)$$

$$\mathcal{H}_E = \sum_{q\lambda} \hbar c|\underline{q}| \left(a_{q\lambda}^\dagger a_{q\lambda} + \tfrac{1}{2}\right) + \sum_j \hat{\tau}_j^z \underline{p}_j \cdot \underline{E}(\underline{r}_j) \qquad (49)$$

The first interaction is between the local strain field $\varepsilon_{\alpha\beta}(\underline{r}_j)$ and the TLS; this strain field changes the bias ϵ_j by a small amount, ie $\delta\epsilon_j = \gamma_{\alpha\beta}^j \varepsilon^{\alpha\beta}(\underline{r}_j)$. where $\gamma_j^{\alpha\beta}$ is the "deformation potential" tensor (more on this later).

The 2nd interaction is with the local electrical field $\underline{E}(\underline{r}_j)$, interacting with the electric dipole moment $\underline{p}_j$ of the TLS. Thus in both of these effective couplings we ignore any effect of the fields on the tunneling splitting itself - this is a good approximation in

many cases.

Consider now what kinds of experiments can examine the TLS. Apart from thermodynamic mmts like specific heat, the most obvious thing to do is look at how the TLS affect the propagation of phonons (in thermal conductivity, or sound propagation) and photons (in dielectric measurements). We look at these in turn:

Specific Heat Mmts: Naively one might suppose that a few parts per million of TLS in a crystal would have a very small effect on the heat capacity $C_V(T)$. This however is not true. Elementary thermodynamics tells us that we expect

$$C_V(T) = C_V^{TLS}(T) + C_V^{\phi}(T) \tag{50}$$

where the phonon specific heat is

$$\left.\begin{aligned} C_V^{\phi}(T) &= \frac{12\pi^4}{5}\frac{N}{V}k_B\left(\frac{T}{\Theta_D}\right)^3 \\ &\frac{12\pi^4}{5}\;\frac{k_B^4}{(2\pi\hbar)^3 C_s^3}\;T^3 \end{aligned}\right\} \tag{51}$$

and the TLS specific heat is

$$\left.\begin{aligned} C_V^{TLS}(T) &= \tfrac{1}{2}\sum_j k_B\left(\frac{E_j}{kT}\right)^2 \operatorname{sech}^2\left(\frac{E_j}{2kT}\right) \\ &\xrightarrow[\epsilon_j = 0]{} \tfrac{1}{2} n_I k_B \left(\frac{\Delta_0}{kT}\right)^2 \operatorname{sech}^2\left(\frac{\Delta_0}{2kT}\right) \end{aligned}\right\} \tag{52}$$

In these equations N/V is the number of host particles per unit volume, and n_I the number of TLS per unit volume (so that $n_I V/N = x$). These specific heats are given for unit volume of the system.

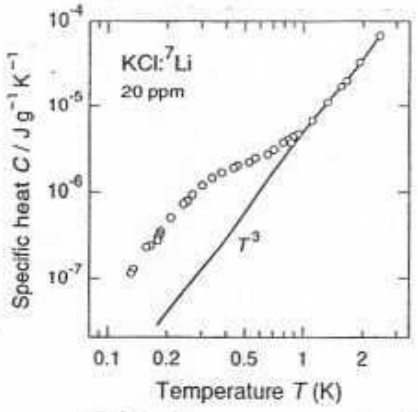

LEFT: Specific heat of a lithium-doped KCl crystal versus temperature. The *full line* indicates the T^3 contribution of the host lattice

The specific heat in any of these systems shows a a very clear anomaly to low T, as we see at left for a concentration $x = 2\times10^{-5}$. This anomaly is known as the "Schottky" anomaly, and is very easily explained using (52). The key is to note how small is the phonon specific heat at low T, and how sharply peaked the TLS concentration is around the energy Δ_0. If we look at the asymptotic behaviour of (52), we get the characteristic behaviour of the "wings" of the Schottky anomaly:

$$\left.\begin{aligned} C_V^{TLS} &\sim \tfrac{1}{2} n_I k_B \left(\frac{\Delta_0}{kT}\right)^2 e^{-\Delta_0/kT} \qquad (kT \ll \Delta_0) \\ &\sim \tfrac{1}{2} n_I k_B \left(\frac{\Delta_0}{kT}\right)^2 \qquad (kT \gg \Delta_0) \end{aligned}\right\} \tag{53}$$

In the experiments it is convenient to subtract off the Debye contribution C_V^{ϕ}

from the data - this is not entirely easy, but can be done quite accurately below 1-2K. The results show a remarkable agreement with theory, with a generalization of (52) to account for the multiple levels in the tunneling defect spectrum:

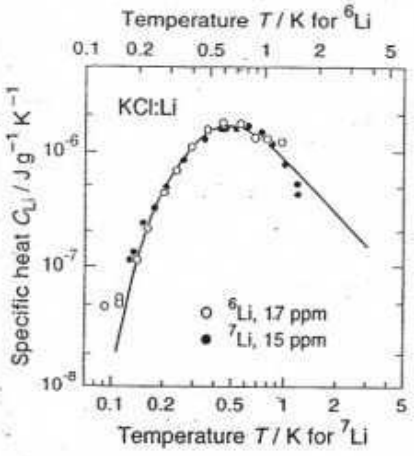

LEFT: Specific heat of lithium-doped KCl after subtracting the lattice contribution. The *upper* temperature scale is valid for ^{6}Li, and the *lower* scale for ^{7}Li. The *full line* represents the prediction of (52)

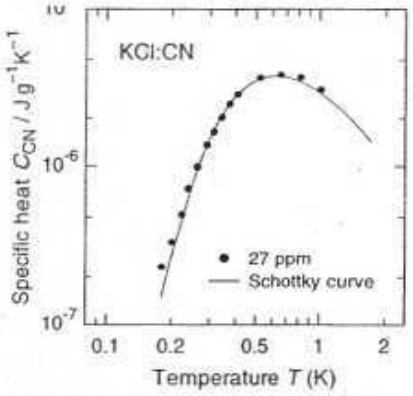

ABOVE: Specific heat of KCl:CN after subtraction of the lattice C_V^{ϕ}

We note that these measurements allow a very accurate determination of the matrix element Δ_0, which can then be used to fit other experiments.

Photon Propagation Mmts: Experiments on EM wave propagation in glasses are usually done at rather low frequency, in the range 10-10,000 Hz typically. The wavelength is of course huge, & we are looking at the very slow response of the 2-level systems to electric field.

Note first that these frequencies are so low (corresponding to energies ~ 0.5-500 nK) that we do not expect any absorption of the photons from single defects - the TLS splittings are much larger. However we certainly do expect the TLS to weakly modify the static polarizability of the system, since they themselves can polarize. We can simply calculate this change as

$$\chi_\varepsilon = -\frac{1}{V}\left.\frac{\partial^2 F(E,T)}{\partial E^2}\right|_{E=0} \equiv \left.\frac{kT}{V}\frac{\partial^2 \ln Z(E,T)}{\partial E^2}\right|_{E=0} = \frac{2}{3} n_z \frac{p^2}{\epsilon_0}\frac{1}{\Delta_0}\tanh\left(\frac{\Delta_0}{2kT}\right) \qquad (54)$$

where ϵ_0 is the vacuum susceptibility, F is the free energy of the TLS system, and Z is the partition function. In experiments one typically measures the dielectric function, which is defined by the "Clausius-Mosotti" relation with the added TLS:

$$\chi_\varepsilon(\omega) = 3\,\frac{(\epsilon(\omega) - \epsilon_{Host}(\omega))}{(2 + \epsilon_{Host}(\omega))} \qquad (55)$$

The fact that $\mathrm{Im}\,\chi_\varepsilon(\omega) = 0$ at low ω does not contradict the finite result for χ_ε in (54). The Kramers-Kronig or "dispersion" relation, that

$$\mathrm{Re}\,\chi_\varepsilon(\omega) = \frac{1}{\pi}\mathcal{P}\int_{-\infty}^{\infty} d\omega'\,\frac{\mathrm{Im}\,\chi_\varepsilon(\omega')}{\omega' - \omega} \qquad (56)$$

simply tells us that most of the Im part of $\chi_E(\omega)$ is coming from higher frequency contributions. We shall study this point in more detail below.

In any case the experimental results on dilute defect systems are rather startling:

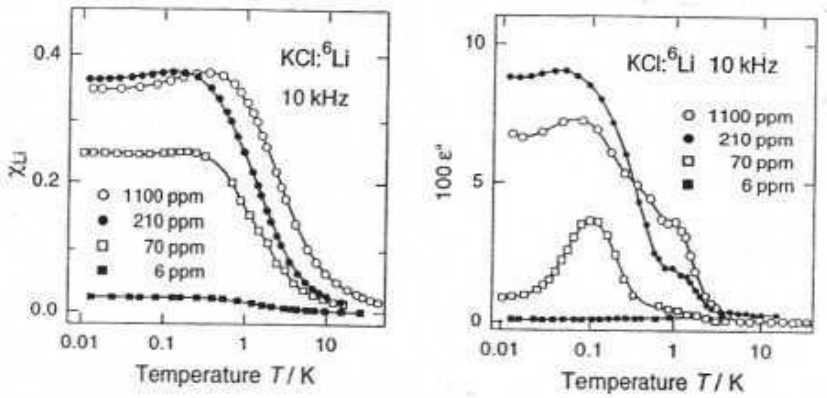

Dielectric susceptibility (a) and dielectric absorption (b) of KCl crystals with different lithium doping — *Full lines* connect the data points

We see immediately that even for $x = 7\times10^{-5}$ concentration of Li TLS in KCl, there is a very significant dielectric absorption. This is prima facie evidence for interaction effects in these systems, even at very low x. Even more striking is how these effects saturate when $x < 10^{-4}$: we even get a <u>reduction</u> in the dielectric response from the TLS when x exceeds 10^{-4}. This shows the profound role of the long-range interactions.

<u>Phonon Propagation Measurements</u>: The propagation of phonons through a dilute elastic medium of TLS is a slightly complicated problem. The phonons can scatter elastically or inelastically off the TLS, as well as interacting resonantly with them. They can also mediate relaxation of the TLS, ie., decay between the levels, which can be spontaneous or stimulated. All of this is quite apart from the interactions between the TLS that they mediate.

There are 4 common experiments used to probe this physics. In straightforward sound propagation, one measures the sound velocity $C_s(\omega,T)$ and the attenuation $\alpha_s(\omega,T)$. This can involve resonant absorption if the TLS frequencies are matched. One can do "phonon echo" experiments, in which the coherent dynamics of the TLS is probed; and finally one can look at heat propagation, ie, the thermal conductivity $K(T)$, which probes the diffusive dynamics of the phonons. We look at these in turn; but first note some of the important quantities that enter into them. Consider the interaction processes shown:

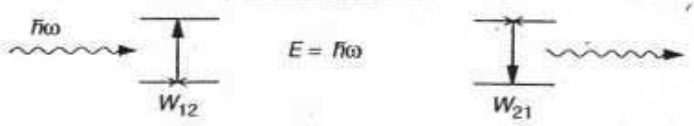

(a) One-phonon process. The transition between the levels occurs via the absorption or emission of a single thermal phonon

(b) Resonant interaction of photons or phonons with two-level systems. Absorption (*left*) and induced emission (*right*) of a photon or phonon with energy $\hbar\omega$

In these figures the phonons coming in may be either thermal or produced by an external source. We can then define a mean free path function $\ell_\lambda(\omega,T)$ given by

$$\ell_\lambda^{-1}(\omega,T) = n_I \frac{\gamma_\lambda^2}{\rho c_\lambda^3}\left(\frac{\Delta_0}{E}\right)^2 \frac{\pi\omega}{\hbar}\, g(\omega,E)\tanh\left(\frac{E}{2kT}\right) \tag{57}$$

and a sound velocity shift caused by the TLS given by

$$\Delta c_\lambda(\omega,T) = n_I \frac{\gamma_\lambda^2}{\rho c_\lambda}\left(\frac{\Delta_0}{E}\right)^2 \frac{\pi}{2\hbar\omega\tau_2}\, g(\omega,E)\tanh\left(\frac{E}{2kT}\right) \tag{58}$$

$$\xrightarrow[\omega \ll E]{} n_I \frac{\gamma_\lambda^2}{\rho c_\lambda}\left(\frac{\Delta_0}{E}\right)^2 \frac{1}{E}\tanh\left(\frac{E}{2kT}\right) \tag{59}$$

In these expressions, $\lambda = \parallel, \perp$ refers to longitudinal & transverse sound modes, and we assume a concentration n_I of TLS all having the same $E = (\Delta_0^2 + \epsilon_0^2)^{1/2}$. There is a phase relaxation time $\tau_2(\omega,T)$ in the problem, to which we come below, and a resonance function

$$g(\omega,E) = \frac{1}{\pi}\,\frac{\tau_2}{1+(\omega-E)^2\tau_2^2} \tag{60}$$

so we see that τ_2^{-1} is telling us the linewidth of the TLS line caused by coupling to phonons. We can easily relate Δc_λ to ℓ_λ via Kramers-Kronig, and we can also define a longitudinal or energy relaxation time $\tau_1(\omega,T)$, given by [1]

$$\tau_1^{-1}(E,T) = \left(\frac{\gamma_\parallel^2}{c_\parallel^5} + 2\frac{\gamma_\perp^2}{c_\perp^5}\right)\left(\frac{\Delta_0}{E}\right)^2 \frac{1}{2\pi\hbar^4\rho}\, E^3 \coth\left(\frac{E}{2kT}\right) \tag{61}$$

where we have put $\omega = E$ here since we are concerned with direct spin-boson relaxation (cf eqtn (269) in section 2.A). Eqtn (61) combines longitudinal and transverse phonon couplings, and its physical meaning will be clear from the work in section 2A. The extra complication in ℓ_λ and Δc_λ comes from the resonance function which very accurately models the line-broadening caused by the phonons.

Thermal conductivity: The simplest experiment interpreted is thermal conductivity. Quite generally we can write for $\kappa(T)$ that

$$\kappa(T) = \tfrac{1}{3} C_V^{\phi}\, \bar{c}_s\, \ell(T) \tag{62}$$

where $\bar{c}_s$ is a suitable average over the longitudinal & transverse sound velocities, and $\ell(T)$ is a thermally weighted average over different phonon frequencies (using a Bose occupation factor).

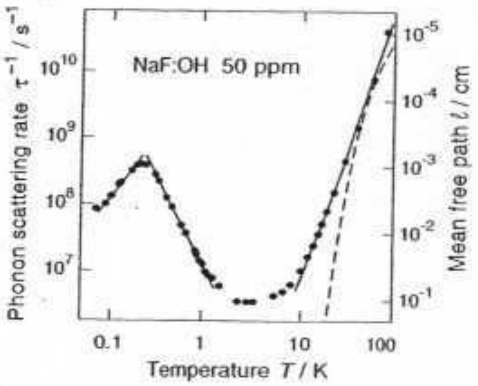

EFT. Scattering rate τ^{-1} of thermal phonons versus temperature in NaF doped with OH [403]. The *left scale* depicts the scattering rate, the *right scale* the mean free path. The *dashed line* represents the variation expected from Umklapp processes

where we note that we can extract $\tau_i^{-1}(T)$ from (42) using $\bar{c}_s \sim \bar{\ell}(T)\bar{\tau}_i^{-1}(T)$. What is actually seen in an experiment is not $\ell(T)$ or $\tau_i(T)$, but $\kappa(T)$ directly. When we look at the data, seen below, we see the following typical results:

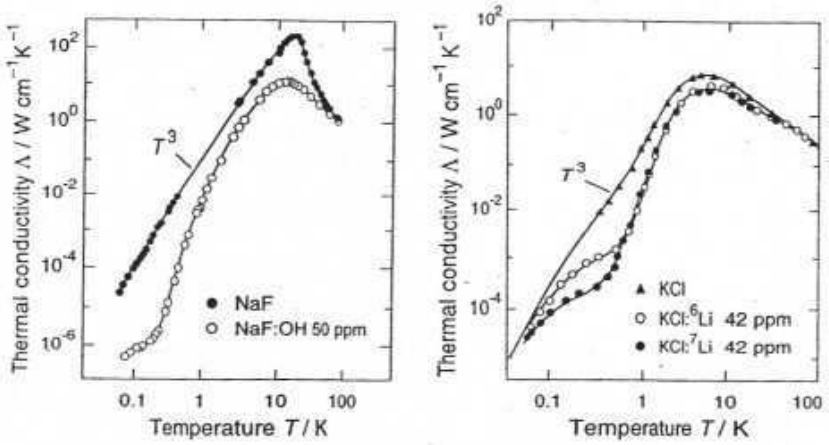

(a) Thermal conductivity of a pure sodium fluoride crystal and of a crystal doped with 50 ppm OH^- ions. (b) Comparison of the thermal conductivity of pure KCl crystal with the conductivity of crystals doped with ^{6}Li and ^{7}Li, respectively.

What we are actually seeing here is a pronounced deficit in $\kappa(T)$ at low T, but only over a certain range of T. In a pure crystal one expects to see $\kappa(T) \sim T^3$ once $\bar{\ell}(T)$ exceeds the size of the sample – as we saw on the last page, $\bar{\ell}(T)$ is already 1 mm in a pure sample when $T \sim 20$ K, reaching several metres when $T = 10$ K (Umklapp scattering typically goes like T^α, where $\alpha \sim 7$-9 depending on the crystal structure). The deficit, ie., the extra scattering, is caused by resonant coupling of the phonons to the TLS, which causes a sharp rise in $\tau_i^{-1}(T)$ as we pass through the temperature range $kT \sim \Delta_0$. As we go still lower in T, τ_i^{-1} falls again, and eventually $\bar{\ell}(T)$ again becomes longer than the sample size.

Sound Propagation: The attenuation of sound gives a very direct measure of $\ell(\omega, T)$ [ie., not the frequency averaged $\bar{\ell}(T)$, but the attenuation for phonons of a specific frequency ω]. The results are complicated to plot as functions of 2 variables, so I don't show them here. In the same way one can plot the sound velocity change Δc at a given frequency as a function of T – such a plot is shown below. The same general behaviour that we might expect from that of $\ell(T)$ is reflected in the T-dependence of δc, ie, a resonant coupling to the TLS which slows the sound down in a broad T-range around Δ_0. Notice that the ratio $\Delta c/c$ is quite small, typically $\sim O(10^{-3})$. Nevertheless one should be impressed – we see at left that a concentration $x = 6\times10^{-5}$ of Li ions gives a $\Delta c/c \sim 1.5\times10^{-3}$. Even more remarkably, we are already in the dense impurity regime here – increasing by 15% causes a 40% decrease in $\Delta c/c$!

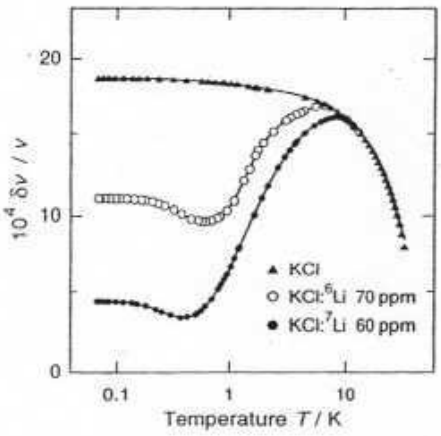

LEFT: Relative variation of the sound velocity $\delta v/v$ versus temperature in pure and lithium-doped KCl at 2 kHz. *Full lines* connect the data points

Phonon Echoes: We can think of the TLS in the system as individual spin ½ systems - the analogue of a magnetic field is simply $\underline{h} = \Delta \hat{h}_x + \epsilon \underline{h}_y$, and if we apply pulsed electric fields to the system, we can "tip" these "spins" in exactly the same way as is done in NMR with nuclear spins, or ESR with electron spins.

Consider the pulse sequence shown at left. We imagine the TLS sitting in its ground state, and then hit it with a pulse which puts it in a superposition of $|0\rangle$ and $|1\rangle$ (ground and excited state). It then oscillates accumulating phase, until we hit it with a second pulse which reverses the "spin", after which it continues to precess.

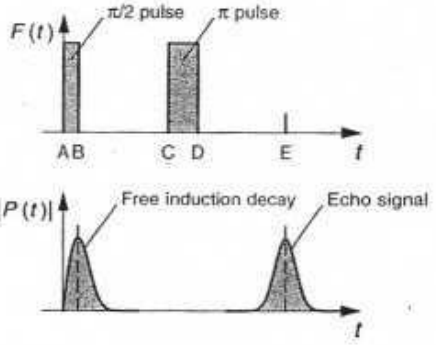

LEFT: Pulse sequence for the generation of a spontaneous echo (*top*), and the corresponding dielectric polarization (*bottom*). *Capital letters* refer to particular times for which the polarization vector is depicted below.

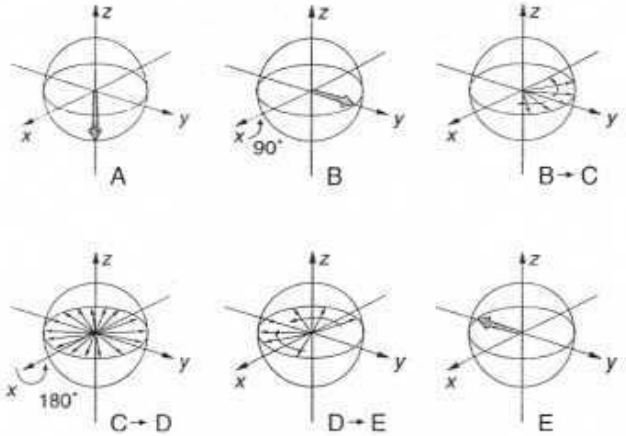

Schematic representation of various stages in the development of a spontaneous echo. The z-component represents the occupation of the energy levels. The x- and y-components reflect the phase of the systems with respect to the applied field. It is assumed that, at the beginning, all tunneling systems are in the ground state. The capital letters refer to particular points in time

The great interest in this thought experiment arises when we imagine a collection of TLS which have slightly different tunneling splittings (come from, eg., a distribution of biases ϵ_0, so that the splitting E is spread out in some distribution. This then corresponds to a real "echo" experiment.

Because of the different splittings, some of the TLS will precess faster (at a frequency $E/\hbar$) than others, during the time between B and C in the figures above. However, the π-pulse flips them, so that those spins that were previously ahead of the more slowly precessing spins now find themselves behind them. If we now let them catch up (by waiting for a time t_{ED} between D and E on the figure, such that $t_{DE} = t_{BC}$, then the TLS spins will all end up aligning together again, leading to an alignment of all their electric fields.

Such experiments have been successfully done. However a further interesting surprise is in store for us when such experiments are done. This is that one also sees echoes in the dense defect regime. We see this at left, where the CN defect concentration is 5%, some 10^3 times larger than the concentration at which one leaves the dilute defect regime. Even more astonishing is that the precession we are seeing here is not that of single defects, but rather of PAIRS of defects, which are strongly coupled to each other. We thus see that these "charge echo" experiments are of very considerable interest in the dense phase as well, to which we now turn.

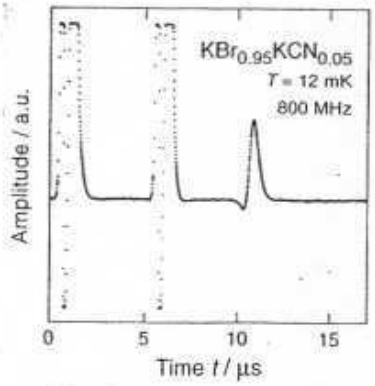

LEFT: Dielectric two-pulse echo in a KBr crystal doped with KCN

(iii) Experiments on Dense Defect & Amorphous Glasses.

We have already seen that the experimental properties of glasses contain some very curious features, already at a rather low defect concentration. These include the extraction of things like excess dielectric constant or sound velocity, and the existence of echoes from defect pairs.

We shall now find, when we get well into the dense defect regime, right into the discussions of amorphous glasses, that there are some quite extraordinary surprises in store for us. What is more, the most important of these features, connected with the UNIVERSALITY of the low T properties, remain quite mysterious – they still have not received an adequate explanation. It is felt by some very well-known physicists (notably Anderson, Leggett, Osheroff, etc) that the explanation of these remain amongst the most important outstanding problems in physics.

We begin with an exploration of some of these basic experimental properties. Consider first the specific heat. We show below left some results for the low-T specific heat of SiO_2 in various states of disorder, and with different concentrations of OH ions. The most obvious results are (i) a massive enhancement of $C_v(T)$ below K over that in crystalline quartz, and (ii) an apparently universal behaviour of the size and form of $C_v(T)$ in the low-T regime – typically

$$C_v(T) \sim T^{1+\delta} \quad (\delta \sim 0.1\text{-}0.3) \qquad (63)$$

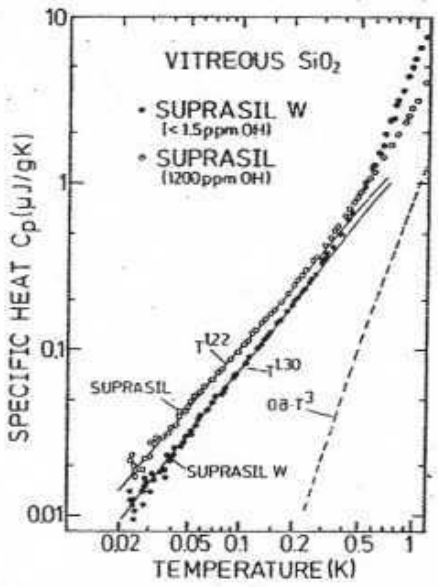

Specific heat as a function of temperature of vitreous silica Suprasil W (<1.5 ppm OH content) and Suprasil (1200 ppm OH). The Debye specific heat is indicated by a dashed line. (After Lasjaunias et al., 1975.)

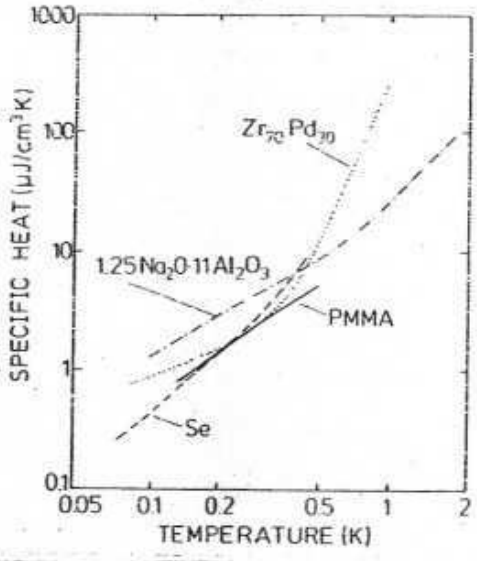

Specific heat versus temperature of different amorphous solids: PMMA (after Stephens et al., 1972), a-Se (after Stephens, 1976), superconducting metallic glass $Zr_{70}Pd_{30}$ (after Graebner et al., 1977) and Na-β-Al_2O_3 (after Anthony and Anderson, 1977).

This behaviour is not confined to quartz or SiO_2; we see other examples at right, and we feel (63) holds for any glass outside the dilute defect regime (amorphous, polymer, metallic, etc).

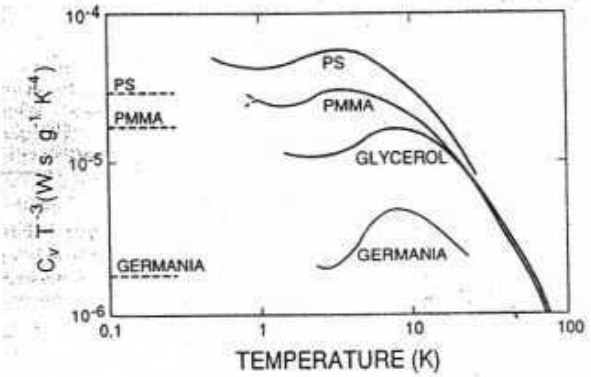

It is interesting to look at the crossover in the specific heat between the low- and high-T regimes. This can be seen by plotting the function $C_v(T)/T^3$ against T (see left). The dashed lines show what one would expect in the pure system – a flat line. We actually find this behaviour nowhere in the whole T-range, but there is a "plateau/hump" crossover regime between low & high-T behaviour. $C_v(T)$ is depleted at higher T ($T > 20\text{-}30$ K).

We see similar universal properties when we turn to the thermal conductivity $K(T)$:

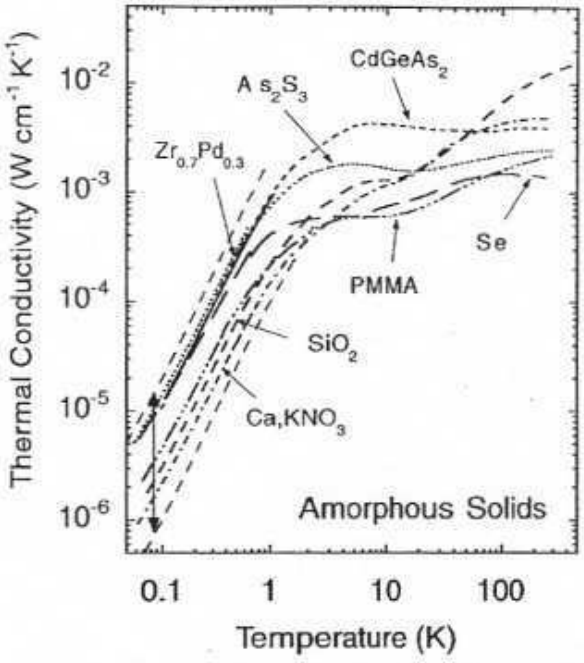

LEFT: Thermal conductivity of several amorphous solids (Cahill and Pohl, 1988a). The conductivities of all glasses measured to date below 1 K lie in the range spanned by the two dashed straight lines shown here, separated by the double arrow.

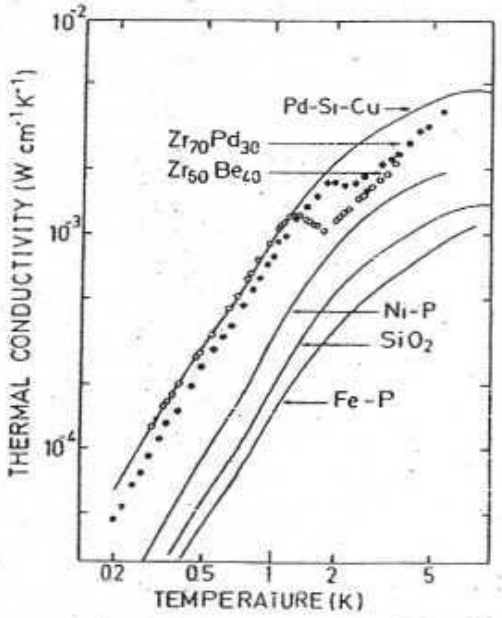

Thermal conductivity versus temperature of the superconducting metallic glasses $Zr_{70}Pd_{30}$ (Graebner et al., 1977) and $Zr_{60}Be_{40}$ together with various other amorphous solids. (From Raychaudhuri and Hasegawa, 1980.)

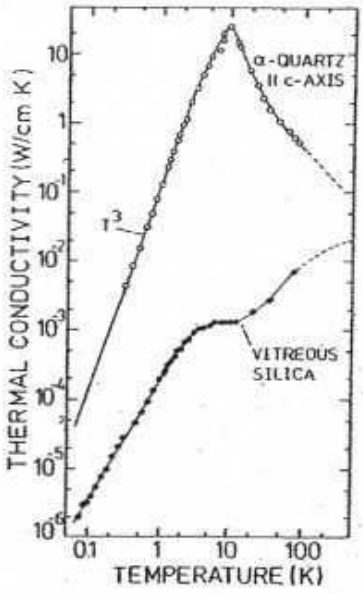

Thermal conductivity as a function of temperature of vitreous silica and crystalline quartz (after Zeller and Pohl, 1971). The amorphous solid exhibits a characteristic plateau at a temperature where a maximum is observed in crystalline materials.

As we see from the figures above, the thermal conductivity also shows universal behaviour below ~ 1K, with a plateau region between 3-30K. One finds

$$K(T) \sim T^{2-\epsilon} \quad (\epsilon \approx 0.05 - 0.2) \qquad (C4)$$

and again this applies no matter what the material (amorphous, polymer, films, metallic, superconducting, etc). The plateau region in $K(T)$ corresponds to the "hump/plateau" region in C_v/T^3; both of indicate a crossover region between a high-T behaviour dominated by ordinary phonons and a very puzzling low-T universal behaviour. The change in $K(T)$, from the behaviour of the pure crystal, is most dramatic in the crossover regime. However we see that there is actually a very large difference over the entire T range between 500K down to the lowest temperatures - even as high as $kT = \Theta_D$.

Before going on with the data it is useful to make a few clarificatory remarks, and introduce a very naive interpretational model. As we see from the results for $K(T)$, we can distinguish 3 regimes for phonon propagation which have the following characteristics:

high T regime: ($T \gtrsim 20-30$K): The phonon transport is very far from being ballistic. In fact one finds that the mean free path $\ell(T)$ of the phonons is roughly equal to their thermal de Broglie wavelength $\lambda_T \sim 2\pi C_s/kT$, which is only 5-10 Å at 30K. Under

these circumstances it makes no sense to talk about conventional propagating phonons - their dynamics is essentially diffusive, and l_c is not a good quantum number at all. Note however that very long-wavelength phonons still propagate ballistically, as collisional pressure waves (just as they do in a gas).

Crossover Regime ($T \sim 3$-$20\,K$): Sometimes called the "plateau" regime, it is characterized by almost flat behaviour of not only $K(T)$, but as will see below, similar behavior in the "internal friction" $Q(\omega,T)$, and in the dielectric loss angle δ.

low-T Regime ($T \lesssim 1K$): In this low T regime we find the remarkable universal properties, to be described fully below. Phonons now have longer mean free paths, and in a naive model one can discuss their propagation in terms of resonant coupling to defects - although as we will see this naive model can't be correct.

The naive model being referred to here is the Anderson-Halperin-Varma/Phillips (AHVP) model of *independent* TLS, in which we assume a distribution function for the tunneling action S_0 and for the bias energies ϵ_0 of the form

$$P(\epsilon_0, S_0) \sim P_0 = \text{const} \quad (S_0 \leq S_0^{max}) \tag{65}$$

so that we also have for the distribution over $E = \sqrt{\epsilon_0^2 + \Delta_0^2}$ and Δ_0 as

$$P(E,\Delta_0) \sim P_0 \frac{1}{\sqrt{E^2-\Delta_0^2}} \frac{E}{\Delta_0} \quad (\Delta_0 \gtrsim \Delta_0^{min}) \tag{66}$$

and a DOS:

$$N_I(E) = \int_{\Delta_0^{min}}^{E} d\Delta_0 P(E,\Delta_0) \sim P_0 \ln\left(\frac{E}{\Delta_0^{min}}\right) \tag{67}$$

From the last equation we see why we need to impose an upper cut-off on the tunneling action - it stops the IR divergence in the low-E density of states for the TLS energy splittings.

While this model clearly makes no sense in terms of the basic physics (we saw already that the defects interact *strongly*, not weakly), the idea of a distribution fn. for Δ_0 and E makes sense - each TLS in an amorphous system will be in some kind of random field from the others, and there will some broad distribution of tunneling barriers and hence of tunneling actions. We will see that the AHVP theory is a useful "zero-th order" interpretational framework to begin with.

Consider first what kind of phonon mean free path will come out of such a theory in the low-T regime. If we go back to eqn (57), then we see that a distribution of mean free paths will now result by substituting $P(E,\Delta_0)$ for $n_I g(\omega) E$ in (57), and putting $E = \omega\hbar$:

$$P[\ell_\lambda^{-1}(\omega,\Delta_0;T)] = \frac{\gamma^2}{\rho c_\lambda^3}\left(\frac{\Delta_0}{\hbar\omega}\right)^2 \frac{\pi\omega}{\hbar} P(\omega,\Delta_0) \tanh\left(\frac{\hbar\omega}{2kT}\right) \tag{68}$$

so that

$$\left.\begin{aligned} \bar{\ell}_\lambda^{-1}(\omega,T) &= \int d\Delta_0 \, P[\ell^{-1}(\omega,\Delta_0;T)] \\ &= P_0 \frac{\gamma^2}{\rho c_\lambda^3} \pi\omega \tanh\left(\hbar\omega/2kT\right) \end{aligned}\right\} \quad (\text{low } T) \tag{69}$$

Of course we will actually find 2 different m.f.p.'s for phonons depending on whether $\lambda = \parallel, \perp$. A fit of (69) to experimental data in the low T regime is shown in the figure at left, at a particular frequency - it is actually a very good fit. To extract these curves, one typically measures the Q-fact or "internal friction" coefficient, given by

$$Q_\lambda^{-1}(\omega, T) = C_\lambda / 2\pi\omega \bar{\ell}_\lambda(\omega, T) \qquad (70)$$

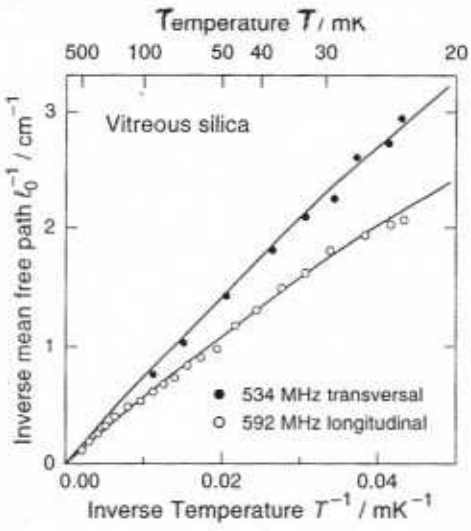

LEFT: Inverse mean free path of longitudinal and transverse sound waves in vitreous silica at 550 MHz plotted as a function of the inverse temperature T^{-1}. *Full lines* depict the hyperbolic tangents

This function essentially tells us how strongly a vibrational oscillation the system will be damped - it is a dimensionless measure of the ratio between the phonon damping and the phonon frequency. Actually plots of the data over the whole temperature and frequency range show us some very interesting features. In the the low-T regime we now see a broad plateau (we show this also for the dielectric loss angle δ, which is the direct analogue of Q^{-1} for photons, and is defined by

$$\tan\delta(\omega) = \frac{\epsilon''(\omega)}{\epsilon'(\omega)} \qquad (71)$$

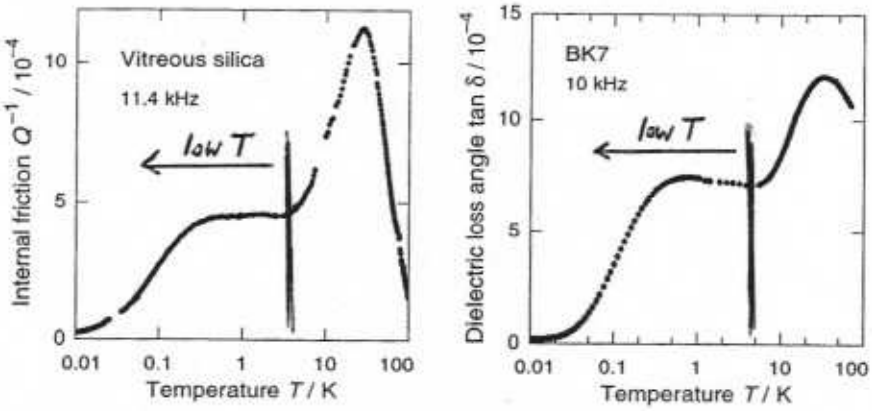

(a) Internal friction of vitreous silica (a-SiO_2) (b) dielectric loss angle tan δ of borosilicate glass (BK7) versus temperature

This plateau is quite remarkable it exists for all amorphous or dense defect glasses, and in the low-T regime below ~3K it shows certain universal properties - irrespective of the defect concentration in the system, it has roughly the same value, viz.,

$$\bar{Q}^{-1}_{plat} \approx 10^{-4} - 10^{-3} \qquad (72)$$

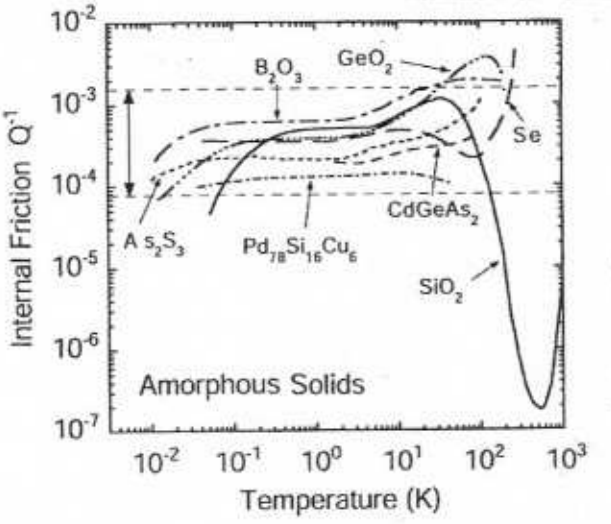

Internal friction of several amorphous solids (Topp and Cahill, 1996). Between 0.1 and 10 K, the internal friction is nearly independent of temperature and measuring frequency. Within this temperature range, the magnitude of the internal friction for all glasses falls within about a factor of 20 as shown here by the dashed straight lines and the double arrow.

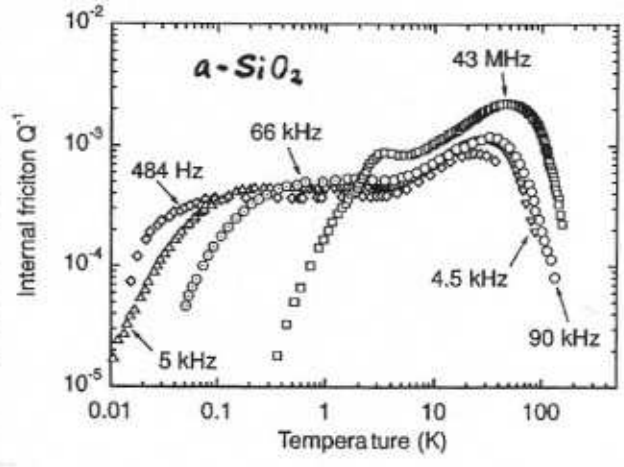

Quite amazingly, this result for $\bar{Q}_{plat}$ is independent of ω in the low-T region, as well as varying over different materials by only a small amount. This is true until we get to a temperature $T_{min} \propto \omega$, where the tanh factor in $\ell_\lambda(\omega,T)$ starts to cause a rapid change in Q^{-1}, as we will explain this below. Note that $Q^{-1}(\omega,T)$ can be measured in various ways independent of propagating phonons - for example, one can do "torsional oscillation" measurements, which simply look at the response of a sample to an oscillatory "twisting" force.

We can summarize the results for $\bar{Q}_{plat}$ for many materials by plotting them against ρc_λ^2:

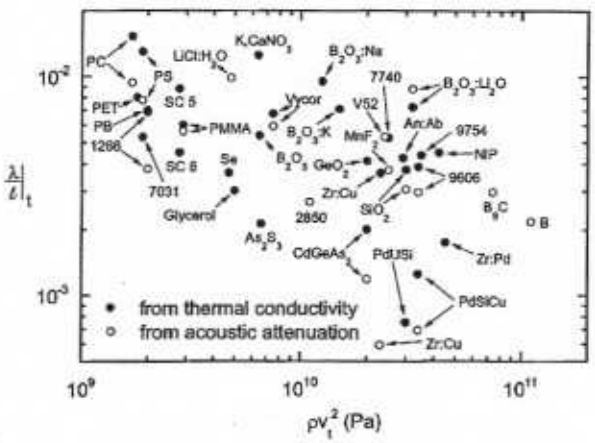

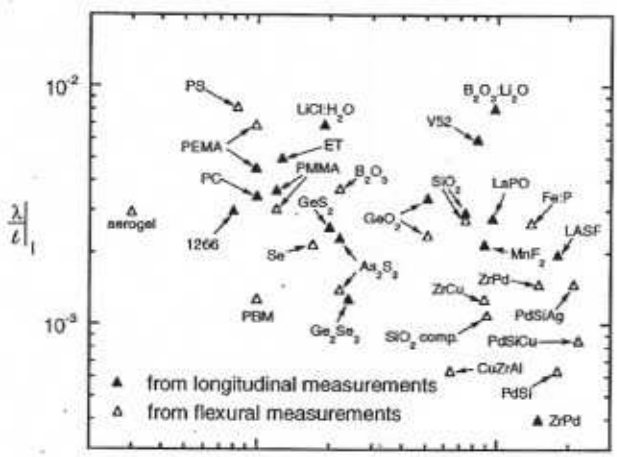

PLOTS OF $(\bar{\lambda}/\bar{\ell})_\lambda = 2\pi\bar{Q}^{-1}_{plat}$ IN UNITS OF $\kappa(T)$, $\alpha(T)$, & TORSIONAL RESPONSE, FOR $\lambda = \parallel, \perp$.

We see that for essentially all materials, no matter what their microscopic parameters, or degree of disorder, there is a low-T plateau, which is quite extraordinarily flat, in the behaviour of $\bar{Q}^{-1}(\omega,T)$, and which extends from $T \sim 3K$ down to the lowest temps measured at very low ω.

There is actually another way to parametrise this, which is very interesting. Let us note that in expressions for quantities like $\kappa(T)$, which involves the phonon mean free path $\ell_\lambda(\omega,T)$, we inevitably end up dealing with phonons whose energy $\hbar\omega$ is $\sim \Theta(kT)$. To get the exact numerical factor we can look at expressions like (57) or (69) and assume a thermal distribution over ω, as we already specified for writing down eqn (62); this means we write

$$\ell_\lambda(T) = \int d\omega\, n(\omega,T)\, \ell_\lambda(\omega,T) \qquad (73)$$

where $n(\omega,T)$ is the Bose function, then we find that the phonons that dominate this expression are those with wavelength $\bar{\omega}(T)$ such that

$$\hbar\bar{\omega}(T) \sim 4.25\, kT \equiv 90\,(GHz\,K^{-1})\,T \qquad (74)$$

One can do the same thing in the analysis of the specific, ie, look at the "dominant phonons contributing to $C_V(T)$"; the factor then becomes ~ 3.65. Suppose we stick with (74); then we can write

$$\bar{\lambda}(T) = \frac{\bar{c}_s}{\bar{\omega}(T)} \sim \frac{\hbar\bar{c}_s}{4.25\,kT} \qquad (75)$$

Now let's go to amorphous glasses, and let's assume that even though the defect

density is high, nevertheless we can still assume ballistic propagation of phonons over a length scale $\bar{l}_\lambda(\omega, T)$, and a mean free path $\bar{l}_\lambda(T)$. Now let's write

$$K(T) \sim \tfrac{1}{3} C_V^{\phi} \bar{C}_s \bar{l}(T) \sim \beta_0 T^2 \tag{76}$$

where we use the experimental result (64) at low T, and we ignore the small correction ϵ to the temperature exponent. We then find that (using 51):

$$\left.\begin{aligned} \beta_0 &= \tfrac{1}{3} A_D \bar{C}_s \bar{l}(T)\, T \\ \text{where} \quad A_D &= \tfrac{2}{5} \pi^2 \frac{k_B^4}{\hbar^3} \frac{1}{\bar{C}_s^3} \end{aligned}\right\} \tag{77}$$

and we can write $\bar{l}(T)$ in terms of β_0 as

$$\left.\begin{aligned} \bar{l}(T) &= \frac{3\beta_0}{A_D \bar{C}_s} \frac{1}{T} \\ &\equiv \frac{15\hbar^3}{2\pi^2 k_B^4} \frac{\beta_0 \bar{C}_s^2}{T} \end{aligned}\right\} \tag{78}$$

But now notice that we can write, using (75), that

$$\frac{\bar{\lambda}(T)}{\bar{l}(T)} = \frac{2}{15} \frac{\pi^2 k_B^4}{4.25 \left(\frac{k_B}{\hbar}\right) \hbar^3} \frac{1}{\beta_0 \bar{C}_s} = 0.46 \left(JK^{-3}s^{-2}\right) \frac{1}{\beta_0 \bar{C}_s} \tag{79}$$

and moreover, comparing (70) & (75), we have when $\omega = \bar{\omega}$ that

$$Q^{-1}(\bar{\omega}, T) = \frac{1}{2\pi} \frac{\bar{\lambda}(T)}{\bar{l}(T)} \tag{80}$$

This is why we have plotted $\bar{\lambda}/\bar{l}$ in the figures on the previous page. We see from these figures that

$$\frac{\bar{\lambda}(T)}{\bar{l}(T)} \sim \frac{1}{200} \qquad Q^{-1}_{\text{phot}} \sim \frac{1}{1300} \tag{81}$$

in the low-T plateau regime, with a spread of a factor ~ 2-3 on either side of these values.

Can we believe this simple picture? Note one astonishing implication of it - that effectively we have a very dilute set of "effective scatterers" of our phonons, since from (81), a phonon is travelling a distance $\sim 200\, \bar{\lambda}(T)$, the thermal wavelength, before it is scattering. But there are no simple naive scatterers - as T increases, so that $\bar{\lambda}(T)$ decreases, so $\bar{l}(T)$ decreases in exactly the same way, so as to maintain the plateau!

We can check against other predictions of this theory in the low-T regime. Consider two such predictions, for the ultrasound attenuation and for the shift in sound velocity in the system. We already know how the ultrasound attenuation will behave,

since we have

$$\bar{\alpha}_\lambda(\omega,T) = \bar{l}_\lambda^{-1}(\omega,T) = \frac{\pi\omega}{c_\lambda}\,\bar{g}_0^\lambda \tanh\left(\frac{\hbar\omega}{2kT}\right) \qquad (82)$$

from (C9), where we define the dimensionless couplings $\bar{g}_0^\lambda = \dfrac{\gamma_\lambda^2}{\rho c_\lambda^2} P_0$ (83)

From (82), which tells us the imaginary part of the sound propagation propagator, we can also deal with the change Δc_λ in the sound velocity, since this just comes from the real part of this propagator - we have (compare (5C)) that

$$\delta\,\frac{\Delta \bar{c}_\lambda}{\bar{c}_\lambda} = -\frac{c_\lambda}{\bar{\omega}}\,\mathcal{P}\int_{-\infty}^{\infty}\frac{d\omega'}{\pi}\,\frac{\bar{\alpha}_\lambda(\omega',T)}{\omega'-\bar{\omega}} \qquad (84)$$

which when evaluated gives

$$\frac{\Delta \bar{c}_\lambda}{\bar{c}_\lambda} \longrightarrow \begin{cases} \bar{g}_0^\lambda \ln\left|\dfrac{T}{T_0}\right| & \text{low } T \\ -\frac{3}{2}\,\bar{g}_0^\lambda \ln\left|\dfrac{T}{T_0}\right| & \text{higher } T \end{cases} \qquad (85)$$

where the crossover temperature again depends on frequency. From the result (85) we see that the contribution Δc_λ will show a turnover at a frequency-dependent temperature T_0, and this is what happens. At left we see the low-T regime and the beginning of the crossover - note the big difference between longitudinal & transverse waves. Below we see the whole range of temperatures, with both the regimes in (85) covered.

One can go through a similar analysis with the real & imaginary parts of the dielectric

Relative variation of the sound velocity versus temperature in $Ni_{81}P_{19}$ for both, longitudinal and transverse sound waves.

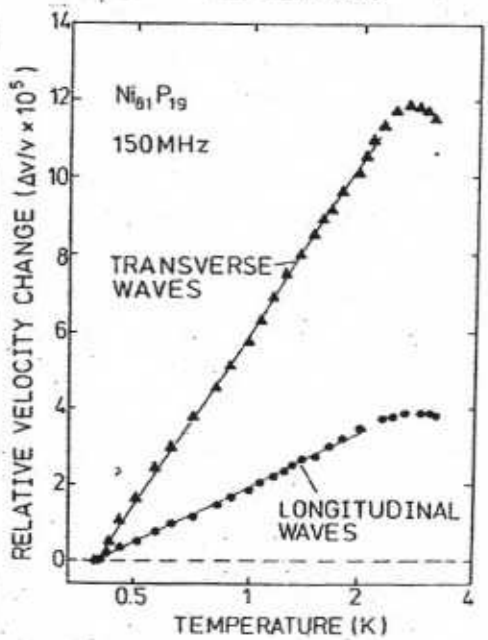

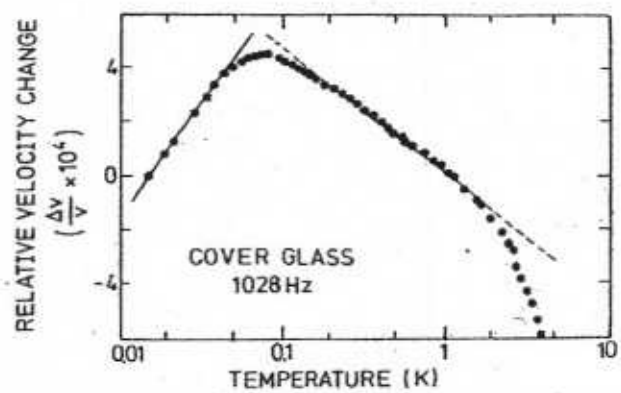

Temperature dependence of the sound velocity of a silica based microscope cover glass at 1028 Hz. The dashed line indicates the logarithmic decrease of the velocity with temperature. Its slope is exactly $-\frac{1}{2}$ of the logarithmic rise represented by the full line. A clear deviation from the expected behaviour is observed above 1.5 K.

function $\epsilon(\omega,T)$, but we will not do this here.

This is by no means the end of the "universal" properties found in low-T glasses. As some interesting further examples we consider the quantities entering $\bar{g}_0^\lambda$ in (83). Notice that we can write

$$\bar{g}_0^\lambda = \frac{1}{\pi}\frac{\bar{\lambda}(T)}{\bar{l}(T)} = 2\bar{P}_{pl}^{-1} \approx \frac{1}{600} \qquad (86)$$

in the low-T regime (compare (75) & (82) with $\omega \to \bar{\omega}$), which we know to be ≈ constant. But what about the individual parts of $\bar{g}_0^\lambda$?

The answers are quite startling and shown below. First, we find that the ratio of the sound velocities $C_{\parallel}$ and $C_{\perp}$ fall on a straight line, no matter what the material this is quite remarkable, given that some are very disordered, even sponge-like, whereas others are almost crystalline (see Figure at left).

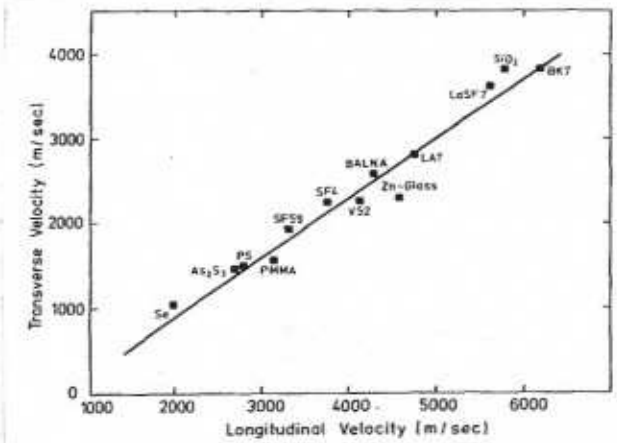

Fig. 1. Transverse versus longitudinal sound velocities for 13 glasses. The straight line is according to a least square fit (see text)

The second plot at right above shows the way in which P_0 varies between materials. It does not vary much - typically we have values in the range

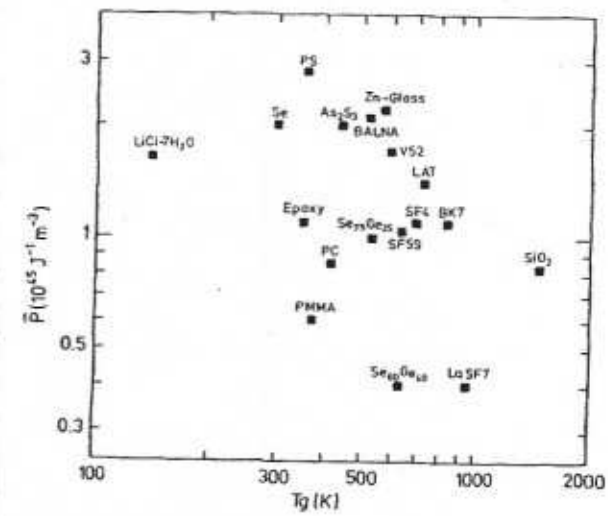

Fig. 2. Variation of the TLS spectral density P with the glass transition temperature T_g

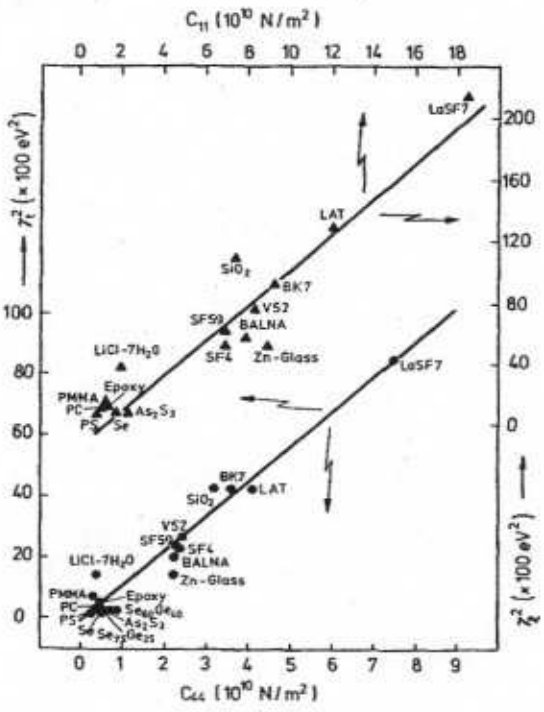

$$P_0 \approx (1.5 \pm 1) \times 10^{45}\,J^{-1}m^{-3} \equiv 2 \times 10^{22}\,K^{-1}m^{-3} \qquad (87)$$

This result immediately makes it interesting, in view of the constancy of $\bar{g}_0^\lambda$, to look at the relationship between the elastic constants

$$C_{11} = \rho C_{\parallel}^2 \qquad C_{44} = \rho C_{\perp}^2 \qquad (88)$$

and the couplings $\gamma_{\parallel}$ and $\gamma_{\perp}$. This is shown at left - as we might expect there is a very clear relationship, which is obeyed surprisingly accurately for almost all glasses in the "dense defect" regime at low T. Note that P_0 is very small, as we might expect from the smallness of $\bar{g}_0^\lambda$.

Relaxation in Dense Defect systems

: Just as in the case of spin glasses, ordinary glassy systems show very interesting dynamics, and again we need to be very careful in any discussion of the thermodynamic properties. There is a transition at some high T to a "frozen" glassy state, but the temperature $T_G(\omega)$ which is measured for this depends on the time or frequency scale - at very low ω the temperature of transition is lowered. Again one may analyse this in terms of activation and a Vogel-Fulcher form (recall (20) and (21)), and T_G is now signalled by a very sharp rise in viscosity as one approaches it from above.

At much lower T, however, the system still has significant dynamics. This can be seen in plots of intensive bulk quantities like the specific heat - see Figure at left) and in extensive quantities like the electric polarization of the electric dipoles in the glass. Both are similar in behaviour to their spin glass counterparts.

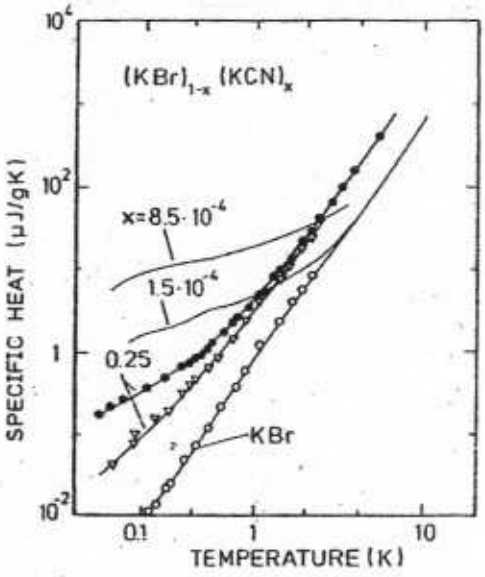

Specific heat of $(KBr)_{1-x}(KCN)_x$ versus temperature. For $x = 0.25$ the specific heat was measured on short- and long-time scale t, indicated by triangles ($t < 1$ ms) and full circles ($t > 50$ ms). For comparison the specific heats of pure KBr ($\Theta_D = 172$ K) and of slightly doped samples ($x = 1.5 \times 10^{-4}$ and $x = 8.5 \times 10^{-4}$) are shown.

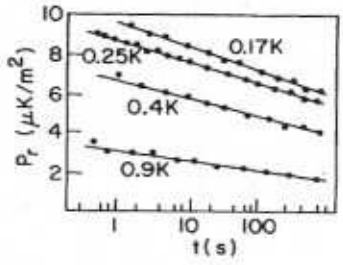

Residual polarization in KCl:Li as a function of time

When one starts to make a detailed study of this, behaviour very reminiscent of that in low-T spin glasses is found. In the last decade some very interesting low-T experiments have been done on the dynamics of both the dielectric & acoustic response of glassy systems over a wide range of timescales.

A nice example of the time dependence of the dielectric function is shown at left. Note that this graph is showing much the same thing as the graph above (the relaxation of the capacitance is just a relaxation of the polarization of the TLS dipoles following a change in applied electric field). The difference between the 2 is solely in the change of material (which we now know is not important) and in the lower T at left. Given the universality shown at low T in the static limit, we might think that this lowering of T is also not so important, but this is not true, because none of what was discussed above took account of the relaxation on very long time scales. As we have seen in quantum spin glasses, these interactions in the system do lead to very interesting new properties on these longer

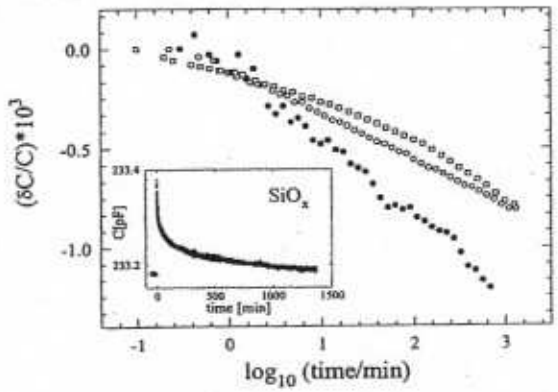

The inset shows the capacitance jump and relaxation in the SiO_x sample 2 upon application of a 10 MV/m dc electric field, measured at $\nu = 1$ kHz at $T = 50$ mK. The graph demonstrates the nearly logarithmic relaxations seen in three samples, SiO_x sample 2 at 50 mK (open circles), SiO_2 sample 3 at 50 mK (solid circles), and polymer sample 5 at 80 mK (squares). The capacitances have been normalized and the SiO_2 fractional change has been multiplied by 100 for clarity. The changes are referred to the initial reading after the field has been applied.

time scales, and the same happens in ordinary glasses. One way to investigate these long-time changes is to do the analogue of a ZFC experiment in spin glasses:

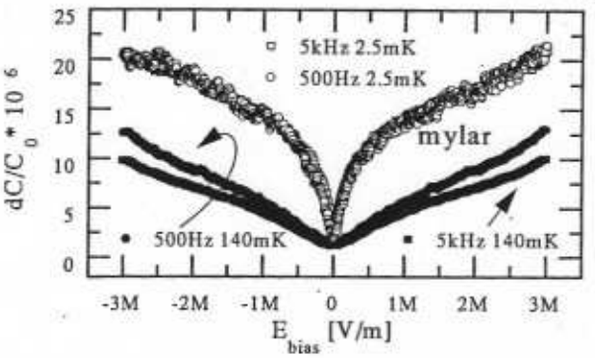

dc bias sweeps on the Mylar sample showing frequency independence at low temperatures and larger response at 500 Hz above the minimum of $\epsilon'(\omega, T)$. This frequency dependence suggests that the minimum in $\epsilon'(\omega, \mathbf{E})$ is very broad.

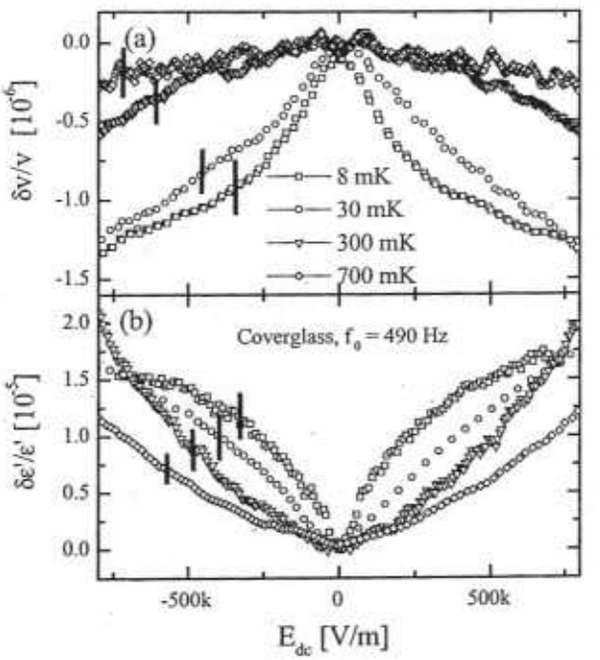

Acoustic (a) and dielectric (b) response of coverglass vs applied E_{dc} at various temperatures, as the field was swept at 1.3 kV/m s. The measuring frequency was 490 Hz, and no excitation or sweep rate dependence was observed. The data have been smoothed by adjacent averaging; statistical errors are indicated by vertical bars.

In all of the experiments shown here, above and at right, the system was cooled in zero electric field, and then left for a long time (perhaps several days) to equilibrate as much as possible). After this, AC dielectric response measurements were done while at the same time the applied DC electric field was changed - the above graphs show essentially the function $\mathrm{Re}\,\epsilon(\omega, T; E)$. In the figure at above right we see a comparison of this function with the real part of the density response of the system, ie., with the sound velocity $\Delta c_1(T; E)$.

In a purely phenomenological way, we can understand these results as a "depletion of states" in the system around zero bias", ie, of those TLS in the system that happened to be in resonance, with no local bias field acting on them. Such a depletion lowers the polarizability when $E = 0$, but applying an extra electric field then biases all the TLS, bringing other TLS into resonance (and taking those TLS which previously had zero bias into a finite bias state, with a new bias $\epsilon_j = \underline{p}_j \cdot \underline{E}$ on them).

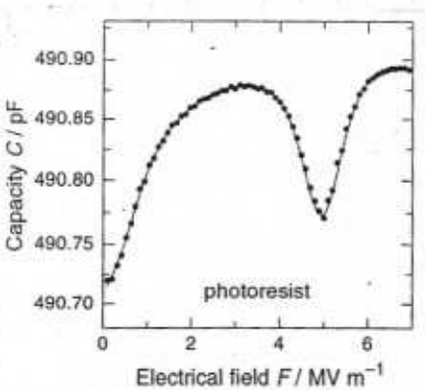

Hole creation in the polymer. After applying a 5 MV/m dc electric field to the polymer for 2 h, the capacitance exhibits a local minimum at this field when the dc field is swept. This suppression in the capacitance was observed to persist for days after the removal of the bias field, consistent with logarithmic relaxation.

Confirmation of this naive picture comes from experiments in which the system is "field cooled" and left sitting at low T for several hours or even days. One now finds the same depletion, but it exists around the field at which the system was allowed to relax. This is what we would expect - the TLS which happened to have zero local bias in the presence of the field are now depleted.

The interesting thing is how rapidly the shape of this depletion hole is still changing as we continue to lower the temperature. This change in shape continues to evolve at even the lowest temperatures at which experiments have been done, with the holes becoming increasingly sharp at lower T.

B.2: THEORY OF GLASSES

There is no unified theory of glassy systems, either spin glasses or non-magnetic glasses. A sometimes enormously sophisticated theoretical apparatus has been developed, but this lives in a very uneasy relationship with more phenomenological theory, and many parts of it are almost completely disconnected from experiment, in a way reminiscent of string theory (which is equally complex mathematically).

What we will do here is first look at some of the important general ideas, which are in some cases quite useful outside the theory of glassy systems. Then we shall go on to discuss some theoretical scenarios. I call them "scenarios" because in no case do they go beyond either general pictures which cannot be applied to real systems, or in some cases more specific discussions of certain systems which cannot be generalized to the whole class of glassy systems.

These scenarios will be divided into 2 classes. The first deals specifically with spin systems, and does not involve phonons except in an incidental way. The second deals with "ordinary" glasses, and is essentially a theory of coupled defects and phonons.

(a) Key General Ideas in the Theory of Glasses

We will discuss 3 key ideas in the theory. The first concerns the general problem of how to deal with the combined effects of frustration and disorder - this is an essential feature of all glassy systems. I will introduce the replica trick & discuss how one can average over different realisations ("replicas") of a glassy system.

The second key idea concerns the idea of an underlying order and an "order parameter" for glasses. The order parameter in question is the "Edwards-Anderson" order parameter, and we will see how it can be deployed in certain approximations.

The 3rd key idea concerns the dynamics, which are really the defining property of a glassy system. We discuss they key role played by the environment in this dynamics, and the difference between the classical and quantum regime. Several different approaches are possible here, and we discuss them in some detail.

(i) Frustration & Disorder: Averaging Techniques

: In statistical mechanics we often need to carry out various averages, and it is sometimes necessary to be quite careful in formulating these. Here are some averages we have to deal with:

- Time Average: This is an average of the properties of some system over a time T. Often we let T be very long, in an effort to explore the entire phase space that the system may move in. For glassy systems it is also common to specify an average over a shorter time T such that there is a separation between timescale of some rapid processes of relaxation, on a timescale $< T$, and much slower ones. In experiments one explores this by doing separate experiments over a timescale T, separated by intervals $t_w \gg T$ (here t_w refers to the "waiting time" between experiments).

- Bath Average: An average we introduced previously in the definition of

the reduced density matrix $\bar{\rho} = Tr_E[\rho]$ was the trace over the environment (the rest of the universe). This average can be done in different ways depending on the initial state assumed for the global or "universal" density matrix $\hat{\rho}$. One common way of doing it is to assume that the system of interest is initially decoupled from the environment, and we then average over both states in a way consistent with our knowledge of the environmental part $\hat{\rho}_E$ of ρ. Alternatively we may have a $\rho_{initial}$ in which the system S and the environment E are already entangled.

It is very common to assume that initially the bath is in thermal equilibrium, but this is by no means necessary - usually however some part of it will be near thermal equilibrium on some timescale of interest.

- Thermal Average : This is a special case of the bath average discussed above. Here we assume that, for some sector of the environment, that

$$\hat{\rho}_E = \left\{ \begin{array}{ll} Z^{-1} e^{-\beta \hat{H}} & (Z = Tr[e^{-\beta \hat{H}}]). \\ Z_N^{-1} e^{-(\beta H + \mu N)} & \end{array} \right\} \quad (89)$$

depending on whether we allow fluctuations of energy only in the environment, or fluctuations of number as well. Note that (89) already supposes that there is an even larger environment (the "universe", or at least a closed box of some kind) in which nothing fluctuates, and which can be described by a microcanonical ensemble.

- Noise Average : This is another special case of the bath average described above, where we now average over some external noise acting on the central system of interest. As we saw, the best way to do this is by functionally averaging over a noise correlator (cf section A, eqtn (213), or the example in eqtn (353)).

- Disorder (Replica) Average : The above Bath Averages are all over the dynamical fluctuations of the environment, or over initial environmental conditions. Another form of bath average, or indeed average over the full ρ, is to assume an average over different realisations of the system, all of which are consistent with some assumed macroscopic "mean". The most common example of this is an average over random variables in the Hamiltonian itself, ie., over different possible couplings in the Hamiltonian. These could be random couplings between particles or spins, or some random local field. The key point is that we assume these variables to be fixed for all time, but that a given disordered system has been prepared in some way so that the different parts of it, all macroscopically similar, nevertheless are different realisations of the disorder. Nowadays we say that we can divide the system into different "replicas" of the system - each replica is a sub-system of the whole, but it is still macroscopic, and it still looks on average like the entire system.

Actually one needs to be very careful in dealing with disorder averages in glassy systems, in the same way as with time averages. The point is that the disorder (in couplings, or random fields) will evolve with time in glassy systems (indeed in random systems in general). We say that the randomness "ANNEALS" with time, and there may be many timescales involved. Physical examples which illustrate this well are the diffusion (classical or quantum) of defects & dislocations, or of impurities, or the slow local and global changes of structure occurring in very viscous liquids, or in processes like crystallisation from liquids or disordered "supercooled"

liquids or glasses. It might be objected that in most or all of these cases, the underlying Hamiltonian is not changing, but again we must remember that we are dealing here with effective Hamiltonians, and these are changing.

Formally, in trying to deal with equilibrium properties on some timescale, it is common to introduce 2 more averages:

Annealed Average: Here we assume that the timescale T of interest for time averages in the system (eg., the experimental time scale) is much longer than the timescale of relaxation or fluctuation of the random variables connected with disorder. The disorder variables are then absorbed into the thermal average we already considered, ie., we can write

$$Tr_E [\cdots] \equiv Tr_{Bath} Tr_{\underline{X}} [\cdots] \tag{90}$$

where the $\{\underline{X}\}$ are the random variables; the density matrix for the environment becomes

$$\hat{\rho}_E = \frac{1}{\langle Z_X \rangle} e^{-\beta \hat{H}[\underline{X}]} \qquad \langle Z_X \rangle = Tr_{Bath} Tr_{\underline{X}} [e^{-\beta H[\underline{X}]}] \tag{91}$$

and we can write an annealed free energy of form

$$F = -\tfrac{1}{\beta} \ln \langle Z_X \rangle \equiv -\tfrac{1}{\beta} \ln \left(Tr_X Z[\underline{X}] \right) \tag{92}$$

Normally in annealed averages of this kind we would not even make explicit reference to the random variables $\underline{X}$.

Quenched Average: Now we go to the opposite limit, where $\tau_X^{fluct} \gg T$, ie., the random variables $\underline{X}$ change on a timescale much longer than of interest in an experimental timescale T. Now we cannot trace over the random variables in the density matrix and partition function as we did above. Instead we must assume that we compute an extensive quantity (the Free energy) for each replica (ie realization for a given X) and then average over these - ie., we have

$$\left.\begin{aligned} \bar{F} &= -\tfrac{1}{\beta} \langle \ln Z[\underline{X}] \rangle \\ &\equiv -\tfrac{1}{\beta} \sum_{\underline{X}} P[\underline{X}] \ln Z[\underline{X}] \equiv \sum_{\underline{X}} P[\underline{X}] f[\underline{X}] \end{aligned}\right\} \tag{93}$$

A lot of the problems that arise in equilibrium statistical mechanics of disordered systems come purely from the difficulty of calculating (93), because it is much harder to average over $\ln Z[X]$ than over $Z[X]$. We assign here a probability $P[X]$ to each replica, with a given configuration of the random variables $\underline{X}$. This is not usually going to be a thermal probability, although it might.

Equations (92) and (93) clearly give different results for physical systems. To see this in a simple way, suppose we assume that the Free energy F for our system is "SELF-AVERAGING", ie., that if we have n replicas of the system, then

$$\Delta F(n) \equiv \left(\bar{F} - \frac{1}{n} \sum_{\alpha=1}^{n} P[\underline{X}_\alpha] f[\underline{X}_\alpha] \right) \xrightarrow[n \to \infty]{} 0 \tag{94}$$

ie., we imagine choosing n replicas, each chosen with a probability $P[x]$, and then look at the fluctuations of the sum about the mean. Usually one assumes a central limit theorem, ie., we assume that

$$\Delta F(n) \sim \sigma_F/\sqrt{n} \tag{95}$$

so that we can assign a probability

$$P[f] \sim e^{-\frac{n}{2\sigma_F^2}(f-\bar{F})^2} \tag{96}$$

where the normalisation factor is ignored. The idea of self-averaging of extensive quantities makes sense if interactions are short-ranged. We then expect that most of the free energy of each replica or sub-system is locked up in bulk contributions, with only a small surface contribution, ie., the free energy of each subsystem can be treated as extensive. Clearly if we have long-range interactions then things become a lot more delicate - I will return to this point later - but we see that in principle it causes problems, not only because the surface contributions will no longer be small, but also because there will be non-trivial interactions between the sub-systems.

Consider now what we get when we use the probability $P[f]$ in the 2 averages. We can, eg., calculate the mean free energy in the system, and we get

$$\left.\begin{aligned} F_{Ann} &= \frac{1}{n}\left(-\tfrac{1}{\beta}\ln\langle Z\rangle\right) \equiv \frac{-1}{\beta n}\ln\langle e^{-n\beta f}\rangle \\ &\equiv -\frac{1}{\beta n}\ln\int df\, P[f]\, e^{-n\beta f} \\ &= \bar{F} + \tfrac{1}{2}\beta\sigma_F^2 \end{aligned}\right\} \tag{97}$$

whereas

$$F_{Quench} = \int df\, P[f]\, f = \bar{F} \tag{98}$$

so that $F_{Ann} > F_{Quench}$ (not surprising - we always expect the free energy to increase if we remove a constraint).

<u>The "Replica Trick"</u>: A useful, though technically rather complicated way to to average over replicas starts by defining the quantity appropriate to an average over n replicas, viz

$$\bar{Z}_n = \left\langle \sum_x P[x]\, Z^n[x] \right\rangle \tag{99}$$

and then makes use of the identity $Z^n = e^{n\ln Z} \longrightarrow 1 + n\ln Z \quad (n \ll 1)$. We can then write

$$\left.\begin{aligned} \langle \ln Z[x]\rangle &= \lim_{n\to 0}\frac{1}{n}\left(\langle Z^n[x]\rangle - 1\right) \\ &\equiv \lim_{n\to 0}\partial/\partial n \langle Z^n[x]\rangle \end{aligned}\right\} \tag{100}$$

Now suppose we consider the total system, which is the sum of all replicas. We clearly have.

$$\left.\begin{aligned} Z_{Tot} &= \prod_{\alpha=1}^{n} Z_\alpha[x] \equiv Z^n[x] \\ &= \prod_{\alpha=1}^{n} e^{-\beta H_\alpha[x_\alpha]} \\ &= \exp\left[-\sum_{\alpha=1}^{n} \beta H_\alpha[x_\alpha]\right] \end{aligned}\right\} \quad (101)$$

and moreover

$$\left.\begin{aligned} \bar{Z}_n &= Tr_{[S_j]}\, Tr_x \exp\left[-\beta \sum_{\alpha=1}^{n} H_\alpha[S_j; x_\alpha]\right] \\ &\equiv Tr_{[S_j]} \exp\left[-\beta \mathcal{H}_{eff}^{(n)}[S_j]\right] \end{aligned}\right\} \quad (102)$$

where $H_\alpha[x_\alpha]$ is the Hamiltonian for the α-th replica, with realisations x_α of the random variables, and $\mathcal{H}_{eff}^{(n)}$ is an effective Hamiltonian now for the total system, in which the random variables have been averaged over but not the other variables of the system (which we denote by $\{S_j\}$ as if they were spin variables, although this is not necessary). A crucial point is that

$$\mathcal{H}_{eff}^{(n)}[S_j] \neq \sum_{\alpha=1}^{n} Tr_x\left(\mathcal{H}_\alpha[S_j; x_\alpha]\right) \quad (104)$$

because in fact the averaging over the $[x]$ in (102) produces interactions between the S_j in $\mathcal{H}_{eff}$ that were not in the original $\mathcal{H}_\alpha$. We shall see this below in an example.

If one wants to calculate correlation functions in the replica trick a further trick needs to be employed. For example, a "1-particle" or "1-spin" operator O operating on a single degree of freedom δ has expectation value

$$\left.\begin{aligned} \langle S_j \rangle &= \left\langle \frac{1}{Z[x]}\, Tr_{[S_j]}\left(S_k\, e^{-\beta \mathcal{H}_{eff}^{(n)}[S_j]}\right)\right\rangle \\ &\equiv \left\langle \frac{Z^{n-1}[x]\; Tr_{[S_j]}\left(S_k\, e^{-\beta \mathcal{H}_{eff}^{(n)}[S_j]}\right)}{Z^n[x]} \right\rangle \end{aligned}\right\} \quad (108)$$

which does not look terribly useful, but is in the limit $n \to 0$, since the denominator of the 2nd form goes to unity. Now the idea is that if we evaluate (108) in the expanded configuration space of the total system, it can only exist in one of the replicas, ie., we have

$$\langle S_k \rangle \equiv \frac{1}{n} \sum_\alpha \langle S_{k\alpha} \rangle \quad (109)$$

where $S_{k\alpha}$ is the k-th spin in the α-th replica. Whenever one uses the replica trick it has to be remembered that we have expanded the configuration space to the total system, ie., to all the replicas, but that a 1-particle operator only acts on a single variable in one of the replicas.

One can do the same thing for higher correlation functions - thus a 2-spin correlation function looks like

$$q = \langle S_k^2 \rangle = \frac{1}{n(n-1)} \sum_{\alpha \neq \beta} q_{\alpha\beta}$$

$$q_{\alpha\beta} \equiv \langle S_{k\alpha} S_{k\beta} \rangle = \left\langle \frac{1}{Z^2[X]} \left[Tr_{S_j} \left(S_k e^{-\beta \mathcal{H}_{eff}[S_\mu]} \right) \right]^2 \right\rangle \qquad (110)$$

and more generally:

$$\langle S_i S_j S_k S_\ell \cdots \rangle = \frac{1}{n(n-1)(n-2)\cdots} \chi_{ijk\ell\ldots}^{\alpha\beta\gamma\delta\ldots}$$

$$\chi_{ijk\ell\ldots}^{\alpha\beta\gamma\delta} = \langle S_{i\alpha} S_{j\beta} S_{k\gamma} S_{\ell\delta} \cdots \rangle \qquad (111)$$

Example : In much of traditional spin glass theory a rather simplified model is studied, with Hamiltonian

$$\mathcal{H}_J = -\tfrac{1}{2} \sum_{ij} J_{ij} \underline{S}_i \cdot \underline{S}_j - \sum_j \underline{h}_j \cdot \underline{S}_j \qquad (112)$$

and usually the spins are taken to be Ising spins. The randomness is typically given to the J_{ij}, with some distribution function $P[J_{ij}]$.

Suppose we now write down $\bar{Z}_n$, using the definition in the form (102). The Trace over X becomes an integral over J_{ij}, and we have

$$\bar{Z}_n = Tr_{[S_{j\alpha}]} \prod_{i,j} \int dJ_{ij} \, P[J_{ij}] \exp\left[\beta \sum_{\alpha=1}^{n} \left(J_{ij} S_{i\alpha} S_{j\alpha} + \underline{h}_j \cdot \underline{S}_{j\alpha} \right) \right] \qquad (11$$

To find the form of $\mathcal{H}_{eff}^{(n)}$ we Taylor expand the exponential, to get for $h_j = 0$

$$\mathcal{H}_{eff}^{(n)} = -\frac{1}{2\beta} \sum_{i,j} \sum_{k=1}^{\infty} \frac{\beta^k}{k!} C_k(J_{ij}) \left(\sum_{\alpha=1}^{n} S_{j\alpha} S_{j\beta} \right)^k \qquad (114)$$

where $C_k(J_{ij})$ is the k-th cumulant of J_{ij}, defined in the usual way (see below)

CUMULANTS The characteristic function of the random variable J is defined as

$$G[\tau] = \langle e^{i\tau J} \rangle \equiv \int dJ \, P[J] e^{i\tau J} \quad (\equiv P[\tau])$$

and we can expand this as $G[\tau] = \sum_k g_k (i\tau)^k / k!$ with moments g_k

The cumulant expansion is an expansion of $\ln G[\tau] = \sum_k C_k \frac{(i\tau)^k}{k!}$

The relation between the cumulants and the moments is:

$C_1 = g_1$ $\quad C_2 = g_2 - g_1^2$ $\quad C_3 = g_3 - 2g_2 g_1 + 2g_1^3$ $\quad$ etc.

so that

$$\left.\begin{aligned} C_1(J_{ij}) &= \langle J_{ij}\rangle \\ C_2(J_{ij}) &= \langle J_{ij}^2\rangle - \langle J_{ij}\rangle^2 \equiv \sigma_J^2 \quad , \text{etc} \end{aligned}\right\} \quad (115).$$

We can find a simpler form for $\mathcal{H}_{eff}^{(n)}[S_i]$ if we assume a simple Gaussian distribution for the J_{ij}, ie, we assume that

$$P[J_{ij}] = \frac{1}{(2\pi)^{1/2} J_0} \exp\left[-J_{ij}^2/2J_0^2\right] \quad (116)$$

so that $\langle J_{ij}\rangle = 0$, and $C_2 = \sigma_J^2 = J_0^2$; all higher moments and cumulants are zero. The model specified by the Hamiltonian (112), with the distribution (116), is known as the "Sherrington-Kirkpatrick" model - it has a physical pathology, which is that the interactions are infinite range (the distribution in (116) is independent of the distance $(\underline{r}_i - \underline{r}_j)$). To give it some sense one assumes that

Using (116) we find

$$\sigma_J^2 = J_0^2 \sim O(1/N) \quad (SK \text{ model}) \quad (117)$$

Using (116) we find that (again for $h_j = 0$)

$$\mathcal{H}_{eff}^{(n)}[S_i] = -\frac{\beta^2}{4} \sum_{ij} J_0^2 \sum_{\alpha\beta} (S_i^\alpha S_j^\alpha)(S_i^\beta S_j^\beta) \quad (118)$$

and we see that we have generated 4-spin interactions in the effective Hamiltonian. We will return to this model later on.

Frustration: We have already noted on several occasions that 2 conditions required for glassy behaviour are frustration and disorder. These are not disconnected, because certain kinds of disorder in the inter-spin coupling leads to frustration as well.

To get an idea of what frustration is, lets look at some simple models where we only have nearest-neighbour exchange couplings between Ising spins. The simplest "plaquette" is the triangle, and we notice that with all AFM bonds $-J$, we cannot simultaneously keep all of these bonds "happy" - there must be at least one bond with a high-energy FM

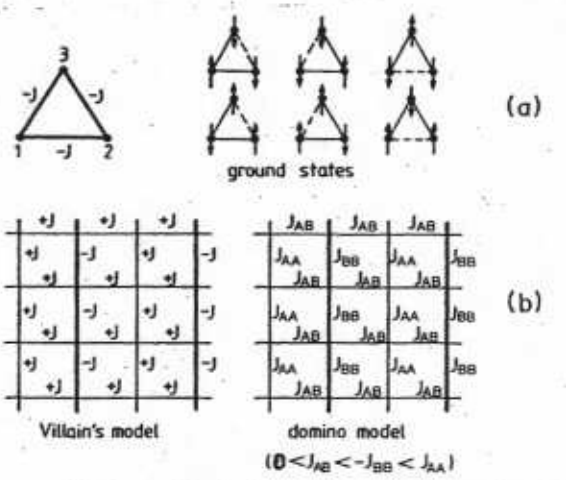

(a) Frustrated triangle and its ground state: "unsatisfied" bond is denoted as a dashed line. (b) Two fully frustrated two-dimensional models, suggested by Villain (1977a) and Vil-

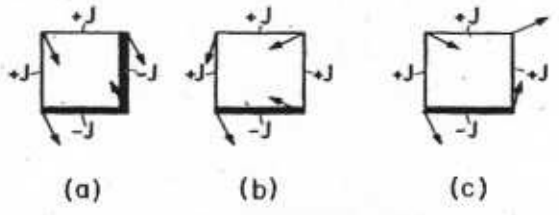

Classical ground state of a set of four spins in the XY model with interactions $\pm J$ (thick bonds are antiferromagnetic, thin bonds are ferromagnetic). (a) Nonfrustrated plaquette; (b) frustrated plaquette, chirality $\tau = +1$; (c) frustrated plaquette, chirality $\tau = -1$.

arrangement (ie., parallel spins). One can generalise this to a lattice, and devise frustrated arrangements of couplings as shown in the figure on the last page.

For these square lattices one can devise a local measure of frustration quite easily. Consider the flux variable defined on the "dual lattice" to the original lattice, so that the vertices of the dual lattice are in the centre of the plaquettes of the original lattice (and vice-versa). Now we define the flux variable on plaquette p as

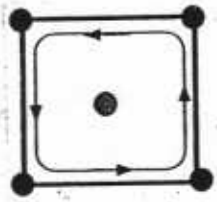

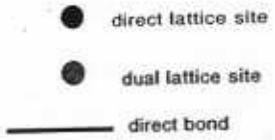

$$\phi_p = \prod_{\langle ij\rangle \in p} \text{sign } J_{ij} \qquad (118)$$

where $\langle ij\rangle \in p$ indicates we take all bonds $\langle ij\rangle$ which border the plaquette p. More generally the flux enclosed by a contour C in the square lattice is given by

$$\phi(C) = \prod_{p \in S} \phi_p \equiv \prod_{\langle ij\rangle \in C} \text{sign } J_{ij} \qquad (119)$$

where $p \in S$ indicates that the plaquette is enclosed by the contour on the original "direct lattice", ie., is part of the enclosed surface S, and $\langle ij\rangle \in C$ means that the link $\langle ij\rangle$ is part of the contour C.

Obviously one can think of all this in terms of a lattice gauge theory, in which the gauge field is defined by the J_{ij} and lives on the links. One nice consequence of this gauge formulation is that only gauge-invariant terms have any physical meaning - thus the "fluxes" ϕ_p are invariant under the relevant Z_2 gauge transformation,

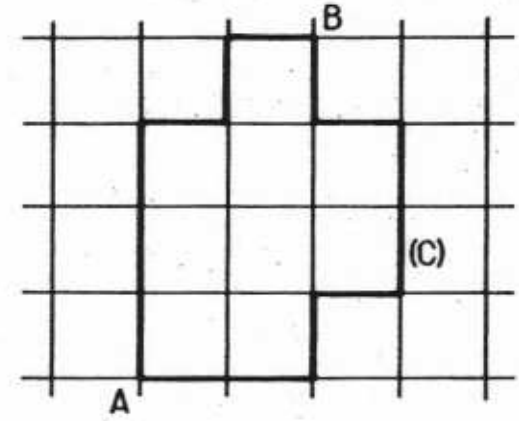

If the frustration function around contour (c) takes the value -1, then A sends to B contradictory orders along the two paths forming (c).

$$\left.\begin{aligned} S_j &\rightarrow -S_j \\ J_{ij} &\rightarrow -J_{ij} \end{aligned}\right\} \qquad (120)$$

which does not physically change the problem - it leaves the Hamiltonian invariant, even if it is applied locally as in the figure at left.

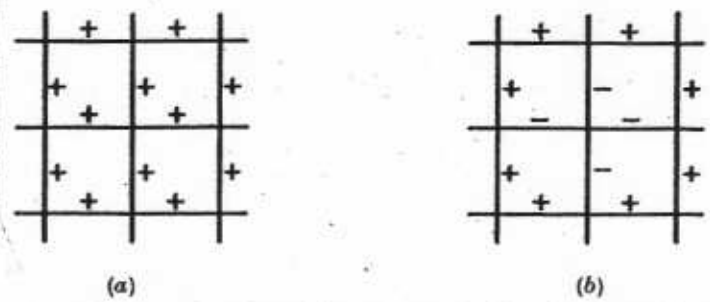

(a) A ferromagnetic configuration of bonds. (b) All bonds around the central site have been made negative; this has the same ground-state energy, with the central spin flipped.

It is obvious how one can generalise this discussion to deal with other lattice structures provided we deal with nearest-neighbour spin-spin couplings. It is not so obvious how to do it for longer-range interactions and I will not go into this topic here. The most interesting thing about the gauge formulation of the problem is that it suggests how one can separate out the physics of glasses into frustration "sources" along with the analogue of curl-free disturbances (like solitons & spin waves).

The above formulation of the gauge theory ignores the actual state of the spins. There is a slightly different formulation which does this as well. Suppose we define "link variables" for the bonds $\langle ij \rangle$ as

$$A_{ij} = S_i S_j \operatorname{sign} J_{ij} \tag{121}$$

(here I assume Ising variables $S_j = \pm 1$ for simplicity).

We now introduce some useful terminology. If $A_{ij} = -1$ on some bond, we say that there is a "kink" on this bond. If the flux ϕ_p associated with a given plaquette is -1, then we say that this plaquette is frustrated. Clearly these variables are not independent - if the number of negative A_{ij} is even, then $\phi_p = +1$, and if it is odd, then $\phi_p = -1$. In fact we have

$$\prod_{\langle ij \rangle \in p} A_{ij} = \phi_p \tag{122}$$

However we can visualize how the system tries to accomodate the frustration using the A_{ij}, which give us an alternative way of looking at the spin state of the system.

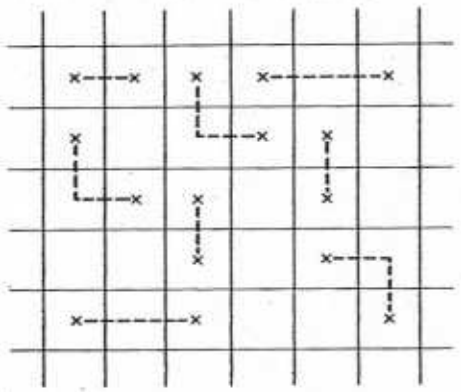

2-DIM: Frustrated plaquettes and strings.

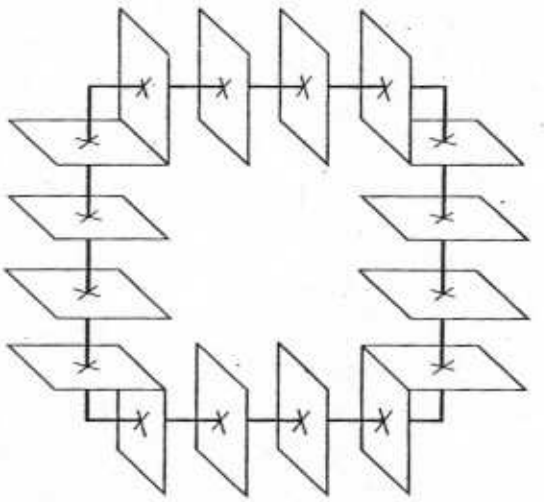

3-DIM: A closed tube of frustrated plaquettes.

We draw a hatched line perpendicular to all "kink bonds", and link these up to get lines of kinks - this looks just like a line of defects, ie, like a dislocation. The same think is easily done in 3-d. Now we notice that for any plaquette where $\phi_p = 1$, all defect lines entering the plaquette must also leave it; but for a frustrated plaquette, there must be a defect line terminating there. Thus the statistical mechanics of the system can be written as that of a set of tethered strings as well as untethered loops. One can actually formulate the statistical mechanics of the system in terms of these variables, using a partition function of form

$$Z[\phi, A] = \operatorname{Tr}_{[A_{ij}]} e^{\beta \sum_{\langle ij \rangle} A_{ij}} \prod_p \delta\left(\phi_p - \prod_{\langle ij \rangle \in p} A_{ij}\right) \tag{123}$$

which can also be written in a continuum approximation for long wavelengths.

We have briefly sketched here how one may formulate the physics of frustration. This still leaves the question of <u>why</u> frustration is necessary for glassy behaviour - and also why it is that we also <u>need</u> disorder as well. (there are now many examples of frustrated systems which exist in ordered arrays, where glassy behaviour is not seen). To answer this we need to go a bit further.

(ii) Order Parameter : Free Energy Landscape

In a system which combines disorder and frustration, it is at first glance hard to understand how there could be an order parameter. Historically the reason why efforts were made to find one is that a clear sign came from experiments for the existence of some kind of transition between a "glassy" state and a simple paramagnetic state. In the case of ordinary glasses, arising from, eg., supercooled liquids, there is similar evidence for a transition. The idea is then that there is some collective phenomenon going on here, and so there must be an order parameter.

In what follows we look only semi-formally at what is going on. This is because a quantitative discussion requires consideration of specific models, and moreover is rather technical, even for quite simple models. Some of this more technical discussion will be given later, when we come to discuss the replica symmetry-breaking scenario for glasses.

"Multi-Valley" Picture of Free Energy :

There is, in much of the spin glass literature, a theoretical picture which underlies quite a few of the general scenarios that have been developed. This picture can be loosely described as follows. We start by noting that on almost any reasonable timescale, a glassy system with $T < T_G$ cannot explore all of its configuration space - its dynamics are confined to some region in this space. The idea then is that all states in a region correspond to roughly the same macroscopic state. The idea is illustrated below, and it is usually formulated in terms of a free energy "landscape" which is supposed to be a function of all the spin configurations, ie., we have

$$F = F(\{S_j\}; T) \qquad (124)$$

which has local minima defined by

$$\left.\frac{\partial F}{\partial S_j}\right|_{\{S_j\} = \{S_j^{min}\}} = 0 \qquad (125)$$

with the condition that the eigenvalues of the matrix

$$M_{ij} = \left.\frac{\partial^2 F}{\partial S_i \partial S_j}\right|_{\{S_j^{min}\}} \qquad (126)$$

are positive definite (ie all curvatures at the bottom of these multi-dimensional Free energy wells are positive).

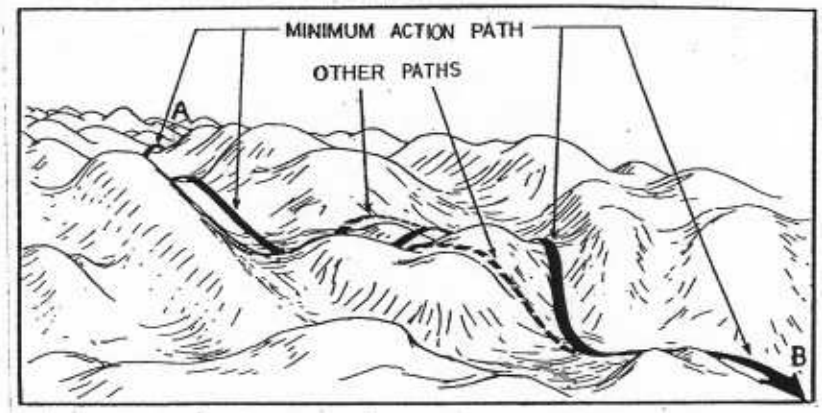

ABOVE : SCHEMATIC FIGURE OF FREE ENERGY LANDSCAPE, SHOWING A FAVOURED PATH OR MINIMUM ACTION FROM STATE A TO STATE B.

BELOW : THE FREE ENERGY ALONG THIS PATH.

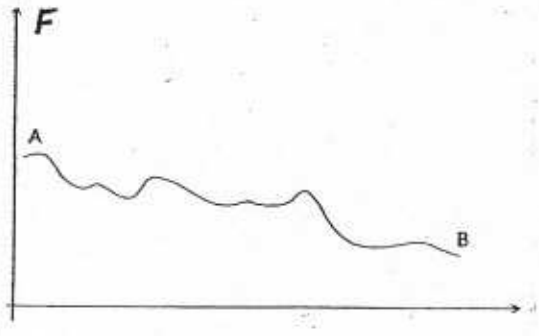

We now imagine that the topography in this $2N$-dimensional "phase space" (it is assumed the spins move on Bloch spheres) is such that there will be a large set of "valleys" separated by very high free energy - Indeed it is usually argued that the "barriers" separating the valleys become infinitely high as one goes to the thermodynamic limit $N \to \infty$. In this case the idea is that

the configuration space of "phase space" divides into seperate regions, which in the literature are sometimes called "basins of attraction" instead of valleys. The idea is that even though the free energy landscape inside a given valley may be very complicated, with lots of hills and dales, crevasses, ridges, etc (all in $2N$-dimensional space!), nevertheless the system can explore a given valley during a specified experimental timescale.

One should be rather suspicious of this picture - it is intuitively attractive but has real problems associated with it, to which I will come below. Before looking at the problems, lets see how far we can go in formulating it mathematically.

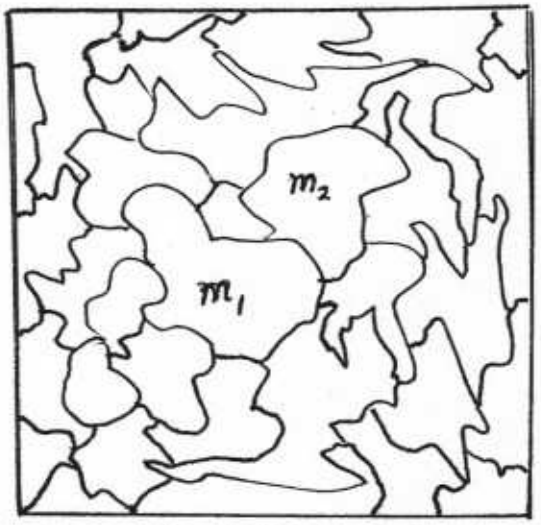

DIVISION OF HILBERT SPACE (OR OF CLASSICAL PHASE) INTO DIFFERENT REGIONS $\mathcal{H}_m$, SEPARATED BY BARRIERS.

Suppose we label each valley by an index m. Then the probability of finding the system in the valley in a full Gibbs average is

$$P_m = \frac{1}{Z} e^{-\beta f_m} \tag{127}$$

$$Z = \sum_{n} Z_m = \sum_{m} e^{-\beta f_m} \tag{128}$$

We can then write the average "expectation" value for some quantity, in thermal equilibrium, but assuming a quenched average, as

$$\langle A \rangle = \sum_m P_m \langle A_m \rangle \tag{129}$$

where in a given valley

$$\langle A_m \rangle = \frac{1}{Z_m} \sum_{\nu \in \mathcal{H}_m} A_\nu e^{-\beta E_\nu} \tag{130}$$

Here we assume the system as a whole has eigenstates $|\nu\rangle$ with energies E_ν, and that inside a given valley, we have some "macroscopic thermodynamic state" which includes a large number N_m of microscopic states $|\nu_m\rangle$; we say that all these states are in some region $\mathcal{H}_m$ of Hilbert space (or phase space for classical spins).

Lets see how this works when we look at some particular expectation value. Consider for example the "annealed" value of $\langle S_j \rangle^2$, produced by averaging over the whole of configuration space with a Gibbs weighting - we have an ensemble average

$$\left.\begin{aligned} [\langle S_j \rangle^2]_{\text{Annealed}} &= [(\sum_m P_m \langle S_j^{(m)} \rangle)^2]_{\text{Annealed}} \\ &\equiv \sum_{m_1} \sum_{m_2} P_{m_1} P_{m_2} [\langle S_j^{(m_1)} \rangle \langle S_j^{(m_2)} \rangle]_{\text{Ann}} \end{aligned}\right\} \tag{131}$$

whereas if we are stuck in a single valley with $m = \ell$, we have for that sample:

$$[\langle S_j \rangle^2]^{\text{1 Sample}}_{\text{Quenched}} \equiv \frac{1}{N} \sum_j (\langle S_j^{(\ell)} \rangle)^2 \tag{132}$$

Now the important point here is that if we have a large collection or ensemble of

such quenched samples, then the ensemble average is now

$$[\langle \underline{S}_j \rangle^2]_{\text{Quenched}} = \sum_m P_m \langle \underline{S}_j^{(m)} \rangle^2 \qquad (133)$$

Thus there is a crucial difference between the 2 results, depending on whether we between the different valleys or not - compare (131) and (133).

Note, to avoid confusion, that although a given sample can be thought of as a particular replica, we should not identify all samples in a given valley with a replica. If we take a whole set of replicas, however, the probability of finding a replica in the m-th valley is just P_m.

It is clear that there are some inadequacies in this whole picture - I have included it primarily because it is so central to much of the theoretical and experimental discussion of glasses. Here are some objections:

(i) The talk of infinite barriers in the thermodynamic limit sounds nice, but what selects out which barriers are infinite & which are finite? In a real system there will be a continuum of states and barrier heights - how do we then define a valley? And what "thermodynamic" states do these valleys correspond to? We know that in real glasses there is always a continuous range of relaxation times.

(ii) The landscape is a free energy landscape, not an energy landscape - it depends on temperature, and the free energy itself is a quantity that fluctuates in time! It is thus a somewhat ill-defined object, especially when we also note that:

(iii) Any spin glass Hamiltonian is in any case an effective Hamiltonian, whose various terms we expect in any case to be temperature dependent (in part the interaction parameters). This makes the whole theoretical framework, in which the free energy landscape needs to be precisely defined, a little shaky.

Order Parameters & Response Functions: In spite of these problems, spin glass theorists have been able to erect an impressive theoretical framework around these ideas. One begins with the definition of several "order parameters". The first is defined as

$$\left.\begin{aligned} q &= \lim_{\underline{H}_0 \to 0} \lim_{N \to \infty} [\langle S_j \rangle^2]_{\text{Annealed}} \\ &\equiv \lim_{\underline{H}_0 \to 0} \lim_{N \to \infty} \sum_{m_1} \sum_{m_2} P_{m_1} P_{m_2} \langle \underline{S}_j^{(m_1)} \rangle \langle S_j^{(m_2)} \rangle \end{aligned}\right\} \qquad (134$$

ie., the same parameter as defined in (131), but where now first take the thermodynamic limit $N \to \infty$, and then let any orienting field go to zero. This is just a standard response function for a system assumed to be in global equilibrium. We shall see below why it is to be thought of as an order parameter.

The second order parameter we shall define is that corresponding to the

ensemble average in (133); it is the famous "Edwards-Anderson" order parameter, given by

$$q_{EA} = \sum_m P_m \langle \underline{S}_j^{(m)} \rangle^2 \tag{135}$$

Finally, we define the time-dependent order parameter

$$\left.\begin{aligned} q(t) &= \left[\langle \underline{S}_j(0)\, \underline{S}_j(t) \rangle_{\tau_{ob}} \right]_{av} \\ &\equiv \left[\frac{1}{\tau_{ob}} \int_0^{\tau_{ob}} dt'\, \underline{S}_j(t')\, \underline{S}_j(t'+t) \right]_{av} \end{aligned}\right\} \tag{136}$$

which is an average over configurations, and over the time-delayed response averaged over an observation time τ_{ob}. We can actually define q and q_{EA} in terms of $q(t)$, via

$$\left.\begin{aligned} q &= \lim_{\underline{H}_0 \to 0} \lim_{N\to\infty} \lim_{t\to\infty} q(t) \\ q_{EA} &= \lim_{t\to\infty} \lim_{N\to\infty} q(t) \end{aligned}\right\} \tag{137}$$

where we see that q_{EA} is defined by only waiting a finite time, even for $N \to \infty$, so that the system always remains in the same valley.

One can also define these order parameters in the language of replicas. The following results will be given without proof, because the proofs are technical, and because the results have an intuitive justification.

One finds first that in replica language the intuitively clear result:

$$q = \lim_{n\to 0} \frac{1}{n(n-1)} \sum_{\alpha \neq \beta} q_{\alpha\beta} \tag{138}$$

(recall eqtn (110), where we had not yet taken the formal limit $n \to 0$). Thus in replica language, q is an average over all the different $q_{\alpha\beta}$. On the other hand, if we think of $q_{\alpha\beta}$ as a matrix in replica space, we find that the Edwards-Anderson order parameter $q_{\alpha\beta}$ is given by the diagonal elements - formally one has

$$q_{EA} = \lim_{n\to 0} \lim_{\alpha\to\beta} q_{\alpha\beta} \tag{139}$$

Now an important point. Up until now we have talked as though the order parameter was a single number. But in both the replica formulation (before we take $n \to 0$) and in the multi-valley formulation, we expect in general that q and q_{EA} actually are distributed over different values with different probabilities. Thus we need to specify a probability distribution for these, as follows:

(i) In replica language, we define the distribution:

$$P(q) = \lim_{n\to 0} \frac{1}{n(n-1)} \sum_{\alpha\neq\beta} \delta(q - q_{\alpha\beta}) \tag{140}$$

(ii) In multi-valley language, we define

$$P(q) = \left[\sum_{m_1, m_2} P_{m_1} P_{m_2} \delta(q - q^{m_1 m_2}) \right]_{AV.} \tag{141}$$

where we write

$$\left.\begin{aligned} q^{m_1 m_2} &\equiv \left[\langle S_j^{(m_1)} \rangle \langle S_j^{(m_2)} \rangle \right]_{AV} \\ &\equiv \frac{1}{N} \sum_j \left[\langle S_j^{(m_1)} \rangle \langle S_j^{(m_2)} \rangle \right]_{AV.} \end{aligned}\right\} \tag{142}$$

Note that we can think of both $q_{\alpha\beta}$ and $q^{m_1 m_2}$ as "overlap" functions, the first as an overlap between different replicas, and the second between different valleys. Thus $q^{m_1 m_2}$ is telling us about the correlations between the spin states in 2 different valleys. This physical interpretation will become much clearer later, when we come to discuss the Parisi scenario for spin glasses.

Finally, let us consider the response function / order parameter which leads to the non-linear susceptibility $\chi_3(T)$ which we defined in eqtn (22). It turns out that we can relate this to one of the correlation functions defined in eqtn (111), in replica language. Without proof, I just give the important results (the proofs are too long to give here):

Define the correlation functions, 4th-order in spin:

$$\chi_{SG} = [\chi_{ij}^2]_{av} = \frac{1}{N} \sum_{ij} \left[\left(\langle S_i S_j \rangle - \langle S_i \rangle \langle S_j \rangle \right)^2 \right]_{av} \tag{143}$$

and

$$\left.\begin{aligned} \chi_3 &= -\frac{\beta^3 N}{3} \left\langle \left(\sum_j S_j \right)^4 \right\rangle_{\substack{cum \\ av.}} = -\frac{\beta^3 N}{3} \sum_{ijkl} \langle S_i S_j S_k S_l \rangle - 3 \langle S_i S_j \rangle \langle S_k S_l \rangle \\ &= \beta^3 N \left(2 - \frac{4N}{3}\right) \sum_{ij} \langle S_i S_j \rangle^2 \\ &= \beta \left(\chi_{SG} - \tfrac{2}{3} \beta^2 \right) \end{aligned}\right\} \tag{144}$$

where χ_{ij} is just also the experimental response function defined by

$$\langle S_i \rangle = \sum_j \chi_{ij} H_j \tag{145}$$

Then it is the task of any theory of spin glasses to show that χ_3 and χ_{SG} must diverge as one approaches the glass transition temperature T_G (all the while remembering that to make such arguments, we have to forget that T_G depends on the timescale!).

(b) Theoretical Scenarios for Dipolar Glasses

Recall that we are dealing here with any glassy system that we think can be modelled as a set of 2-level systems which couple to each other via dipolar interactions. Thus this includes spins in an insulator, as well as defects in some otherwise crystalline system - and in principle it also includes defects in an amorphous system. All of these systems are insulators, and the dipolar interactions are either phonon-mediated or mediated by electric or magnetic dipolar fields.

In what follows we look at 2 scenarios that have produced results that can be compared directly with experiment, and 2 scenarios that attempt a rather general synthesis but which cannot be made sufficiently precise (at least not yet) for this comparison to be made. The first of these deals with spin systems, the latter 3 with insulating glasses.

(i) 1st Scenario: Kinetic Equation Approach to Dipolar Spin Systems

This approach attacks the problem of dynamics directly, by making a separation of timescales between the dipole interaction-driven dynamics, and the dynamics given to the system by its coupling to the environment.

To see how and when such an approach can work, we consider first the application to the problem of a dipole-interacting spin system, in interaction with phonons & nuclear spins. It is useful to consider what are the important parameters in this problem. We assume we are at low-T, in the "qubit" or "quantum regime, where the spin system has truncated to a set of 2-level systems. Ignoring the temperature for the moment, we look at the parameter space of couplings in the Hamiltonian for the system. The general form of this Hamiltonian was already given in eqtn (5); here we specialise to a dipolar interaction between the spins, whose form will be specified below. The strength of this interaction will be such that the interaction between nearest-neighbour dipoles is $\sim V_0 \tau_i^z \tau_j^z$. Each spin will have a quantum dynamics parameter Δ_j, and we assume that $\Delta_j \sim \Delta_0$; and finally there will be an interaction with the environment of strength $\sim \xi_0$. The definition of these 3 parameters will be given more precisely below.

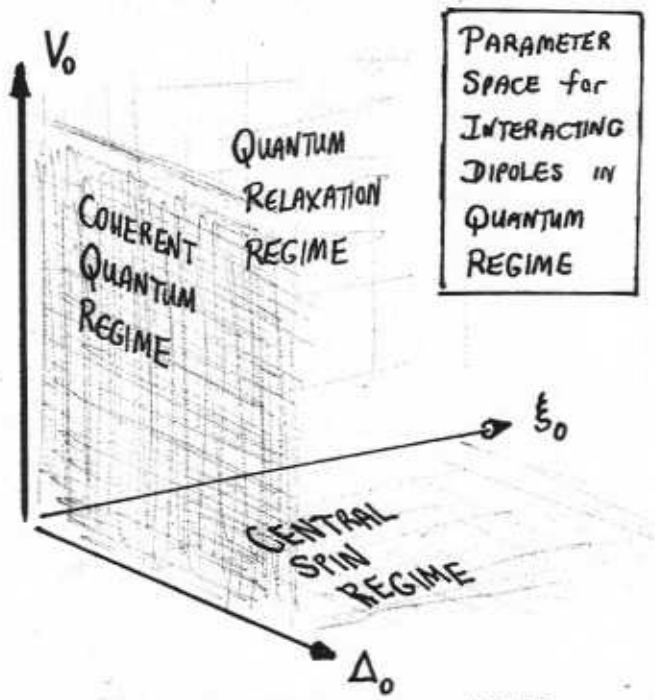

PARAMETER SPACE for INTERACTING DIPOLES in QUANTUM REGIME

THE PARAMETER SPACE FOR THE LOW-T DIPOLAR-INTERACTING "QUBIT" PROBLEM. THE PARAMETERS ARE THE nn DIPOLAR INTERACTION STRENGTH V_0, THE "TUNNELING" PARAMETER Δ_0, AND THE COUPLING STRENGTH ξ_0 TO THE ENVIRONMENT

We have already looked at the "central spin" regime where V_0 can be neglected - this is the regime of individual qubit dynamics, discussed in Part 2, section A. The question now is how to deal with these interactions in calculating the dynamics of this system.

The 2 regimes of interest here are (i) the "coherent quantum regime", in which we

assume that $\xi_0 \ll \Delta_0, V_0$; and (ii) the "quantum relaxation" regime, where the quantum parameter $\Delta_0 \ll V_0, \xi_0$. It turns out that even though the small parameters in these 2 regimes may be very much smaller than the other 2, - we still cannot ignore them - this actually makes the theory rather interesting.

The basic Hamiltonian we shall use is (5), in which the interaction is assumed to have the form

$$\mathcal{H}_{int}(\{\underline{\tau}_j\}) = \tfrac{1}{2} V_0 \sum_{i \neq j} \frac{1}{\bar{r}_{ij}^3} \left[\hat{\underline{\tau}}_i \cdot \hat{\underline{\tau}}_j - 3 \frac{(\hat{\underline{\tau}}_i \cdot \bar{\underline{r}}_{ij})(\hat{\underline{\tau}}_j \cdot \bar{\underline{r}}_{ij})}{\bar{r}_{ij}^2} \right] \tag{146}$$

where we measure distances in units such that $\bar{r}_{ij} = r_{ij} n$ (147)

where n is the number density of spins in the system: $x = n/N$ (148)

The concentration x of spins per site we will take to vary between 0 and 1 - we will be interested in all of these cases. In terms of the original spins $\underline{S}_i$, we have

$$V_0 = (4 g \mu_B S)^2 n = (4 g \mu_B S)^2 / r_0^3 \tag{149}$$

where $r_0^3 = 1/n$ is the mean distance between the spins.

There are 2 cases of this kind of system. One is where the spins are found on some regular lattice, so that their orientations are fixed to lie in one or more specific directions. This is the case for spin systems like magnetic molecule crystals, or the RE spin glass systems like $LiHo_x Y_{1-x} F_4$. It is also the case for glassy systems like $KCl:Li$, where the dipoles are oriented along one of a limited number of directions fixed by the lattice. The simplest such case is where there is only one allowed direction, which we choose to be the $\hat{z}$-axis; then we have

$$\left.\begin{aligned} \mathcal{H}_{int}(\{\underline{\tau}_j\}) &\longrightarrow \tfrac{1}{2} V_0 \sum_{ij} \frac{1}{\bar{r}_{ij}^3} (1 - 3\cos^2\theta_{ij}) \hat{\tau}_i^z \hat{\tau}_j^z \\ &= \tfrac{1}{2} V_{ij}^D \hat{\tau}_i^z \hat{\tau}_j^z \qquad \text{(oriented easy axis system)} \end{aligned}\right\} \tag{150}$$

where θ_{ij} is the polar angle, and we have only included the $\tau_i^z \tau_j^z$ parts of the interaction (this approximation is discussed below in more detail); the full Hamiltonian then becomes

$$\mathcal{H} = \sum_j \Delta_0 \tau_j^x + \tfrac{1}{2} \sum_{i \neq j} V_{ij}^D \tau_i^z \tau_j^z + \mathcal{H}_{env} \tag{151}$$

where we assume that all the spins are the same, ie., we that we do not have several species of spin. The term $\mathcal{H}_{env}$ includes all couplings to spin & oscillator baths (nuclear spins & phonons for magnetic insulators). We ignore external fields in (151) for the moment.

The other important case is where the orientations of the spin axes are random. This is the case of amorphous spin glasses, or amorphous glasses. In this case we will have

Axes

to average over the directions of the spin axes in (14C); we discuss this below.

To find the dynamics of these systems we need to find some sort of kinetic equation to describe the coupled dynamics of the spin density matrices, after integrating out the bath. We show how to do this in 2 cases below, from which the general method will become clear.

(a) Dynamics in Coherent Quantum Regime : We consider a set of M qubits, described by the Hamiltonian (5); our general problem is to understand the dynamics of the M-qubit reduced density matrix defined by

$$\bar{\rho}_M(\tau_1 .. \tau_M ; t) = Tr_E \rho_{Tot}(\{\tau_j\}; \underline{X}; t) \qquad (152)$$

where $\underline{X}$ describes the environment. More generally we wish to calculate expectation values of the form

$$\langle A(\{\tau_j\}; t)\rangle = Tr_{\{\tau\}} [A(\{\hat{\tau}_j\}) \bar{\rho}(\{\tau_j\}, t)] \qquad (153)$$

where $\hat{A}(\{\tau_j\})$ is some operator acting on the $\{\tau_j\}$ (eg., $\sum_j \tau_j^z$, or $\sum_j \sum_{l \neq j} A_{lj}^{\alpha\beta} \tau_j^\alpha \tau_j^\beta$). Under some circumstances we may even want to calculate correlation functions of the form

$$\langle C(\{\tau_j\}; X)\rangle = Tr_{\{\tau\}} Tr_E [\hat{C}(\tau_j; X) \hat{\rho}_{Tot}(\tau_j, X)] \qquad (154)$$

in which we want to find out about correlations between the system and the environment, for example, entanglement correlations

Clearly this is a very hard problem, so in what follows we will do a particular example of this problem which is of considerable current interest. Consider a scheme where we have a set of spin qubits interacting via dipolar couplings, and we start off with the system in some coherent state - to be specific we will assume that all spins are oriented in the same direction, but with no mutual entanglement, and no correlations between the qubit system and the environment. Thus we start with

$$\hat{\rho}_{Tot}(t=0) = \hat{\rho}_0(\{\tau_j\}) \otimes \hat{\rho}_E^{Th}(X;\beta) \qquad (155)$$

where $\rho_E^{Th}(X;\beta)$ is a thermal density matrix for the environment, and ρ_0 is a pure state density matrix for the system, which we will assume to have one of 2 forms:

$$\hat{\rho}_0 = |\Psi_0^{(M)}\rangle\langle\Psi_0^{(M)}| \qquad \Psi_0^{(M)} = \left\{ \begin{array}{l} \prod_{j=1}^{M} |\uparrow\rangle_j \quad \text{(oriented spins)}. \\ \frac{1}{2^{M/2}} \prod_{j=1}^{M} (|\uparrow\rangle_j \pm |\downarrow\rangle_j) \equiv \prod_{j=1}^{M} |\pm\rangle_j \end{array} \right\} \qquad (156)$$

The second form assumes a set of M qubits in one or other of the eigenstates of the qubit Hamiltonian; whereas the first "oriented" state is what would result if we "field cooled" the system, polarizing the spins.

What we now want to do is calculate the dynamics of the 1-qubit density matrix for this system, with these initial conditions. Thus we are actually doing the same as was

done for the central spin model, but the crucial difference now is in the interactions between the qubits. In fact, at any given time the net field on a i-th qubit along the important z-direction is

$$\xi(t) = \xi_i^D(t) + \eta_i(t) = \left(\epsilon_i + \sum_j V_{ij}^D \tau_j(t)\right) + \eta_i(t) \qquad (157)$$

where $\eta_i(t)$ is the field from the environment (spin and oscillator baths). All the new complexity of the problem comes because the dipole field contribution from the other spins is also time-dependent. Thus when we calculate the 1-particle density matrix

$$\bar{\rho}(\tau_i; t) = Tr_{\tau_1 \ldots \tau_{i-1}, \tau_{i+1} \ldots \tau_M} \bar{\rho}_M(\tau_1 \ldots \tau_M; t) \qquad (158)$$

or alternatively the average

$$\bar{\rho}_1(\tau; t) = \frac{1}{M} \sum_j \bar{\rho}(\tau_j; t) \qquad (159)$$

we also need to average over the contribution $\sum_j V_{ij}^D \tau_j(t)$ from the other qubits.

In what follows I will not solve for the dynamics starting from the equation of motion for $\bar{\rho}(\tau_i; t)$, since this is a little lengthy, but instead simply give some of the results, along with arguments which justify them intuitively.

Note first that if we start from one or other of the states in (156), we can classify the states to which it couples using spin wave theory. Recall that for a Hamiltonian like (151), if we ignore the environment, we have excitations of momentum $|q\rangle$, with energies

$$\left.\begin{aligned} \omega_q &= \left[(\omega_0 + \alpha_1 q^2)(\omega_0 + \alpha_1 q^2 + \alpha^2\left(\frac{q_x^2 + q_y^2}{q^2}\right)\right]^{1/2} \\ \text{where} \quad \hbar\omega_0 &= \Delta_0 + 4\pi g \mu_B N_z M_0 \\ \alpha_1 &= 2JSa_0^2 \\ \alpha_2 &= 4\pi g \mu_B M_0 \\ N_z &= \tfrac{1}{3} + \frac{1}{4\pi N} \sum_{j=1}^{M} \frac{1}{r_{ij}^3}\left(1 - 3\frac{(\hat{z}\cdot r_{ij})^2}{r_{ij}^2}\right) \end{aligned}\right\} \text{ordered lattice array} \qquad (160)$$

This result is for a pure "crystalline" ordered array of spins that is polarized - we have included an exchange coupling in here for good measure. If the spins are *not* in an ordered array - if, for example, we have spins on some fraction x of sites, with the positions being random - then we cannot classify the states in such a simple way. Their nature can be classified using the general framework of the Anderson theory of localization, and we have

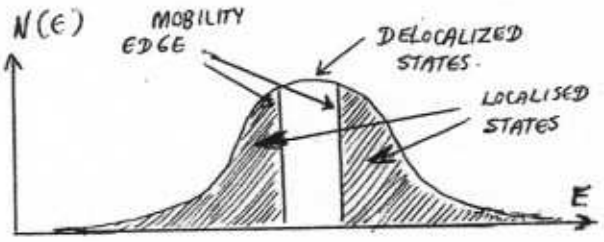

ANDERSON LOCALISATION: A MIXTURE OF LOCALISED & DELOCALISED STATES

(i) $V_0 > \Delta_0$ — Anderson localised states

(ii) $V_0 < \Delta_0$ — mixture of localised & delocalised states; mobility edge (161)

A theory of all these states would take us far afield

from the present discussion - but it makes it clear how the theory of glasses is directly connected to the theory of localization. Here we are interested in the coherence properties in the coherent quantum regime, without all the complications associated with disorder, so we will focus on these, and deal later with the effects of disorder.

In the case where the spins are on an ordered lattice, we can distinguish 2 cases, viz., strong dipole interactions (i.e., $V_0 > \Delta_0$), and weak dipole interactions ($V_0 < \Delta_0$). To understand the results we have to make a slight detour to look at the distribution of fields in the system.

Distribution of Internal Fields: We consider an initial density matrix $\bar{\rho}(\xi_1 \ldots \xi_N; t)$, & define:

$$\langle \xi_i^D(t) \rangle = Tr\left[\bar{\rho}\, \xi_i^D(t)\right] \tag{162a}$$

In general we can separate this quantity into 2 parts:

$$\langle \xi_i^D(t) \rangle = \bar{\xi}_D(r,t) + \delta\xi_i(t) \tag{162b}$$

where $\bar{\xi}_D(r,t)$ varies slowly in space, and can be formally defined in terms of the original $\langle \xi_i^D(t) \rangle$ by doing a coarse-grained average around the site i; and $\delta\xi_i(t)$ refers to the fluctuations about $\bar{\xi}_D(r,t)$

Now typically, when dipolar interactions are involved, the length scale over which $\bar{\xi}_D(r,t)$ varies can be rather long, and it will be governed by the sample geometry - in fact we can identify $\bar{\xi}_D(r,t)$ with the longitudinal component of the internal field:

$$\bar{\xi}_D(r,t) = g\mu_B S_z \left(H_0^z + H_{DM}^z(r,t)\right) \tag{164}$$

where $H_{DM}(r,t)$ is just the internal demagnetization field coming from the sum over all the dipole fields of the individual qubits. One can usefully visualize the behaviour of $\bar{\xi}_D(r,t)$ in 2 ways. First, we can plot surfaces of constant $\bar{\xi}_D(r,t)$ in space, defined by the equation

$$\bar{\xi}(r,t) = \bar{\xi}_D(r,t) \tag{165}$$

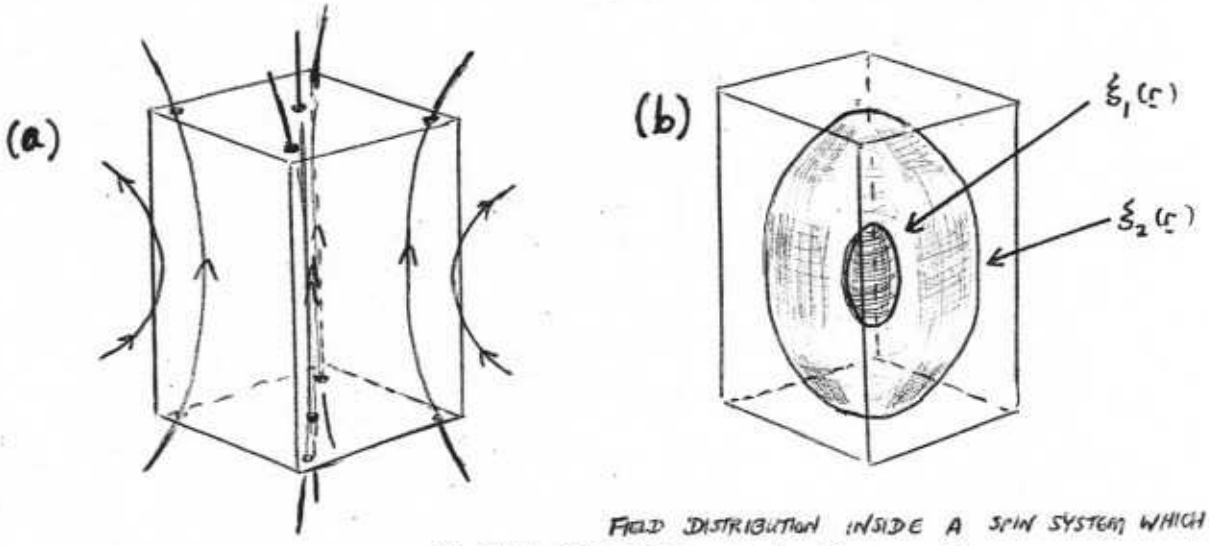

FIELD DISTRIBUTION INSIDE A SPIN SYSTEM WHICH IS FULLY POLARIZED ALONG $\hat{z}$. IN (a) WE SEE THE DIRECTION OF THE FIELD, PLOTTING FIELD LINES OF $H_{dm}(r)$. IN (b) WE SEE TWO SURFACES OF CONSTANT $\bar{\xi}_D(r)$, VIZ., $\bar{\xi}_D(r) = \xi_1$ AND $\bar{\xi}_D(r) = \xi_2$.

The calculation of $\underline{H}_{Dm}(\underline{r},t)$, and hence of $\xi_D(\underline{r},t)$, for a given distribution $\underline{M}(\underline{r},t)$ of magnetisation in the sample, is a matter of elementary magnetostatic theory (see part I, section C.3.1). Another way to visualise the results is to define the "density of states" function

$$N(\xi,t) = \frac{1}{N}\sum_j \delta(\xi - \langle \xi_j^D(t)\rangle) \xrightarrow[\text{Sample}]{\text{Polarized}} \frac{1}{V_0}\int d^3r\, \delta(\xi - \bar{\xi}_D(\underline{r},t)) \qquad (166)$$

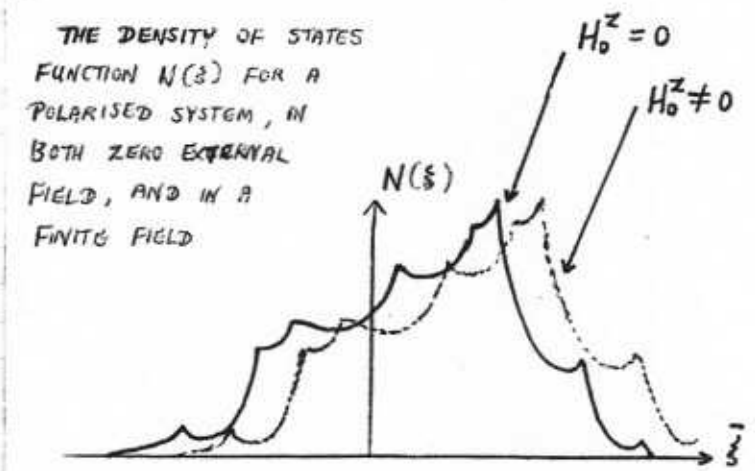

which tells us how much of the sample is inside the surface $\bar{\xi}_D(r,t) = \xi$.

If we plot $N(\xi)$ for a polarised sample we notice that there will be "Van Hove" singularities at certain specific values of ξ. These are a generic feature of such calculations - one sees the same thing, eg., in calculations of the electronic density of states for some band structure. One can get a general understanding of them using topological methods (using "Morse theory"), but they are intuitively rather easy to understand in terms of the surfaces $\bar{\xi}(\underline{r})$. Suppose we slowly change the value of ξ, so that the surfaces of constant ξ are swept gradually through the sample. We see that $N(\xi)$ in (166) above is just measuring the total area of the surface with $\bar{\xi}_D(r) = \xi$, and that at the point where this surface begins to touch an edge or corner of the sample, we will have

$$\left.\frac{d^2N(\xi)}{d\xi^2}\right|_{\xi=\xi_m} \to \pm\infty \qquad (167)$$

simply because the rate of change of area with ξ changes suddenly as a surface vanishes or appears - at the points where $\xi = \xi_m$. These are the Van Hove points.

Notice that if we add an external field $\epsilon = g\mu_B S H_0^z$ (for electronic spins), then the density of states must shift; we have $\xi \to \xi + \epsilon$, so that

$$N(\xi,t) \to N(\xi+\epsilon,t) = \frac{1}{V_0}\int d^3r\, \delta(\xi - (\bar{\xi}_D(r,t) - \epsilon)) \qquad (168)$$

ie., the surface ξ is now probing energies $\bar{\xi}_D - \epsilon$.

The figure above shows what $N(\xi,t)$ looks like for a polarised system. What if the spins are completely annealed, with the spins oriented completely randomly (ie with no correlation between nearby spins). In this case the demagnetisation contribution $\xi_D(\underline{r},t) \to 0$ if there is no external field, and to $+\epsilon$ if we apply a field. Now the contribution of the rapidly fluctuating contribution $\delta\xi_1(t)$ is crucial:

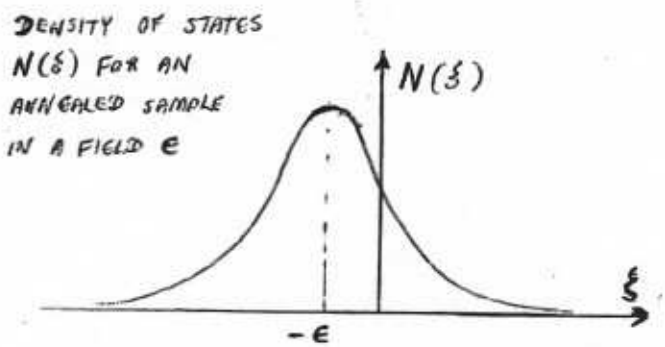

$$N(\xi) \to \frac{1}{(2\pi)^{1/2}W_0} e^{-(\xi+\epsilon)^2/2W_0^2} \qquad (169)$$

where the width W_0 depends on the lattice structure

Let us now return to our problem, which is the calculation of the dynamics of the reduced density matrix, in particular of the single-spin reduced density matrix $\bar{\rho}_1(t)$.

The first thing to emphasize is that consideration of $\bar{\rho}_1$ inevitably leads us to consider the higher interactions as well, because we have split the Hamiltonian into a kinetic K an interacting term. Thus the interactions inevitably generate correlations between the spins which can only be described by the higher reduced density matrices - moreover, these correlations inevitably react back on the dynamics of ρ_1.

There exist well-developed but rather complex techniques for systematically evaluating these higher correlations. Suppose, for example, that $V_0 \ll \Delta_0$, so that a perturbation expansion in V_0/Δ_0 makes sense. Then we see that $\bar{\rho}_1$ must couple to $\bar{\rho}_2$ via processes in which a pair-flip process occurs involving the spin τ_1 of interest in $\bar{\rho}_1$, and the spins τ_1 and τ_2 in $\bar{\rho}_2$.

There is no space here to develop these systematic techniques. Instead we will analyze the problem described above, in which we start with a polarised sample – and we will look at the detailed dynamics of the system in one limit, that where $V_0 \ll \Delta_0$. The opposite limit $V_0 \gg \Delta_0$ will be discussed later, in the context of electric dipole glasses.

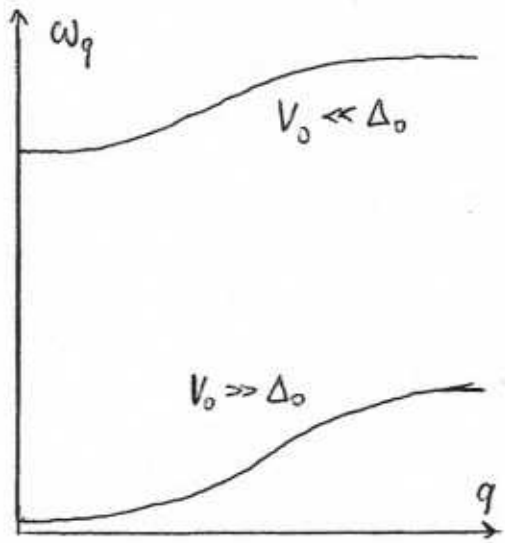

TYPICAL MAGNON SPECTRUM FOR FULLY-POLARISED SYSTEM, IN 2 LIMITS.

We consider the system in the initial polarised state described by $\hat{\rho}_0$ in (156). Then the excitations of the system are spin waves, as noted above, with an effective Hamiltonian at very low T given by:

$$\left.\begin{aligned} \mathcal{H}_{eff} &= \sum_q \omega_q \left(b_q^+ b_q + \tfrac{1}{2}\right) + \\ &\quad + \frac{1}{2N} \sum_{\substack{q_1 q_2 \\ \kappa}} \Gamma^{(4)}_{q_1 q_2}(\kappa)\, b^+_{q_1+\kappa}\, b^+_{q_2-\kappa}\, b_{q_1} b_{q_2} + \cdots \end{aligned}\right\} \quad (171)$$

and with ω_q given by (160) above. Since $\Delta_0 \gg V_0$, the non-interacting magnon spectrum has the form shown in the Figure at left.

We see that in this regime we are able to completely transform the problem described by (151) into a problem of spin waves. The question now is how to find the dynamics of the Hamiltonian (171). The obvious way to do this is perturbatively, using the small parameter $\Gamma^{(4)}/\Delta_0$. Just for the record we give the form of $\Gamma^{(4)}$ for the relevant case where $\kappa = 0$:

$$\left.\begin{aligned} \Gamma^{(4)}_{q_1 q_2}(\kappa \to 0) &= \frac{1}{4N}\left(K^{(4)}(q_1, q_2) + K^{(4)}(0, q_2)\right) \\ \text{where} \quad K^{(4)}_{zz}(q, q') &= \sum_{j \neq i} V_{ij}^{zz}\, e^{i(q-q')\cdot \underline{r}_{ij}} \end{aligned}\right\} \quad (172)$$

We concentrate on the $\kappa = 0$ case because we are interested in the initial state (156), in which a set of oriented spins (all pointed along $\hat{z}$) then precesses in the fields $\Delta_0 \tau_j^x$, all at the same rate Δ_0. This uniform precession is equivalent to a $\kappa = 0$ spin wave. However it can decay with the emission of magnons, at a rate

$$\tau_\phi^{-1} = \frac{2\pi}{\hbar} \sum_{qq'} \left|\Gamma^{(4)}_{qq'}(\kappa = 0)\right|^2 \mathcal{F}[n_q]\, \delta(\omega_0 + \omega_q - \omega_{q'} - \omega_{q-q'}) \quad (173)$$

(for $kT \ll \omega_0$)

where $\mathcal{F}[n_q]$ is a Bose statistical factor and $\omega_0 = \Delta_0$:

$$\mathcal{F}[n_q] = n_q(1+n_{q'})(1+n_{q-q'}) - (1-n_q)\, n_{q'}\, n_{q-q'} \tag{174}$$

$$n_q = \frac{1}{e^{\beta\hbar\omega_q} - 1} \tag{175}$$

in which we see the rate is governed by the competition between ingoing and outgoing processes. Note that while the easiest way to get this result is using a straightforward Feynman diagram expansion, it is easiest to understand it physically as the result of a lowest order decay process appearing in a kinetic equation of the form

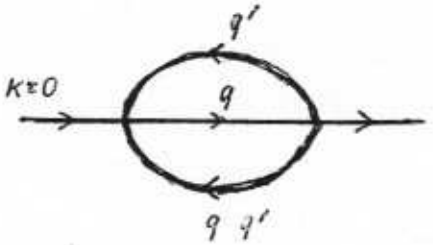

THE 3-MAGNON PROCESS WHICH IS COMPUTED IN EQTN (173), WITH THE DECAY/SCATTERING OF A UNIFORM PRECESSION MODE

$$\frac{dn(K=0)}{dt} = -\tau_\phi^{-1}\, n(K=0) \tag{176}$$

So far this calculation has ignored the fact that in any real sample, the distribution of fields will be inhomogeneous, as we saw above. Under these circumstances the magnon dispersion relation itself becomes inhomogeneous, ie, $\omega_q \to \omega_q(\underline{r})$, where

$$\omega_q(\underline{r}) = \omega_q + \bar{\xi}_D(\underline{r}) \tag{177}$$

and we assume that $\xi_D(\underline{r})$ varies slowly as before. This inhomogeneity makes the problem more complicated – we do not pursue it here.

All of this analysis has assumed that the population density of magnons is low, otherwise we need to go beyond the lowest-order interactions in (171). It is interesting that we can also go away from the low-T limit $kT \ll \omega_0$, and study what happens at high-T, provided we have another small parameter. In fact we do, because $V_0 \ll \Delta_0$ still. The problem can then be solved even though there is a large thermal population of excited states, so that the system is essentially disordered. – one expands in V_0/Δ_0, thereby taking account only of pair-flip processes at lowest order.

The simplest way to do this is rather interesting. Notice that because we now have a significant population of excited states, $N(\xi)$ will be dominated by the rapid fluctuations $\delta\xi_i$, and it will be broadened. Let us therefore define the moments of $N(\xi)$ as

$$M_n = \int d\xi\, N(\xi)\, (\xi - \bar{\xi})^n \tag{178}$$

where $\bar{\xi}$ is the mean value of ξ, ie

$$\bar{\xi} = \int d\xi\, \xi\, N(\xi) \tag{179}$$

Now M_n can be calculated in terms of V_0/Δ_0, by a very nice trick. Suppose we define the exact eigenstates of the Hamiltonian (151), excluding the environment; we call these states $|n\rangle$, defined by

$$\left.\begin{aligned} \mathcal{H}_0 |n\rangle &= E_n |n\rangle \\ \mathcal{H}_0 &= \sum_j \Delta_0 \tau_x^j + \sum_{ij} V_y^{zz} \tau_i^z \tau_j^z \end{aligned}\right\} \tag{180}$$

Now we notice that we can also write these moments in terms of operators acting on the exact eigenstates of the system:

$$M_2 = \frac{Tr\{\hat\rho\,([\hat{\mathcal{H}}_0, \hat S_x])^2\}}{Tr\{\hat\rho\, S_x^2\}} \equiv \frac{\sum_n\sum_m (e^{-\beta\epsilon_m} - e^{-\beta\epsilon_n})\,|\langle n|\hat S_x|m\rangle|^2\,(E_m - E_n)^2}{\sum_n\sum_m (e^{-\beta E_m} - e^{-\beta E_n})\,|\langle n|S_x|m\rangle|^2} \xrightarrow{kT \gg V_0} \frac{\sum_m\sum_n (E_m - E_n)^2\,|\langle n|\hat S_x|m\rangle|^2}{\sum_n\sum_m |\langle n|\hat S_x|m\rangle|^2} \qquad (181)$$

Now what use is this quantity? The answer is that it measures the variance of the fields acting on pairs of spins, causing us we see from flip-flop processes between them. But this variance also tells us what is the dephasing rate of the spin dynamics, caused not by actual decay but purely because different spins move out of phase with each other because of these flip-flop processes. Thus we have a dephasing rate. $\tau_\phi^{-1} \equiv T_2^{-1}$ given by

$$\tau_\phi^{-1} = M_2^{1/2} = \left[1 - \tanh^2\left(\frac{\Delta_0}{kT}\right)\right]^{1/2} \sum_{j\neq 1} V_{1j}^{zz} \qquad (kT \gtrsim \Delta_0) \qquad (182)$$

where the last result follows from detailed evaluation of the commutator in (181); note that we don't actually need to know the eigenstates $|n\rangle$ to find this commutator.

Thus in the results (182) and (173) we have found out the most interesting fact about the 1-spin density matrix for the ensemble of spins, viz., the decay rate of its off-diagonal matrix elements. Note the restriction again – we have assumed an initially oriented state, and we assume the spins are all on a lattice.

To apply this theory to a real experimental system one needs to also include decoherence from spin-phonon interactions, which occurs at a rate

$$(\tau_\phi^{ph})^{-1} = \frac{M_{ph}^2}{\pi\hbar^3}\frac{\Delta_0^3}{\rho c_s^5}\coth\left(\frac{\Delta_0}{2kT}\right) \qquad (183)$$

(compare eqtn (226) in section A), where M_{ph} is a spin-phonon matrix element, and also include the nuclear spin decoherence. One also needs to include all the components of the dipole interaction, along with the anisotropic spin g-factors, etc. The results for a particular system, the Fe-8 molecule, are shown at left. These results, & others on similar systems, are crucial for the design of solid-state qubit systems.

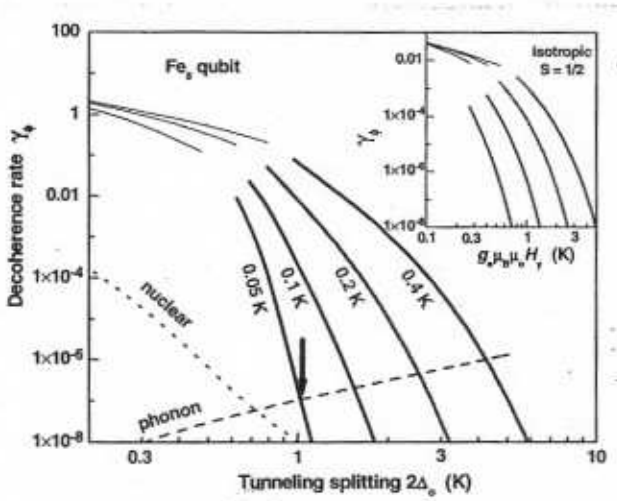

EXAMPLE: Dimensionless decoherence rates $\gamma_\phi = \hbar/T_2\Delta_0$ as a function of tunneling gap $2\Delta_0$ in Fe_8, at the indicated T. Thin lines: γ_ϕ^{vV} arising from pair-flip processes, Eq. 182. We omit γ_ϕ^{vV} at $T = 0.05\ K \ll U_d/k_B$. Thick lines: γ_ϕ^m from magnon scattering, Eq. 173. The gap between the γ_ϕ^{vV} and γ_ϕ^m lines is the crossover region between the validity of the two methods. The dashed and dotted lines show, respectively, the phonon [γ_ϕ^{ph}, Eq. 183] and nuclear (γ_ϕ^{NS}) decoherence rates at $T = 0.05$ K. The arrow indicates the optimal operation point of the Fe_8 spin qubit at $T = 0.05$ K. Inset: γ_ϕ^{vV} and γ_ϕ^m for an isotropic spin-1/2 on the same Fe_8 lattice, as a function of the Zeeman gap $g_e\mu_B\mu_0 H_y$.

(b) Dynamics in Quantum Relaxation Regime

: Let us now turn from the coherent quantum regime, which is very difficult to analyse because one is dealing with multi-spin entanglement, to the much easier problem of the relaxational dynamics in the regime where $\Delta_0 \ll V_0, \xi_0$.

In what follows I first develop the general theory for this problem, in terms of a hierarchy of kinetic equations. Then the dynamics is worked out for 2 cases - the first being a FC (field-cooled) starting state, and the second an annealed ZFC state. Finally, we make contact with experiments on systems in this regime - these experiments were already discussed in section B.1 (a).

Kinetic Equations in Quantum Relaxation Regime

: In the discussion of the coherent Q. regime just above, it was noted that one could develop a hierarchy of quantum kinetic equations for the density matrices of the system, but that these were very complicated & so they were not given (in fact it is an outstanding & very important research problem to give a proper discussion of these equations).

However in the quantum relaxation regime things become a lot easier. This is because we never have to deal with off-diagonal elements of the n-spin density matrices - these have been suppressed already by the coupling to the environment. Thus even though the dynamics is entirely driven by the quantum parameter Δ_0, as we shall see, we can nevertheless deal with classical distribution functions.

To do this, we begin by defining a sequence of distribution functions as follows:

Probability of finding a spin at site $\underline{r}_j$, with local bias ξ_j, and with polarisation state $\alpha = \uparrow, \downarrow$, at time t } $P_\alpha^{(1)}(\underline{r}_i, \xi_i; t)$

Probability of finding spins in states α_1, α_2, with local biases ξ_1, ξ_2, at sites $\underline{r}_1$ and $\underline{r}_2$, call all at time t } $P_{\alpha_1\alpha_2}^{(2)}(\underline{r}_1, \underline{r}_2, \xi_1, \xi_2; t)$

$\vdots$

and so on to the n-spin distribution function: $P_{\alpha_1 \ldots \alpha_n}^{(n)}(\underline{r}_1 \ldots \underline{r}_n; \xi_1 \ldots \xi_n; t)$ } (18)

Note that these distributions are readily defined in terms of the relevant reduced density matrices; we have, e.g., a 1-particle density matrix $\hat{\rho}_1$, which has matrix elements $\rho_1^{\alpha\alpha'} = \langle \alpha | \hat{\rho}_1 | \alpha' \rangle$, and we simply want to enforce the conditions $\alpha = \alpha'$, as well as the local bias and position values - thus we can write

$$\left.\begin{aligned} P_\alpha(\underline{r}_j, \xi_j; t) &= \langle \alpha | \hat{\rho}_1 | \alpha \rangle \, \delta(\underline{r} - \underline{r}_j)\, \delta(\xi - \xi_j) \\ &\equiv \langle \alpha \underline{r} | \hat{\rho}_1 | \alpha' \underline{r}' \rangle \, \delta(\underline{r} - \underline{r}_j)\, \delta(\underline{r}' - \underline{r}_j)\, \delta_{\alpha\alpha'}\, \delta\left(\xi_j - \mathrm{Tr}\left[\bar{\rho}_1 \xi\right]\right) \end{aligned}\right\} \quad (18)$$

Now we can link together the equations of motion for the different $P^{(n)}$. The hierarchy of equations is basically an adaptation of the celebrated "BBGKY" hierarchy of equations first developed for interacting gases.

BBGKY hierarchy

: These were first developed as a generalisation of Boltzmann's famous equation for gases. We begin by defining a set of classical distributions of form.

$$f_1(\underline{r}, \underline{p}; t) \; ; \; f_2(\underline{r}_1, \underline{r}_2; \underline{p}_1, \underline{p}_2; t), \text{ etc.} \qquad (18c)$$

where $f_1(\underline{r},\underline{p};t)$ defines the probability of finding a particle at a particular point in phase space with momentum $\underline{r}$ and position $\underline{p}$; and so on.

The BBGKY hierarchy of equations is written as follows; for a system with N particles and with a Hamiltonian

$$\mathcal{H} = \sum_{j=1}^{N} \frac{\underline{p}_j^2}{2m} + \frac{1}{2}\sum\sum_{i\neq j} V(|\underline{r}_i - \underline{r}_j|) \tag{187}$$

Then the N-particle distribution function satisfies the equation of motion

$$\left.\begin{aligned} \mathcal{D}_t f_N &\equiv \partial_t f_N(\underline{X}_N;t) + \{\mathcal{H}, f_N\} \\ &\equiv \partial_t f_N - i\hat{\mathcal{L}}_N f_N \end{aligned}\right\} = 0 \tag{188}$$

where $\underline{X}_N \equiv (\underline{p}_1 \cdots \underline{p}_N, \underline{r}_1 \cdots \underline{r}_N)$ is a point in $6N$-dimensional phase space, and

$$\hat{\mathcal{L}}_N = -i \sum_{j=1}^{N} \left(\frac{\partial \mathcal{H}}{\partial \underline{p}_j} \cdot \frac{\partial}{\partial \underline{r}_j} - \frac{\partial \mathcal{H}}{\partial \underline{r}_j} \cdot \frac{\partial}{\partial \underline{p}_j} \right) \tag{189}$$

is the "Liouville operator", so that $\{\mathcal{H}, f_N\}$ is the Poisson bracket between $\mathcal{H}$ and f_N. The equation $\mathcal{D}_t f_N = 0$ just says that the total time derivative of f_N is zero, i.e., that the volume of phase space occupied by some region as it flows does not change, no matter how much it distorts.

For the Hamiltonian (187), integrating $N-n$ times over different coordinates of $\underline{X}$ produces the equation

$$\mathcal{D}_t f_n(\underline{X}_n) = \sum_{j=1}^{n} \iint d^3\underline{r}_{n+1}\, d^3\underline{p}_{n+1}\, \hat{\mathcal{M}}_{j,n+1}\, f_{n+1}(\underline{X}_{n+1}) \tag{190}$$

where

$$\hat{\mathcal{M}}_{ij} = N\left[\frac{\partial V_{ij}}{\partial \underline{r}_i} \cdot \frac{\partial}{\partial \underline{p}_i} + \frac{\partial V_{ij}}{\partial r_j} \cdot \frac{\partial}{\partial p_j} \right] \tag{191}$$

and $V_{ij} \equiv V(|\underline{r}_i - \underline{r}_j|)$. In words, the BBGKY eqtn. is telling us that the phase volume of f_n does change, and the change is caused by the net coupling of f_n to the higher distribution f_{n+1} via the averaged effect of the interactions of the n particles in the distribution f_n with the one extra particle in f_{n+1}. The 2 lowest members of the BBGKY hierarchy are, for the Hamiltonian (187), given by

$$\left(\partial_t + \frac{\underline{p}_1}{m} \cdot \frac{\partial}{\partial \underline{r}_1}\right) f_1(\underline{r}_1,\underline{p}_1;t) = \iint d^3\underline{r}_2\, d^3\underline{p}_2\, \hat{\mathcal{M}}_{12}\, f_2(\underline{r}_1\underline{r}_2\underline{p}_1\underline{p}_2;t) \tag{192}$$

$$\left[\partial_t + \left(\frac{\underline{p}_1}{m} \cdot \frac{\partial}{\partial \underline{r}_1} + \frac{\underline{p}_2}{m} \cdot \frac{\partial}{\partial \underline{r}_2} - \hat{\mathcal{M}}_{12}\right)\right] f_2 = \iint d^3\underline{r}_3\, d^3\underline{p}_3\, (\hat{\mathcal{M}}_{13} + \hat{\mathcal{M}}_{23})\, f_3 \tag{193}$$

The famous Boltzmann equation is produced by assuming that we can factorize f_2 as

$$f_2(\underline{r}_1\underline{p}_1;\underline{r}_2\underline{p}_2;t) \sim f_1(\underline{r}_1,\underline{p}_1)\, f_2(\underline{r}_2\underline{p}_2) \tag{194}$$

which when substituted into (192) then produces a closed form for f_1 ; all higher distributions are then just products over f_1. This product form implies that there are no correlations between the distribution at $r_1 p_1$ and $r_2 p_2$. This assumption was called by Boltzmann the assumption of "molecular chaos", and it implies that all memory of correlations in f_2 have been lost. It is actually of some interest to give the explicit form of the Boltzmann eqtn: We define a scattering probability

$$W_{p_1 p_2 ; p_1' p_2'} = \delta(p_1 \to p_1' ; p_2 \to p_2') \qquad (195)$$

for the process where a pair of particles scatters from (p_1, p_2) to $(p_1' p_2')$; because we assume that $V(|r_1 - r_2|)$ is time-symmetric, the probability is the same for the reverse process. Here $\delta_{p_1 p_2 ; p_1' p_2'}$ is the scattering cross-section for this process.

Boltzmann's eqtn is then

$$\left(\partial_t + \frac{p_1}{m} \cdot \partial / \partial r_1 \right) f_1(r_1, p_1 ; t) = I[f_1] \qquad (196)$$

where the "Boltzmann collision integral" is

$$I[f_1] = \int d^3 p_2 \int d^3 p_1' \int d^3 p_2' \; W(p_1 p_2 ; p_1' p_2') \left(f_1(p_1' ; r t) f_1(p_2' ; r t) - f_1(p_1 r t) f_1(p_2 r t) \right) \qquad (197)$$

I will not give the derivation of (197) here from (192) since it is quite lengthy, and in this case the result is fairly intuitively clear - we have a form for $I[f]$ which looks like:

$$I[f_1] = - \sum_{p_2 p_1' p_2'} W \times \underbrace{\left(f_1(1) f_1(2) \right)}_{\text{scattering out}} - \underbrace{f_1(1') f_1(2')}_{\text{scattering in}} \Big\} \qquad (198)$$

in which the rate of change of f_1 inside its moving volume element is produced by the difference between processes where a collision between particles in state $p_1' p_2'$ scatters them into p_1, p_2 (and we integrate over all p_2), and the reverse scattering out process.

Now let's return to our problem of interacting spins. Without derivation, I give the first equation in the series, corresponding to (193); it is

$$\dot{P}_\alpha^{(1)}(\xi, r ; t) = - \tau^{-1}(\xi) \left[P_\alpha^{(1)}(\xi, r ; t) - P_\alpha^{(1)}(\xi, r t) \right]$$
$$- \sum_{\alpha'} \int d^3 r' \int d\xi' \, \tau^{-1}(\xi') \left[P_{\alpha\alpha'}^{(2)}(\xi \xi' r r' ; t) - P_{\alpha\alpha'}^{(2)}(\xi - \alpha\alpha' V(r - r'), \xi' ; r r' ; t \right. \qquad (199)$$

scattering out — scattering in

in which $\tau^{-1}(\xi)$ is the 1-spin quantum relaxation rate for a part in bias field ξ, something we already worked out in the last section (section (A)). This equation tells us that the rate of change of $\dot{P}_\alpha^{(1)}$ is the sum of a local 1-spin term $(P_\alpha - P_{-\alpha})$, which does not involve the interactions at all, and a "2-body" term which does. Again,